JANUS STARCH PARTICLES:
SYNTHESIS AND CHARACTERIZATION

A Dissertation

Presented to the Faculty of the Graduate School

of Cornell University

In Partial Fulfillment of the Requirements for the Degree of

Doctor of Philosophy

by

Arkaye Kierulf

May 2021

© 2021 Arkaye Kierulf

JANUS STARCH PARTICLES:

SYNTHESIS AND CHARACTERIZATION

Arkaye Kierulf, Ph. D.

Cornell University 2021

Starches are one of the most widely used ingredients in the food industry, owing to their incredible versatility as texturizers and emulsifiers. To fine-tune their properties for a wide array of applications, over 100 kinds of modified starches have been made in the last 70 years by homogeneous methods—via chemical, enzymatic, and physical means—to produce one-faced particles, i.e., particles whose entire surface has been modified to have only one and the same physical or chemical functionality. Very little research, however, exists on the potential applications of the heterogeneous modification of starch to produce Janus or two-faced particles, i.e., particles with two opposite halves that have two different functionalities.

In this dissertation, various methods were explored to synthesize starch Janus particles and characterize their self-assembly, texturizing, and emulsifying abilities. In Chapter 1, a 2D mask approach via a spin-coating spray method was developed to produce half-hydrophobic, amaranth starch Janus granules by octenyl succinic anhydride (OSA) esterification. These Janus particles were found to exhibit unique self-assembly behavior into worm-like strings. Low yield, however, prevented further characterization, so a more scalable 3D mask approach via a wax Pickering emulsion

method was developed next. To make this method work, however, starch's emulsifying ability first had to be improved so it could embed itself halfway into a wax droplet. In Chapter 2, it was found that retaining a high protein content when extracting starch from flour played a key role in making sure the starch would embed itself halfway into the wax droplet. In Chapter 3, using these high-protein starches, a scalable 3D mask approach was then developed that could make Janus particles with 49% Janus balance. Janus starch granules with one half side modified with OSA were found to self-assemble into worm-like strings in water. These Janus starch granules outperformed the unmodified and homogeneously modified controls as thickening and gelling agents, as evidenced by their fourfold increase in water-holding capacity, a 30% lower critical caking concentration, a viscosity greater by orders of magnitude, and their formation of gels that were stiffer and stronger also by orders of magnitude. In fact, such was the improved thickening ability of these Janus starch particles that we could achieve similar viscosities as the controls by using less than half the amount of Janus starch. These Janus particles thus show promise as high-performance, plant-based texturizers for potential calorie reduction, pointing to an emerging field of food-based Janus particles that, if pursued, may bring to the table exciting, new applications in the future of our food.

BIOGRAPHICAL SKETCH

Arkaye Kierulf was born and raised in Tacloban City, Philippines. He received a B.S. in Chemistry from the Ateneo de Manila University, where he also received the Dean's Award. After college, he worked for seven years as a Quality Manager and Analytical Chemist for the Philippine Institute of Pure and Applied Chemistry, before pursuing a Ph.D. in Food Science and Technology at Cornell University in Ithaca, New York.

ACKNOWLEDGMENTS

I owe a debt of gratitude to my brilliant academic advisor, Dr. Alireza Abbaspourrad, and my supportive academic committee, Dr. Carmen Moraru and Dr. Robin Dando, for their wisdom, guidance, and patience.

Thanks are also due to the Abbaspourrad Lab, the Cornell Food Science Department, Dairy One, and the Cornell Statistical Consulting Unit for their assistance, especially Dr. Mojtaba Enayati, Dr. Michael Selig, Dr. Hamed Eskandarloo, Dr. Morteza Azizi, Dr. Javad Amani Shams Abad, Dr. Alexandra Brozena, Mohammad Yaghoobi, Brenda Werner, Aaron Jacobsen, Andrew Melychenko, Kyle Kriner, Anthony M. Condo Jr., Philip Carubia, Joseph Dumpler, David Wise, Rebecca Williams, Jennifer Burlew, Marti-Jo Russell, William Guzman, Dr. Brook Luers, Dr. Erika Louise Mudrak, and Erin Atkins.

Guidance from Tate & Lyle Ingredients Americas LLC was crucial to this project, and I would like to thank Dr. Judith Whaley, Dr. Weichang Liu, Dr. Mariana Perez-Herrera, and Dr. Zheng You for their mentorship.

I would also like to thank the Cornell Center for Materials Research Shared Facilities, supported through the NSF MRSEC program (DMR-1719875) and NSF-MRI grant CHE-1531632.

Lastly, I would like to thank my family and my fiancée, Maria Alejandra Zamorano, for their understanding, support, and love throughout my Ph.D. journey.

TABLE OF CONTENTS

LIST OF FIGURES

Introduction

Chapter 1

LIST OF TABLES

LIST OF ABBREVIATIONS

AOAC	Association of Official Analytical Chemists
APTMAC	3-acrylamidopropyl trimethylammonium chloride
CCC	Critical caking concentration
DS	Degree of substitution
DSC	Differential Scanning Calorimetry
EI	Emulsion index
EtOH	Ethanol
FTIR-ATR	Fourier Transform Infrared Spectroscopy with Attenuated Total Reflectance
HLB	hydrophile-lipophile balance
LA	Lauric acid
LVR	Linear viscoelastic region
NMR	Nuclear Magnetic Resonance Spectroscopy
OSA	Octenyl succinic anhydride
O/W	Oil in water (emulsion)
PDI	Polydispersity index
PDMS	polydimethylsiloxane
SD	Standard deviation
SEM	Scanning electron microscopy
SEM-EDX	Scanning electron microscopy- Energy dispersive X-Ray Spectroscopy
SR-SIM	Super resolution-structured illumination microscopy
WHC	Water-holding capacity
W/O	Water in oil (emulsion)
XRD	X-Ray Diffraction

INTRODUCTION

Homogeneous modification of starch

Starch is one of the most widely available and cheapest materials on earth, with a global market projected to reach over USD 100 billion by 2026 (Markets and Markets Research Private Ltd., 2015). Starch is biodegradable, non-allergenic, and GRAS, and thus often used in the food industry as a texturizer and emulsifier (Khlestkin, Peltek, & Kolchanov, 2018; Timgren, Rayner, Dejmek, Marku, & Sjoo, 2013; Zhu, Starch based Pickering emulsions: Fabrication, properties, and applications, 2019; Din, Xiong, & Fei, 2017). In their native form, many starches, however, are unsuitable for certain processes and applications, due to their poor shear or thermal stability, and their tendency for retrogradation (Din, Xiong, & Fei, 2017). Thus, in the last 70 years, starch has often been modified homogeneously, via chemical, enzymatic, and physical means, to produce isotropic or one-faced particles that have fine-tuned or improved properties (Khlestkin, Peltek, & Kolchanov, 2018; Din, Xiong, & Fei, 2017). By "homogeneous modification," we mean the uniform modification of a starch granule over its entire surface. This homogeneous modification of starch produces what we call "one-faced particles," i.e., particles whose entire surface has only one and the same physical or chemical functionality (hence the term "one-faced"). Homogeneous octenyl succinylation of starch has been used for many years, for example, to improve starch's emulsifying and encapsulation ability, thickening ability, and freeze-thaw stability (Sweedman, Tizzotti, Schäfer, & Gilbert, 2013). Homogeneous treatment with *alpha*-amylase, to give another example, has also been used to increase starch's overall

porosity and improve its adsorptive capacity as an ingredient carrier for food, medicine, and cosmetics (Gao, Li, Bi, Mao, & Adhikari, 2014; Wang, et al., 2016; Zhang, et al., 2012; Zhu, Encapsulation and delivery of food ingredients using starch based systems, 2017).

Heterogeneous modification of starch: Janus particles

While homogeneous modification of starch has given starch many improved properties in the last 70 years, very little is known in the literature about what benefits heterogeneous modification of food ingredients would provide. "Heterogeneous modification" of starch is a different type of modification in which, instead of modifying the entire surface of the starch granule, we are only modifying a certain portion of its surface. A Janus particle (Fig. I.1b) is one such product of heterogeneous modification, in which one-half side has a different physical or chemical functionality than the other half; i.e., a Janus particle is anisotropic or two-faced (Zhang, Grzybowski, & Granick, 2017; Hu, Zhou, Sun, Fang, & Wu, 2012). For example, one side of a Janus particle may be hydrophilic and the other side hydrophobic; or one side may contain a certain functional group or molecule, while the other side may contain a different functional group or molecule. By contrast, a homogeneously modified particle is generally uniform over its entire surface (Fig. I.1c). We are aware of only one starch study that was able to produce cornstarch-polystyrene Janus particles. However, they also used a synthetic polymer together with the starch, they did not further study the Janus particles' resultant properties, and they did not explore potential applications (Pei, et al., 2018). The

production of Janus particles using only natural biopolymers like starch is thus an open field that remains to be explored.

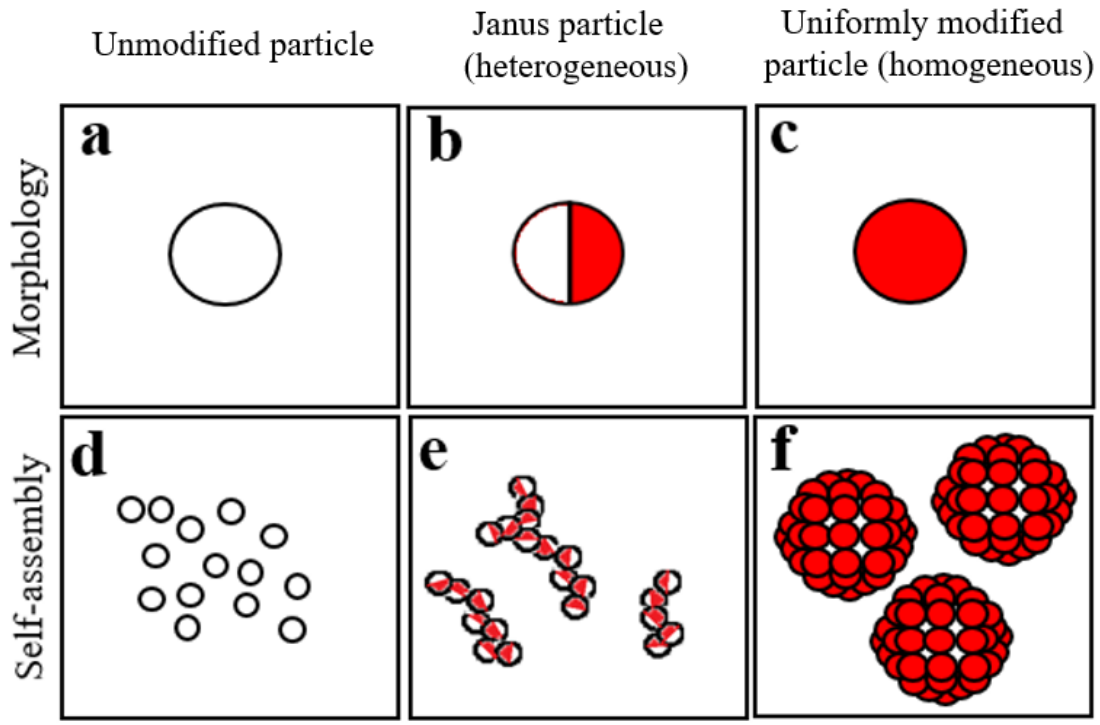

Figure I.1. Morphology of (a) unmodified, (b) Janus particle (heterogeneously modified), and (c) uniformly modified particle (homogeneous). Their respective self-assembly behaviors are shown in d-f.

Exploration of functionalities of starch Janus particles

Many Janus particles have been produced using synthetic polymers via different techniques in the last two or three decades. These synthetic polymer-based Janus particles have been shown to have extraordinary properties, such as unique elf-assembly behavior, improved emulsifying ability (Poggi & Gohy, 2017; Tanaka, Okayama, Minami, & Okubo, 2010), self-propulsion (Poggi & Gohy, 2017; Tanaka, Okayama, Minami, & Okubo, 2010), sensor abilities (Takei & Shimizu, 1997), and tailored drug

delivery (Wang, et al., 2013; Poggi & Gohy, 2017), among others. What is particularly interesting is that several studies have shown that Janus particles self-assemble in ways different than do non-Janus (uniformly modified) particles (Fig. I.1d-f). Synthetic Janus particles tend to form wormlike strings in solution, depending on their Janus balance, while homogeneously modified particles form large aggregates or supermicelles (Li, Lu, Sun, & An, 2012). Recent work from our group in which we produced starch-based Janus particles shows that they exhibit the same self-assembly behavior (Kierulf, et al., 2019). We suspect that these differences in interaction or self-assembly behavior of Janus particles (whether synthetic or starch-based) versus their non-Janus counterparts will also lead to differences in rheology because of their higher effective dispersed phase volume, and that this in turn may lead to better thickening, gelling, and/or emulsifying abilities, with the possibility of being reversible to shear. This can lead to reduction in calories or cost and improved processing stability if these starch Janus particles can be produced in bulk and incorporated into food products.

Method development to make starch Janus particles

In the field of synthetic polymers in the past two or three decades, Janus particles have been produced using five approaches: 2D masking, 3D masking, seeded polymerization, phase separation, and self-assembly of co-block polymers (Fig. I. 2a) (Hu, Zhou, Sun, Fang, & Wu, 2012). In our case, in which our starting material is a solid particle (i.e., starch granule), the most applicable methods are 2D masking and 3D masking.

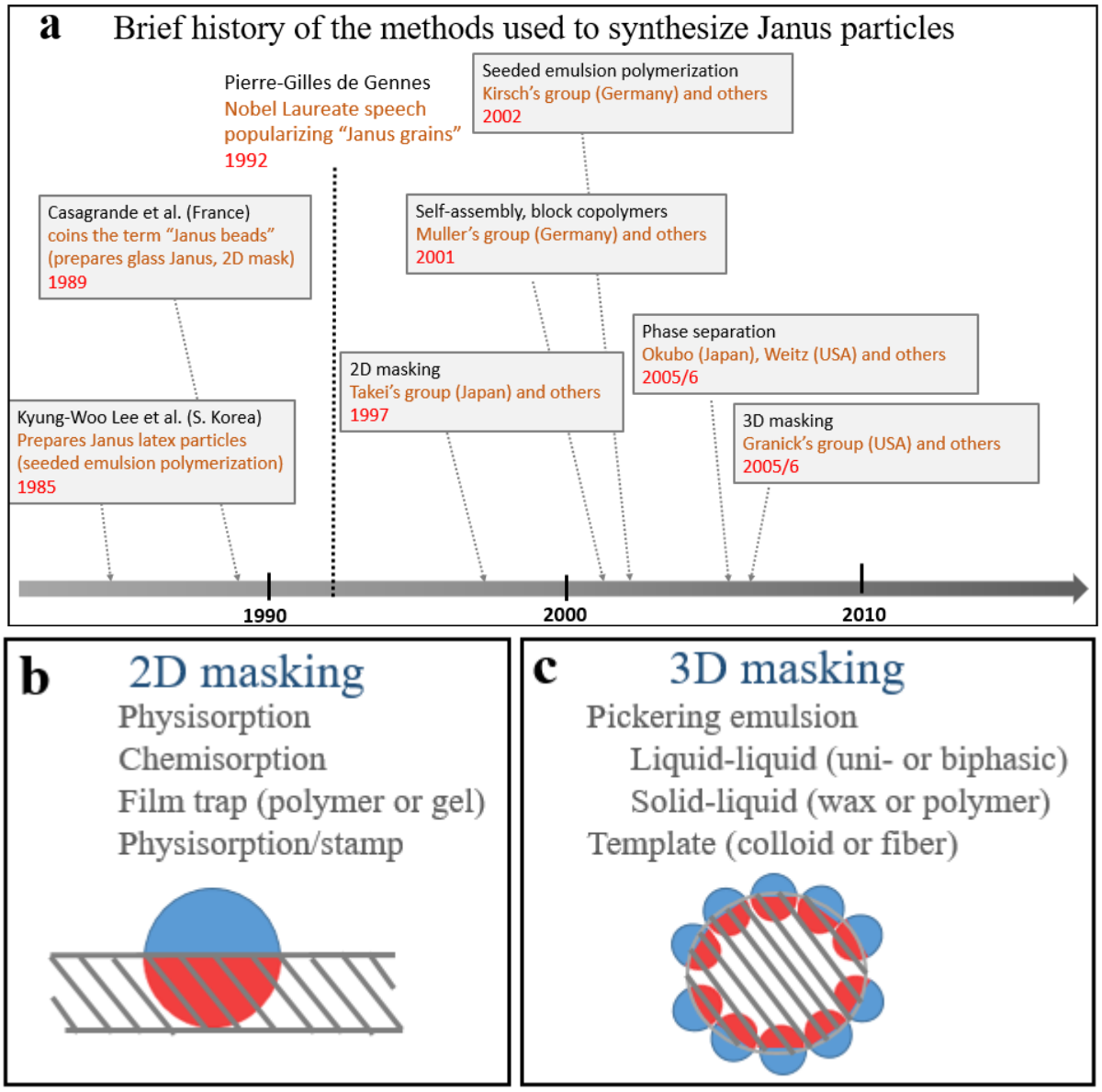

Figure I.2. (a) Brief history of methods used to synthesize Janus particles. Schematic illustration of (b) 2D masking approach, and (c) 3D masking approach to produce Janus particles.

In the 2D masking approach, we mask or trap one side of the particle using essentially a 2D film or a flat substrate, then modify the free or un-trapped half with a reagent (Fig. I.2b) (Takei & Shimizu, 1997). This approach has been shown to produce monodisperse Janus particles but has low yield. In the 3D masking approach, instead of a 2D flat substrate, we use a 3D emulsion droplet substrate to trap our solid particles in what is essentially a Pickering emulsion (Fig. I.2c) (Gu, Yang, Gao, Chang, & Xu, 2005; Hong, Jiang, & Granick, 2006). A Pickering emulsion, by definition, is an emulsion stabilized by solid particles (Bon, 2015; Aveyard, Binks, & Clint, 2003; Timgren, Rayner, Sjoo, & Dejmek, 2011; Yang, et al., 2017). The emulsion droplet can be either an oil, wax, or polymer. This 3D approach has been shown to have a higher yield than the 2D approach, but has problems in preventing the rotation or detachment of the solid particles embedded at the interface, which may lead to polydisperse particles. Using a solid emulsion droplet (wax) rather than a liquid emulsion droplet (oil) has been shown to improve yield (Hong, Jiang, & Granick, 2006).

Overall, the goal of this dissertation is to develop a method to produce starch Janus particles, and to characterize these Janus particles in terms of self-assembly and their texturizing and emulsifying abilities, with an eye to reducing calories or cost and improving processing stability. In Chapter 1, we explored using a 2D approach in a preliminary study to produce Janus particles from starch and studied their self-assembly behavior (Kierulf, et al., 2019). Because the yield was expectedly low, we then explored a 3D approach (using oil or wax). Since the 3D approach depended on the ability of starch to embed at the oil/water or wax/water interface to form Pickering emulsions, in Chapter 2, we first did another preliminary study to optimize starch's emulsifying ability

by increasing its residual protein content (Kierulf, et al., 2020). Then, in Chapter 3, we proceeded to explore the feasibility of employing a scalable 3D masking approach, by using paraffin wax as the emulsion droplet substrate and high-protein amaranth starch as the starting material, and characterized the starch Janus particles produced and assessed their texturizing functionality.

References

Aveyard, R., Binks, B. P., & Clint, J. H. (2003). Emulsions stabilized solely by colloidal particles. *Advances in colloid and interface science, 100-102*, 503-546.

Bon, S. A. (2015). The Phenomenon of Pickering Stabilization: A Basic Introduction. In S. B. To Ngai, *Particle-Stabilized Emulsions and Colloids: Formation and Applications* (p. 1). Cambridge, UK: The Royal Society of Chemistry.

Din, Z.-U., Xiong, H., & Fei, P. (2017). Physical and chemical modification of starches: A review. *Critical Reviews in Food Science and Nutrition, 57*(12), 2691-2705.

Eskandarloo, H., Kierulf, A., & Abbaspourrad, A. (2017). Light-harvesting synthetic nano- and micromotors: a review. *Nanoscale, 9*, 12218–12230.

Gao, F., Li, D., Bi, C.-h., Mao, Z.-h., & Adhikari, B. (2014). Preparation and characterization of starch crosslinked with sodium trimetaphosphate and hydrolyzed by enzymes. *Carbohydrate Polymers , 103*, 310-318.

Gu, H., Yang, Z., Gao, J., Chang, C. K., & Xu, B. (2005). Heterodimers of Nanoparticles: Formation at a Liquid-Liquid Interface and Particle-Specific Surface Modification by Functional Molecules. *Journal of the American Chemical Society, 127*, 34-35.

Hong, L., Jiang, S., & Granick, S. (2006). Simple method to produce Janus colloidal particles in large quantity. *Langmuir , 22*, 9495-99.

Hu, J., Zhou, S., Sun, Y., Fang, X., & Wu, L. (2012). Fabrication,properties and applications of Janus particles. *Chemical Society Reviews, 41*, 4356-4378.

Khlestkin, V., Peltek, S., & Kolchanov, N. (2018). Review of direct chemical and biochemical transformations of starch. *Carbohydrate Polymers, 181*, 460-476.

Kierulf, A., Azizi, M., Eskandarloo, H., Whaley, J., Liu, W., Perez-Herrera, M., . . . Abbaspourrad, A. (2019). Starch-based Janus particles: Proof-of-concept heterogeneous design via a spin-coating spray approach. *Food Hydrocolloids, 91*, 301-310.

Kierulf, A., Whaley, J., Liu, W., Enayati, M., Tan, C., Perez-Herrera, M., . . . Abbaspourrad, A. (2020). Protein content of amaranth and quinoa starch plays a key role in their ability as Pickering emulsifiers. *Food Chemistry, 315*, 126246.

Li, Z.-W., Lu, Z.-Y., Sun, Z.-Y., & An, L.-J. (2012). Model, self-assembly structures, and phase diagram of soft Janus particles. *Soft Matter, 8*, 6693-6697.

Markets and Markets Research Private Ltd. (2015). *"Industrial Starch Market by Type (Native, Starch Derivatives & Sweeteners), Source (Corn, Wheat, Cassava, Potato), Application (Food, Feed, Paper Making & Corrugation, Pharmaceutical), Form (Dry, Liquid), and Region - Global Forecast to 2022.*

Orozco, J., Mercante, L., Pola, R., & Merkoci, A. (2016). Graphene-based Janus micromotors for the drynamic removal of pollutants. *Journal of Materials Chemistry A, 4*, 3371-3378.

Pei, X., Zhai, K., Liang, X., Deng, Y., Xu, K., Tan, Y., . . . Pixin, W. (2018). Fabricaiton of shape-tunable macroparticles by seeded polymerization of styrene using non-crosslinked starch-based seed. *Journal of Colloid and Interface Science, 512*, 600-608.

Poggi, E., & Gohy, J.-F. (2017). Janus particles: from synthesis to application. *Colloid & Polymer Science, 295*, 2083-2108.

Sweedman, M., Tizzotti, M., Schäfer, C., & Gilbert, R. (2013). Structure and physicochemical properties of octenyl succinic anhydride modified. *Carbohydrate Polymers, 92*, 905-920.

Takei, H., & Shimizu, N. (1997). Gradient Sensitive Microscopic Probes Prepared by Gold Evaporation and Chemisorption on Latex Spheres. *Langmuir, 13*(7).

Tanaka, T., Okayama, M., Minami, H., & Okubo, M. (2010). Dual stimuli-responsive "mushroom-like" Janus Polymer particles as Particulate Surfactants. *Langmuir, 26*(14), 11732-11736.

Timgren, A., Rayner, M., Dejmek, P., Marku, D., & Sjoo, M. (2013). Emulsion stabilizing capacity of intact starch granules modified by heat treatment or octenyl succinic anhydride. *Food Science and Nutrition, 1*(2), 157-171.

Timgren, A., Rayner, M., Sjoo, M., & Dejmek, P. (2011). Starch particles for food based Pickering emulsions. *Procedia Food Science , 1*, 95-103.

Wang, F., Pauletti, G., Wang, J., Zhang, J., Ewing, R. W., & Shi, D. (2013). Dual surface-functionalized Janus nanocomposites of polystyrene/Fe3O4@SiO2 for simultaneous tumor cell targeting and stimulus-induced drug release. *Advanced Materials, 25*, 3485-3489.

Wang, H., Lv, J., Jiang, S., Niu, B., Pang, M., & Jiang, S. (2016). Preparation and characterization of porous corn starch and its adsorption toward grape seed proanthocyanidins. *Starch/Starke, 68*, 1254-1263.

Yang, Y., Fang, Z., Chen, X., Zhang, W., Xie, Y., Chen, Y., . . . Yuan, W. (2017). An overview of Pickering emulsions: Solid-particle Materials, Classification, morphology, and applications. *Frontiers in Pharmacology, 8*(287), 1-20.

Zhang, B., Cui, D., Liu, M., Gong, H., Huang, Y., & Han, F. (2012). Corn porous starch: Preparation, characterization, and adsorption property. *International Journal of Biological Macromolecules, 50*, 250-256.

Zhang, J., Grzybowski, B., & Granick, S. (2017). Janus particle synthesis, assembly, application. *Langmuir, 33*, 6964-6977.

Zhu, F. (2017). Encapsulation and delivery of food ingredients using starch based systems. *Food Chemistry, 229*, 542-552.

Zhu, F. (2019). Starch based Pickering emulsions: Fabrication, properties, and applications. *Trends in Food Science & Technology, 85*, 129-137.

OBJECTIVES AND JUSTIFICATIONS FOR THIS RESEARCH

The overall objective of this dissertation is to develop a method via a 2D and 3D mask approach to produce starch Janus particles and to characterize their self-assembly behavior and texturizing properties, with a view to producing better thickening, gelling, and/or emulsifying agents in the food industry that are potentially process-friendly and can potentially reduce calories or cost.

Objective 1: To develop a proof-of-concept 2D mask approach to produce Janus particles from starch with unique self-assembly behavior (Chapter 1)

Justification: Starch modifications in the last 70 years in the food industry via chemical, enzymatic, and physical means, have all been done homogeneously, producing only one-faced particles, but not Janus or two-faced particles. While these homogeneous modifications have made it possible to fine-tune starch's properties, no heterogeneous modifications to produce starch Janus particles in the food industry so far have been performed, so we know very little about their properties or possible applications. Research progress in the area of synthetic polymers in the past three decades have shown, however, that Janus particles made from synthetic polymers exhibit unique self-assembly behaviors, improved surface activity, and many other potential applications. We aim to demonstrate that we can also make Janus particles from starch with similarly unique self-assembly behavior that could lead to improved texturizing abilities in food.

Objective 2: To study the role that protein content plays in starch's Pickering emulsifying ability (Chapter 2)

Justification: Having demonstrated that we can make Janus particles from starch using a 2D mask approach (with low yield), we proceeded to develop a more scalable 3D mask approach via a wax Pickering emulsion method. However, for this method to work, we need to first improve starch's Pickering emulsifying ability by studying the role of its residual protein content. Very little is known in the literature about what makes certain starches more effective than others as Pickering emulsifiers, and this project aims to fill this gap, with a view to developing non-chemically modified plant-based alternative emulsifiers to synthetic or animal-based emulsifiers.

Objective 3: To develop a scalable 3D mask approach to produce Janus particles from starch and assess their texturizing and emulsifying properties (Chapter 3)

Justification: While the 2D approach in Chapter 1 was able to demonstrate that Janus particles made from starch showed promising self-assembly behaviors, low yield prevented further characterization. Development of a scalable 3D method using a wax Pickering emulsion approach, employing high-protein starch with improved emulsifying ability, is therefore needed. Characterization of the starch Janus particles thus produced would be helpful in assessing their improved texturizing abilities in food for potential calorie reduction.

CHAPTER 1

Janus starch particles: Proof-of-concept 2D mask approach via a spin-coating spray method

Abstract

The asymmetric nature of Janus particles made from synthetic polymers gives them intriguing properties that have found applications in a wide variety of fields, such as drug delivery, emulsion stabilization, and environmental decontamination. The potential of using natural biopolymers as base materials for Janus particles in the food industry, however, has not yet been fully explored. Here we demonstrate for the first time the design of a starch-only-based Janus particle. Using a spin-coating spray approach, we produced both large (12.2 μm) half-porous, waxy cornstarch Janus granules by *alpha*-amylase treatment and small (1.2 μm) half-hydrophobic, amaranth starch Janus granules by octenyl succinic anhydride esterification. Optical microscopy, scanning electron microscopy, super resolution-structured illumination spectroscopy, and infrared spectroscopy were used to confirm the binary nature of these particles. A methylene blue adsorption test further showed that the unmodified (non-porous), half-porous Janus, and fully porous waxy cornstarch granules had five-hour adsorption rates of 20.5, 72.1, and 100%, respectively, and adsorption capacities of 0.82, 2.88, and 3.96 mg/g. Meanwhile, unmodified amaranth starch granules were shown not to interact with each other in water, while > 68% of the half-hydrophobic granules self-assembled into wormlike strings and micelles, and > 66% of the fully hydrophobic granules aggregated

into spherical, complex supermicelles. While the low yield typical of Janus particle formation prevents a more detailed characterization of these starch-based Janus particles, the unique properties they displayed here may open exciting, future applications in the food industry as texturants or surface-active agents, as well as in other fields requiring such extraordinary materials.

1. Introduction

"Janus particles"—i.e., solid particles featuring two different faces or sides—were first popularized by Nobel Laureate P.G. de Gennes in the 1990s, largely due to properties that were uniquely different from that of their isotropic or one-faced counterparts (de Gennes, 1992; Zhang, Grzybowski, & Granick, 2017; Hu, Zhou, Sun, Fang, & Wu, 2012). Research progress in this area over the last two decades has produced a variety of distinctly shaped particles made using different methods and designed for different applications. For example, Tanaka *et al.* (2010) used a solvent evaporation approach followed by radical polymerization to produce amphiphilic, mushroom-shaped, synthetic polymer-based particles that could be used to stabilize Pickering oil-in-water emulsions better than homogeneous particles due to their increased surface activity (Poggi & Gohy, 2017; Tanaka, Okayama, Minami, & Okubo, 2010). Orozco *et al.* (2016) sputter-coated a Pt catalyst onto one side of graphene oxide-covered SiO_2 spheres so that the Pt side would generate O_2 bubbles (by catalyzing the decomposition of hydrogen peroxide in water) and self-propel the particles to enable the graphene oxide side to remove organic pollutants more efficiently as the particles moved (Orozco, Mercante, Pola, & Merkoci, 2016; Eskandarloo, Kierulf, &

Abbaspourrad, Nano- and micromotors for cleaning polluted waters: Focused review on pollutant removal mechanisms, 2017; Eskandarloo, Kierulf, & Abbaspourrad, Light-harvesting synthetic nano- and micromotors: a review, 2017). In medicinal research, by using a mini-emulsion and sol-gel reaction, Wang *et al.* (2013) functionalized one side of a polystyrene nanoparticle with folic acid to make it preferentially bind to tumor cells, and then on the other side immobilized the anti-tumor agent doxorubicin for the purpose of targeted release (Wang, et al., 2013; Poggi & Gohy, 2017).

The versatility of synthetic polymers and inorganic materials has made them the main building blocks of Janus particles produced thus far in the fields of materials science and biomedical engineering (Hu, Zhou, Sun, Fang, & Wu, 2012; Groschel, et al., 2012; Bahrami, Groschel, Schmalz, Muller, & Altstadt, 2014; Walther & Muller, 2013). The use of synthetic polymers, however, carries certain financial and environmental burdens, such as their high cost and the need to use environmentally harmful organic solvents, monomers, and reagents during their synthesis. In addition, due to concerns of toxicity and regulatory limits, Janus particles made from synthetic polymers are not easily applicable to other industries, especially the food industry where safety is a main concern, which is a shame given how these Janus particles have been shown to exhibit unique properties depending on their binary design (e.g., surface activity, self-assembly, targeted release, self-propulsion, etc.), which may find surprising applications in the food industry and other fields if pursued. We argue here that these issues can be resolved by replacing synthetic polymers with alternative materials such as naturally occurring biopolymers like starch that are not only very cheap and widely available, but also sustainable, biodegradable, and safe for

consumption (Simkovic, 2008). Thus, exploring the use of naturally occurring biopolymers instead of synthetic polymers in making Janus particles may prove fruitful and open up new applications in industries where Janus particles are not typically used, like in the food industry.

Very little research indeed has been done in this area. The majority of carbohydrate modifications in the last 70 years, for example, via chemical, enzymatic, and physical means, have all been homogeneous, producing only anisotropic or one-faced particles, but not Janus (Khlestkin, Peltek, & Kolchanov, 2018). We are aware of only one starch study that was able to produce cornstarch-polystyrene Janus particles via seeded polymerization. However, they also used a synthetic polymer, did not further study the Janus particles' properties, and did not explore potential applications (Pei, et al., 2018). In the food industry, in particular, we are aware of only one study that tried to produce Janus particles specifically for food applications—silver/chitosan Janus nanoparticles, in particular—which were demonstrated to have long-lasting antimicrobial activity, due in part to the chitosan half preventing the antimicrobial silver components from aggregating with each other, thus better extending food shelf life (Jia, Jiang, Jin, Wang, & Huang, 2015).

The production of Janus particles using only natural biopolymers like starch is thus an open field that remains to be explored. To fill this knowledge gap, we demonstrate in this study a spin-coating spray method to produce starch-only-based Janus particles. Typically, in the past, when starch granules were modified homogeneously, a reagent was simply added to a starch solution, and the solution was mixed until the reaction was complete, producing a homogeneously modified granule.

For example, *alpha*-amylase has been added to starch in this way to increase its overall porosity and improve its adsorptive capacity as an ingredient carrier for food, medicine, and cosmetics (Gao, Li, Bi, Mao, & Adhikari, 2014; Wang, et al., 2016; Zhang, et al., 2012; Zhu, Encapsulation and delivery of food ingredients using starch based systems, 2017). In the same way, octenyl succinic anhydride (OSA) has been added to starch to induce esterification over the granule's entire surface, thus adding hydrophobicity and improving starch's ability as an emulsion stabilizer, encapsulating agent, and thickener (Sweedman, Tizzotti, Schafer, & Gilbert, 2013; Bhosale & Singhal, 2007). If instead of just directly adding a reagent to starch and mixing them, we first fix the starch granules beforehand onto a solid, spin-coated film—such that their bottom halves are trapped in the film and unavailable for modification, while their top halves are free in the air and available for modification—we can then add a reagent to the top (either *alpha*-amylase or OSA, for example) and modify only the top half of each granule to produce a Janus granule.

Using this spin-coating spray approach, we aimed to produce two different starch-only-based Janus particles: 1) half-porous waxy cornstarch Janus granules (i.e., with one side porous due to *alpha*-amylase treatment, and the other side unmodified and non-porous) and 2) half-hydrophobic amaranth starch Janus granules (i.e., with one side hydrophobic due to OSA treatment, and the other side unmodified and hydrophilic). We used large waxy cornstarch granules for *alpha*-amylase treatment because their large size (12.2 μm diameter) and their low resistance to enzyme treatment made it easier to visually verify whether a Janus granule was indeed produced, i.e., that one side of a granule was made porous but the other side was not. After showing that the spin-coating

spray approach worked for enzyme treatment, we then proceeded to show that it could also work for OSA treatment. This time we chose to use small amaranth starch granules (1.2 μm diameter) for OSA treatment to demonstrate that the spin-coating spray approach can be applied to different size granules, and because the small size of amaranth granules, after we attach hydrophobic OSA groups to them, may lend themselves better to self-assembly than larger granules, making it easier to detect differences in self-assembly behavior between granules with an entirely hydrophobic surface vs. granules with only one side hydrophobic.

We verified the binary nature of these micron-size Janus granules by optical microscopy, scanning electron microscopy, super resolution-structured illumination spectroscopy, and infrared spectroscopy. A methylene blue adsorption test was also used to differentiate between the fully porous and the half-porous waxy cornstarch Janus granules, while the difference between the fully hydrophobic and the half-hydrophobic amaranth Janus granules was investigated through their self-assembly behavior in water. As far as we know, this is the first time that Janus particles made only from starch has been produced, and the first time that a Janus particle made only from a natural biopolymer has been shown to exhibit amphiphilicity and self-assembly behavior similar to that of synthetic-polymer-based Janus particles. While the low yield of the spin-coating spray method prevents a more detailed characterization of these particles, we expect that the amphiphilicity already exhibited by these starch-based Janus particles may improve starch's ability to stabilize emulsions, and that their unique self-assembly behavior could impart new textures in food. Further research into natural biopolymer-based Janus particles, however, is needed, and likewise an exploration of other more

scalable approaches for production. We expect that making these advanced functional materials from natural ingredients may open up exciting new applications not only in the food industry as texturants or surface-active agents but in other fields as well.

2. Materials and Methods

2.1 Materials

Waxy cornstarch was provided by Tate & Lyle Ingredients Americas LLC (Hoffman Estates, IL, USA). Amaranth starch was isolated from commercially available amaranth grains (see section 2.2 for isolation method). Termamyl SC (*alpha*-amylase, 134 U/g) was purchased from Novozymes (Bagsvaerd, Denmark). *n*-Octenyl succinic anhydride (OSA) was provided by Dixie Chemical Company (Pasadena, Texas, USA). Lauric acid and Nile Red (microscopy-grade fluorescent dye) were obtained from Sigma-Aldrich Chemical Co. (St. Louis, MO, USA). Sylgard 184 (polydimethylsiloxane, PDMS) was obtained from Dow Corning Corporation (Midland, MI, USA). 100-mm low-density polyethylene (LDPE) petri dishes were purchased from Gosselin (Corning). All other chemicals used were reagent grade and purchased from Sigma-Aldrich Chemical Co.

2.2 Isolation of amaranth starch from grains

We isolated starch from amaranth grains using an alkaline steeping method modified from Xia *et al* (Xia, et al., 2015). The grains were first soaked in 0.25% NaOH for 24 h at a ratio of 1:6 w/w grain:solution. They were then washed thoroughly with water to remove NaOH and ground using a kitchen blender at high speed for 2 min. The slurry was filtered stepwise for 15 min using a laboratory test sieve vibrator (Derrick

Mfg. Co., Buffalo, NY, USA) with 80-mesh (180 µm), 200-mesh (75 µm), and 270-mesh (53 µm) sieves. The remaining residue was re-blended and re-filtered twice. The pooled, liquid filtrate was centrifuged at 5000 g for 10 min and the supernatant discarded. The starch pellet formed at the bottom had a yellow top layer (protein) that was then removed using a spatula. The starch pellet was then further washed with deionized water, ethanol, and deionized water, successively, each time scraping off the top yellow layer after centrifugation. The isolated amaranth starch was then freeze-dried for 24 h and ground ultra-fine using a conical burr grinder. The yield was approximately 30%.

2.3 Particle size analysis

Waxy corn starch and amaranth starch (both in their native forms before any treatment) were dispersed in water separately on a microscope slide and five random images were taken using a Leica Model DMIL LED Inverted Phase Contrast Microscope at 20x and 100x, respectively. ImageJ 1.51w software was used to measure the diameter of 200+ granules of each starch sample. The corresponding volume mean diameter (d_{43}) and polydispersity index (PDI) were computed as follows:

$$d_{43} = \frac{\sum di^4}{\sum di^3} \quad (1.1)$$

$$\text{PDI} = \frac{d_{43}}{\sum di/N} \quad (1.2)$$

in which d_i is the diameter of one granule and N is the total number of granules (Bechtel, Zayas, Kaleikau, & Pomeranz, 1990; McClements, 2016).

2.4 Spin-coating spray approach for making half-porous, waxy cornstarch Janus granules

Melted lauric acid (0.5 mL) was pipetted onto a 100-mm petri dish preheated beforehand to ~ 60 °C, then spin-coated at 6100 rpm for 50 s to form a ~5 μm-thick film (Fig. 1.1, steps i-v, option a). After cooling, the petri dish was placed on a hot plate at 50 ºC to re-melt the lauric acid film, then waxy cornstarch granules (12.2 μm in diameter) were sprayed onto the film using an air gun. With the starch granules half-submerged in the lauric acid film, the other free half was then modified with 3.3 U/mL *alpha*-amylase in a pH 6 buffer (0.1 M citric acid-sodium citrate) for 6 h at room temperature, lightly shaking the petri dish using an orbital shaker. The enzyme treatment conditions used (enzyme type, pH, and reaction time) were based on preliminary trials that we conducted, which in turn were based on several optimization studies (Benavent-Gil & Rosell, 2017; Dura, Blaszczak, & Rosell, 2014). After this enzyme treatment, the petri dish was washed 3-times with deionized water. The film, together with the modified granules, were then dissolved in isopropyl alcohol, washed 3-times again with deionized water (centrifuging at 5000 g for 10 min each time), then dried. The yield was <1 mg starch/petri dish. A control (fully porous waxy cornstarch) was prepared by mixing unbound waxy cornstarch granules (1:5 w/v) with the same *alpha*-amylase solution for 6h at room temperature and then washing and drying in the same manner as previously described.

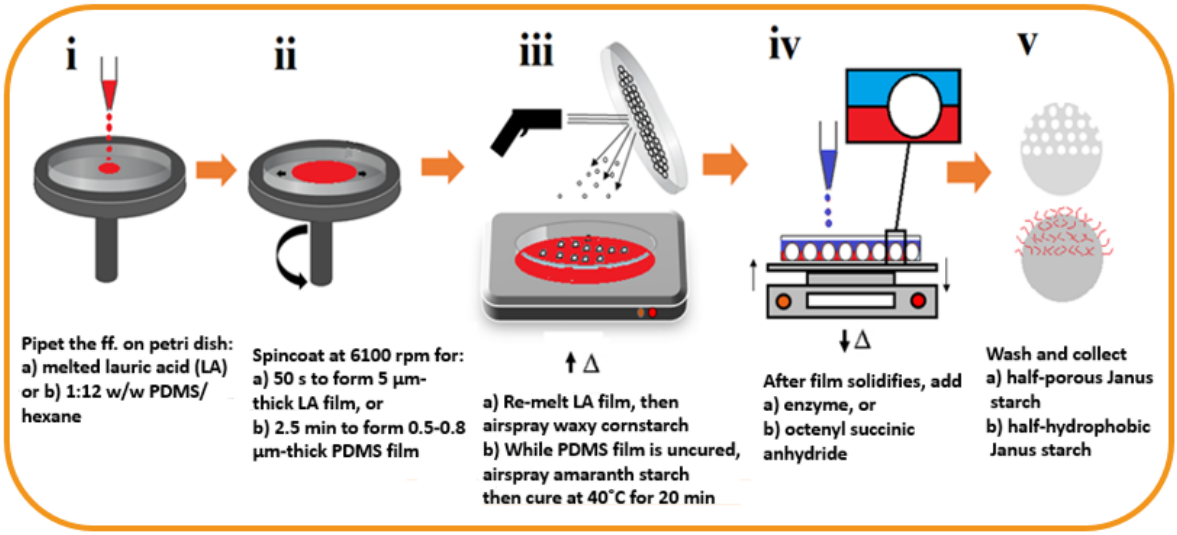

Fig. 1.1. Schematic illustration of the spin-coating spray approach (steps i-v) to produce Janus particles. (a) Steps to produce the half-porous waxy cornstarch Janus granules**;** (b) Steps to produce the half-hydrophobic amaranth starch Janus granules.

2.5 Spin-coating spray approach for making half-hydrophobic, amaranth starch Janus granules

An ultrathin PDMS film was first made based on a method from Thangawng *et al* (Thangawng, Ruoff, Swartz, & Glucksberg, 2007). A 1:12 w/w uncured PDMS:hexane solution (1 mL) was pipetted onto a 100-mm petri dish, then spin-coated at 6100 rpm for 2.5 min to form a ~0.5–0.8 µm-thick film (Fig. 1.1, steps i-v, option b). Amaranth starch granules (1.2 µm in diameter) were then sprayed onto the film using an air gun. The PDMS film, now containing half-submerged granules, was cured at 40 ºC inside an oven for 20 min and left overnight at room temperature. With the starch granules half-submerged in the cross-linked film, the free half was then modified with OSA. The conditions used here for OSA treatment (pH, concentration, and reaction time) were based on preliminary trials we conducted, which in turn were based on

several optimization studies (Hui, Qi-he, Ming-liang, Qiong, & Guo-qing, 2009; Abiddin, Yusoff, & Ahmad, 2015). OSA treatment was performed using the following steps: First, 15 mL of a pH 8–8.5 solution of NaOH was added to the petri dish and slowly mixed on an orbital shaker for 15 min. Next, 15 mL of a 3% OSA aqueous solution was added and allowed to slowly mix and react for another 15 min. The solution inside the petri dish was then decanted out, and a fresh 15 mL of NaOH solution of pH 8–8.5 was added to lightly wash the petri dish, followed by the addition of 15 mL of 3% OSA solution again. This procedure of NaOH-then-OSA addition was repeated for 3 h total (or 6 repetitions). After the treatment, the granules, together with the PDMS film were dislodged using hexane and water. The granules were then separated by centrifugation at 10,000 g for 5 min, followed by removing the top hexane/PDMS layer. The starch was then washed with ethanol and water twice, centrifuged, and dried overnight in an oven at 40 ºC. The yield was < 0.1 mg starch/petri dish. A control (fully hydrophobic amaranth starch) was prepared by mixing unbound amaranth starch granules (1:5 w/v) sequentially with NaOH then OSA solutions in the same manner as previously described.

2.6 Optical microscopy & scanning electron microscopy (SEM)

The lauric acid film formed on the petri dish in section 2.4 was imaged using a digital camera and an Olympus BX51 microscope (MA, USA). For better focus, a segment of the lauric acid film (with the waxy cornstarch granules submerged) was scraped off from the petri dish using a blade and mounted on an SEM stub with conductive carbon tape. The sample was then sputter-coated with gold and examined

using a JCM-6000 Benchtop SEM (JEOL Ltd., Japan) at an accelerating voltage of 15 kV using a secondary electron detector.

Due to the difficulty of scraping off the ultrathin PDMS film (with the amaranth starch granules submerged) from the petri dish produced in section 2.5, a 12-mm-diameter circular section of the petri dish was cut off entirely and mounted on an SEM stub with conductive tape, sputter-coated with gold, and examined under SEM with the same conditions as above.

2.7 Super resolution-structured illumination microscopy (SR-SIM)

While the SEM can show differences between a half-porous Janus and a fully porous waxy cornstarch granule, it cannot show a difference between a half-hydrophobic Janus and a fully hydrophobic amaranth starch granule. For this purpose, SR-SIM was used to image the amaranth starch granules modified with OSA in section 2.5. A Nile Red solution in hexane was added to the half-hydrophobic Janus granules, and vortexed for 1 min. Water was added to the mixture, then shaken upside-down by hand several times. The hexane-water mixture was allowed to separate, enabling the Janus granules to settle to the bottom. Once settled, the Nile Red-treated Janus granules were pipetted onto a glass slide and covered with a 0.15-mm-thick cover slip. The sample was then observed under a Zeiss Elyra Super Resolution Microscope with Structured Illumination (SR-SIM), using a 63x/1.4 Plan-Apochromat oil objective and 561 nm excitation. The same was done to the control.

2.8 Attenuated total reflectance-Fourier transform infrared spectroscopy (ATR-FTIR)

The FTIR spectra of the unmodified, half-hydrophobic Janus, and fully hydrophobic amaranth starch granules were obtained using an ATR-FTIR Shimadzu Affinity-1S, in order to detect ester and carboxylate peaks due to reaction with OSA. The 400–4000 cm^{-1} region was scanned in transmittance mode with 2 cm^{-1} resolution and 120 scans. FTIR was not performed on the unmodified, half-porous Janus, and fully porous waxy cornstarch granules because *alpha*-amylase treatment only creates pores and does not attach any functional groups that may have distinct absorption bands.

2.9 Methylene blue adsorption study of the half-porous Janus and fully porous waxy cornstarch granules

The adsorption of methylene blue, as a model organic pollutant, by the unmodified (non-porous), half-porous Janus, and fully porous waxy cornstarch granules were tested to study their absorption capabilities, and, by extension, their porosity. Fifty milligrams each of the unmodified, half-porous Janus, and fully porous waxy cornstarch granules were added to a 10 mL aqueous solution of methylene blue (20 mg L^{-1}). The mixed solution was then shaken at 25 °C. At selected times, we removed a 100 µL sample from the aqueous solution using a syringe filter and estimated the methylene blue concentration in the supernatant by measuring the absorbance changes at 663 nm on a SpectraMax iD3 Multi-Mode Microplate Reader (Molecular Devices; Sunnyvale, CA). A standard curve plotting absorbance *vs.* concentration of methylene blue was made. The concentration of methylene blue in solution was estimated from the standard

curve. The adsorption rate (%) and adsorption capacity (mg/g) of the samples were calculated in duplicate from the following equations:

$$Adsorption\ rate\ (\%) = \frac{C_0 - C_t}{C_0} \times 100 \qquad (1.3)$$

$$q_e = \frac{(C_0 - C_t) \times V}{m} \qquad (1.4)$$

in which q_e is the amount of methylene blue adsorbed per unit weight of the adsorbents (mg/g), C_0 and C_e are the initial and residual concentrations of methylene blue, respectively, V is the volume of the methylene blue aqueous solution (L), and m is the weight of the adsorbent (g).

2.10 Self-assembly of half-hydrophobic Janus and fully hydrophobic amaranth starch granules

The unmodified, half-hydrophobic Janus, and fully hydrophobic amaranth starch granules were sonicated in an ultrasonic bath at neutral pH for 5–10 min, then pipetted onto a cover slip. Their self-assembly behavior was observed under a Leica Model DMIL LED Inverted Phase Contrast Microscope at 100x magnification.

To estimate the size distribution of the aggregates formed, the cross-sectional area of each discrete element (e.g., both one separate granule and one aggregate of granules would be considered just one discrete element) was measured using ImageJ 1.51w. The discrete elements were divided into five categories, defined here as: a) no aggregates (i.e., separate granules), b) 2- or 3-granule clusters, c) wormlike strings (11–

50 μm^2), d) wormlike strings or micelles (51–100 μm^2), and e) supermicelles (> 100 μm^2, roughly spherical in shape). Once the discrete elements were categorized, their subgroup total area was computed and divided by the overall total area. This gives an estimate of the size distribution of the self-assembled aggregates. Two replicates were performed for each sample. For each replicate, the samples were sonicated, pipetted onto a microscope slide, and three images were taken to measure a total of about 200+ discrete elements to estimate the size distribution.

3. Results and Discussion

3.1 Particle size analysis

Using ImageJ software, the unmodified waxy cornstarch and unmodified amaranth starch granules were found to have volume mean diameters (d_{43}) of 12.2 µm (PDI = 1.45) and 1.2 µm (PDI=1.16), respectively, which are consistent with the literature in which other techniques were used to characterize the size distribution, such as dynamic light scattering (Xia, et al., 2015; Zhu, Structures, physicochemical properties, and applications of amaranth starch, 2017; Qiu, Yang, Ge, Chang, & Xiong, 2016).

3.2 Lauric acid film and formation of half-porous waxy cornstarch Janus granules

Lauric acid was chosen to create the film in which the waxy cornstarch granules were embedded because it is an inexpensive, non-toxic, 12-carbon saturated fatty acid that can be easily melted for the purposes of spin-coating a film (lauric acid's melting point is low at 43.2ºC). Meanwhile, it solidifies at room temperature due to van der

Waals forces between its long fatty acid chains, enabling it to hold starch granules while further enzymatic treatment is performed at room temperature. *Alpha*-amylase modification—a treatment used to impart an adsorption/encapsulation/carrier functionality to starch—was the treatment of choice because 1) *alpha*-amylase creates pores in the granule that can easily be observed under SEM, which allowed us to quickly confirm the reaction, and 2) *alpha*-amylase, compared to other enzymes, is more efficient at creating numerous pin-hole sized pores (~0.15 μm diameter), (Benavent-Gil & Rosell, 2017; Dura, Blaszczak, & Rosell, 2014) which makes them again easy to observe under SEM but not large enough to break the granules apart. The choice of waxy cornstarch was based on the fact that among corn starches of different amylose contents, it appears to be the least resistant to enzyme treatment based on preliminary tests we conducted (data not shown).

After the lauric acid was melted and pipetted onto a preheated petri dish and spin-coated at 6100 rpm for 50 s, centrifugal forces push it radially outwards to form a thin film. This thin film solidifies very quickly and must be melted again at 50 ºC before the waxy cornstarch granules (12.2 μm diameter) can be sprayed onto it and become half-submerged (Fig. 1.2a). After cooling, the surface of the film, as seen under a microscope (Fig. 1.2b), displays wrinkles that are perpendicular to the direction of the centrifugal force. These wrinkles could be due to some segments of the lauric acid prematurely solidifying during the spin-coating process and being pushed radially outward, causing them to bunch up. Figure 1.2d shows an SEM image of the scraped film, with the bottom part of the image showing some granules half-submerged in it, and the top part showing the film curving up, allowing us to approximate the thickness

to be ~5μm. Figure 1.2c (optical microscope) shows a top view of starch granules half-submerged within the film, with the other half above the surface, available for treatment. Figure 1.2e (SEM) shows two starch granules half-submerged in the film.

Corn starch granules, before any treatment, tend to have relatively smooth surfaces (Fig. 1.2g), but they are known to already have very small channels/pores (~7–100 nm) that run from their surfaces down to their central hylum or core. Upon treatment with *alpha*-amylase, which is 3–4 nm in size, the enzyme seeps into these pores and randomly hydrolyzes the (1→4)-α-glycosidic bonds along the starch chain, thus widening the channels/pores and making the granule more porous (Dhital, Warren, Butterworth, Ellis, & Gidley, 2017). If unbound waxy corn starch is modified with *alpha*-amylase homogeneously, the granule becomes fully porous (Fig. 1.2h). However, if only half of the granule is modified with *alpha*-amylase because the other half is submerged in a lauric acid film, then only the half of the granule that is exposed becomes porous (Figs. 1.2f,i). These results show that the spin-coating spray approach with enzyme treatment does indeed produce half-porous waxy cornstarch Janus granules.

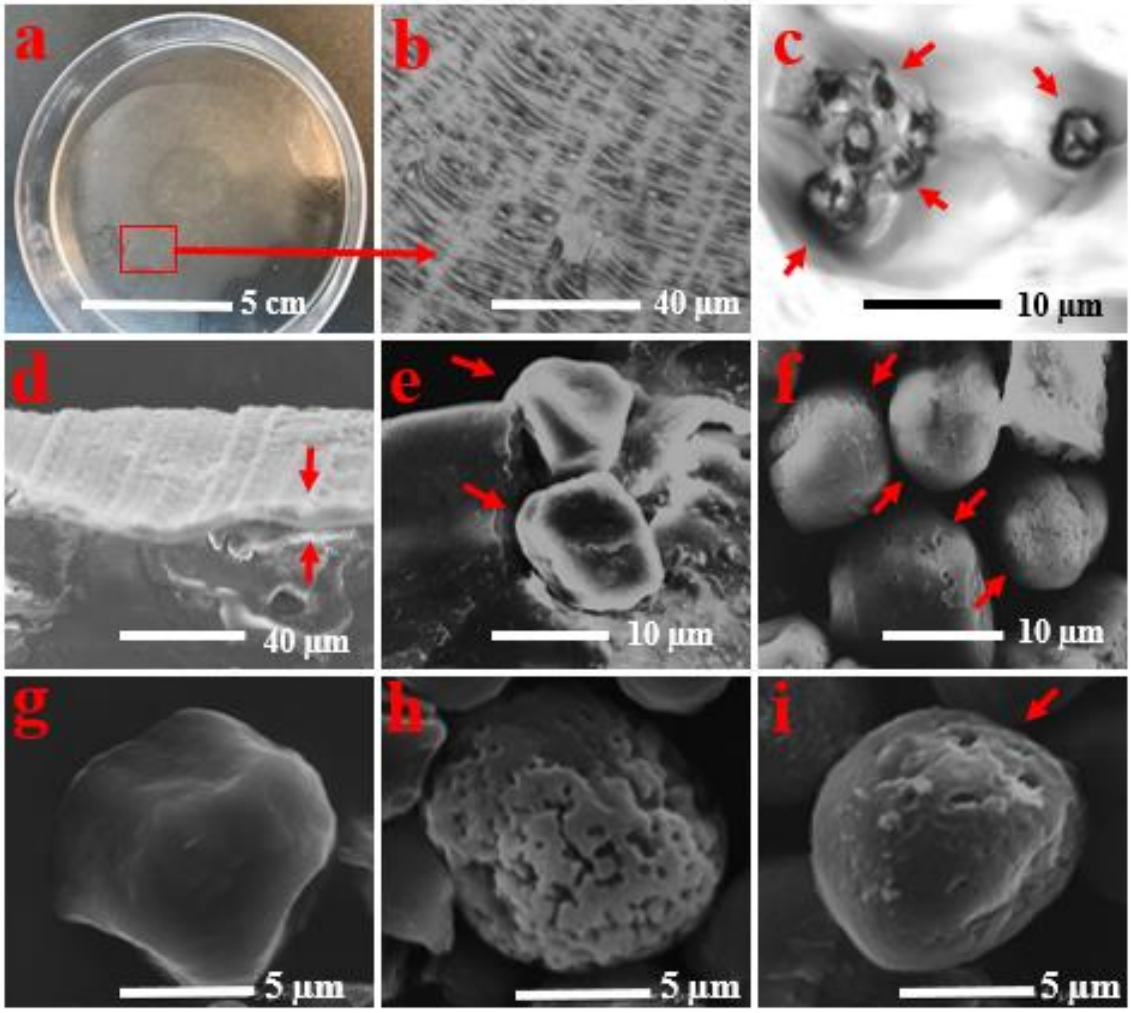

Fig. 1.2. (a) Digital camera image of a lauric acid film in a petri dish after spraying waxy corn starch; (b) microscope image at 20x magnification of the lauric acid film, demonstrating its surface roughness; (c) and at 100x showing the half-submerged waxy cornstarch ; (d) SEM image of a scraped-off lauric acid film, with the bottom part showing some granules half-submerged, and the top part showing the film curving up to show ~5 µm thickness; (e) SEM image of half-submerged waxy cornstarch in lauric acid film (e); (f) and half-porous waxy cornstarch Janus granules after enzyme treatment and collection; a comparison between an (g) unmodified, (h) fully porous, and (i) half-porous waxy cornstarch Janus granule made using the spin-coating spray approach.

3.3 PDMS film and formation of half-hydrophobic amaranth starch granules

The same spin-coating spray approach was also used to perform another common starch modification technique—esterification using OSA. At basic conditions, alcoholate ions are formed on the starch granule surface, which act as nucleophiles that attack OSA's anhydride moiety, resulting in the attachment of a hydrophobic octenyl group via an ester bond (Hui, Qi-he, Ming-liang, Qiong, & Guo-qing, 2009). This imparts an amphiphilic nature to the starch and improves its emulsification properties. For this part of the study, we performed OSA treatment on smaller amaranth granules (1.2 μm) instead of large waxy cornstarch (12.2 μm) in order to show that 1) the spin-coating spray approach is tunable—by changing the film thickness, we can also change the particle size, or even the amount of patch we want our Janus granule to have (i.e., the surface proportion of the particle we want to be hydrophobic); and 2) a small hydrophobic octenyl group attached to a small granule will have a greater effect on its added hydrophobicity than if it were attached to a bigger granule, due to the larger size difference. This should make it easier to distinguish any differences in self-assembly behaviors between half-hydrophobic and fully hydrophobic granules.

Based on preliminary tests, however, lauric acid dissolves at the basic conditions required for OSA treatment, and so a switch was made to use PDMS for the film, which is resistant to basic conditions after curing. PDMS is a common material used in making thin membrane devices, but by itself cannot form a film thinner than 3 μm by spin-coating (Thangawng, Ruoff, Swartz, & Glucksberg, 2007). Because amaranth starch granules are 1.2 μm in diameter, an ultrathin PDMS film of about 0.6 μm thick is necessary to just halfway submerge the material. A 1:12 ratio of PDMS to hexane during

the spin-coating process serves this purpose, lowering the viscosity of the PDMS enough to allow it to be dispersed more thinly, forming a ~0.5–0.8 μm-thick film (Fig. 1.3a). Once the PDMS film was spin-coated, the amaranth starch granules were then sprayed onto the surface, causing them to be half-submerged within the polymer (Fig. 1.3b).

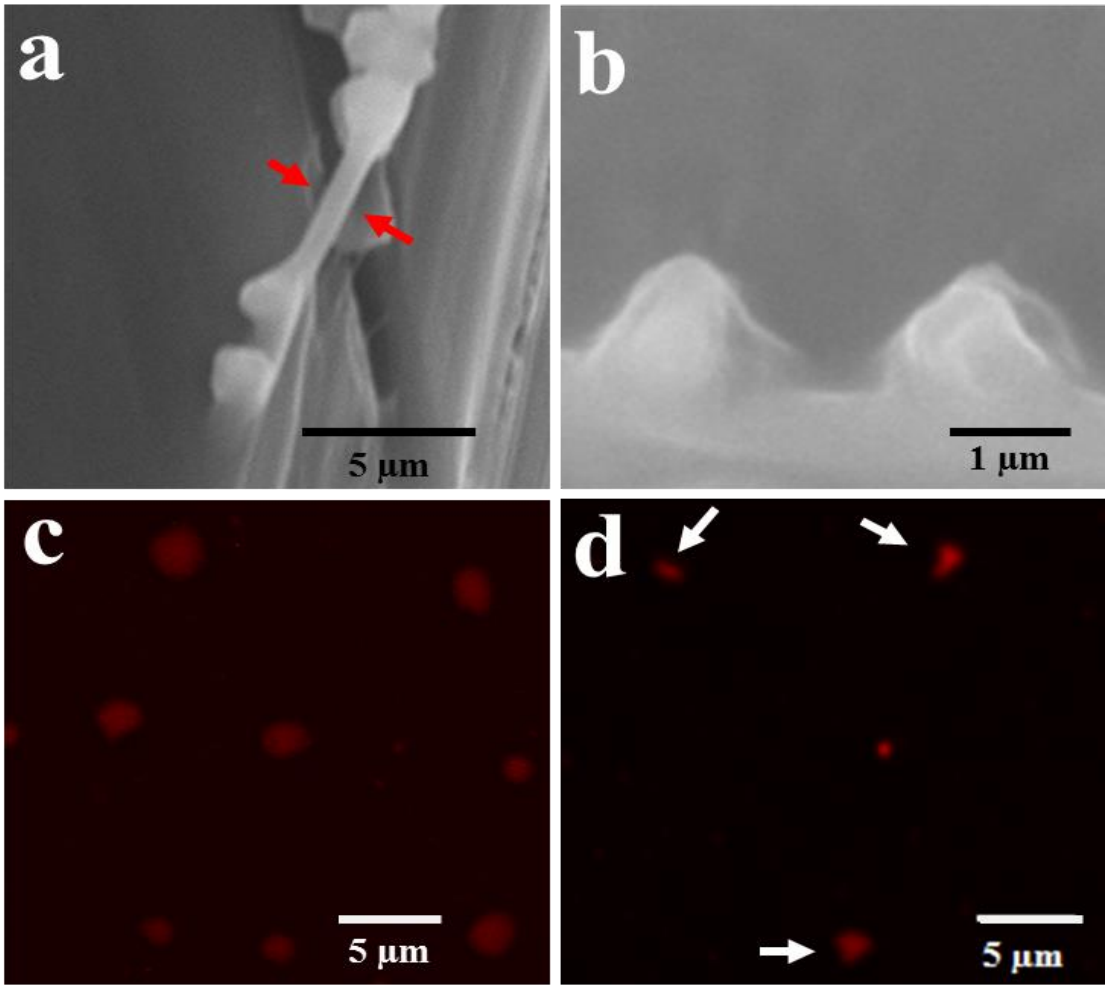

Fig. 1.3. (a) SEM images of a ~0.5–0.8-μm-thick PDMS film and (b) amaranth starch granules half-submerged in the PDMS film (b); (c) SR-SIM images of amaranth starch colored with hydrophobic Red Nile dye after OSA treatment, showing red spheres (fully hydrophobic) for the control and (d) red half-spheres or red crescents for the half-hydrophobic amaranth Janus granules made using the spin-coating spray approach.

After curing, the free half of the submerged granules was modified with OSA to produce half-hydrophobic amaranth Janus granules. To confirm the difference between the fully-hydrophobic control—made by mixing unbound granules with OSA—vs. the half-hydrophobic Janus granules, both were treated with a hydrophobic Nile Red dye. It was expected that the control granule's surface would be fully covered by the red dye due to hydrophobic interactions and appear as red spheres under SR-SIM, and this was indeed the case (Fig. 1.3c). On the other hand, the half-hydrophobic Janus granules appeared as red half-spheres or red crescents (indicating amphiphilicity), depending on the angle from which they were observed (Fig. 1.3d). This result confirms that the spin-coating spray approach via OSA treatment produces half-hydrophobic amaranth starch Janus granules.

3.4 Adsorption study of half-porous Janus and fully porous waxy cornstarch granules

A porous structure provides a larger specific surface area and larger surface-to-volume ratio compared to a less porous or non-porous structure (Ai, Yue, & Jiang, 2012; Yamada, Kayama, Saito, & Hara, 1986). Thus, the porosity of a material is proportional to its adsorptive capacity. Studies have shown that the adsorption mechanism between starch and methylene blue at neutral pH is a typical physical adsorption, which may be due to a combination of van der Waals forces, hydrogen bonding, and π-stacking between the starch pyranose rings and the methylene blue rings (Guo, Li, Liu, Meng, & Tang, 2013; Asensio, Arda, Canada, & Jimenez-Barbero, 2013; Eltaboni, Imragaa, Edbey, & Mousa, 2015; Bertolini, 2009).

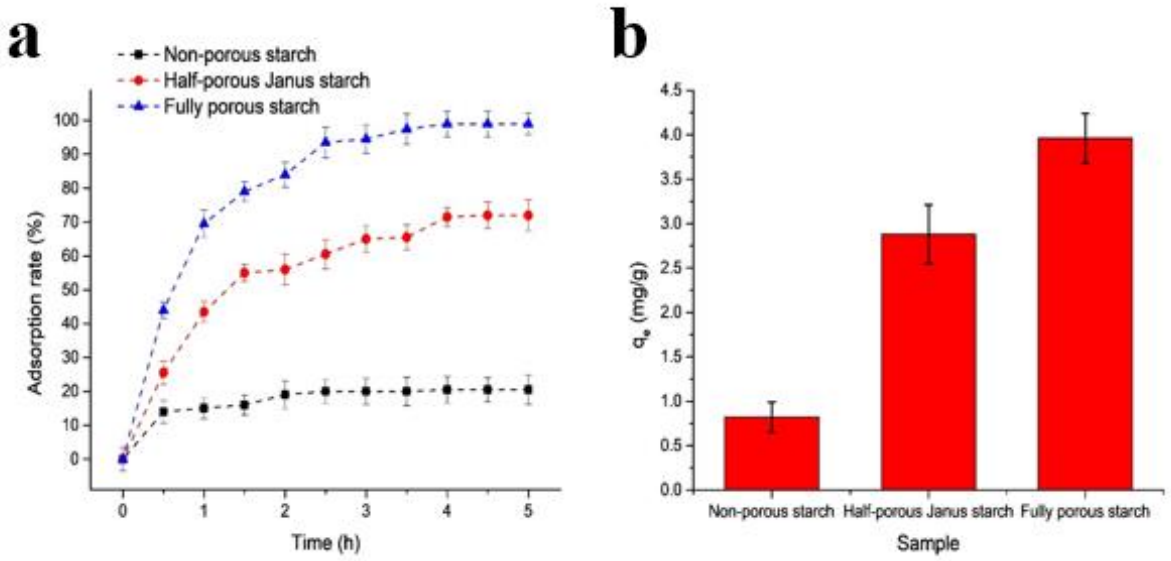

Fig. 1.4. (a) Adsorption rate (%) of methylene blue for the waxy cornstarch samples of different porosities as a function of time. (b) Adsorption capacity (q_e, mg/g) for methylene blue of the waxy cornstarch samples of different porosities.

The waxy cornstarch samples, including unmodified (non-porous), Janus (half-porous), and fully porous (control), were added to aqueous solutions of methylene blue. The concentration of methylene blue in the solution was then monitored over time. Figure 1.4a shows the adsorption rate (%) of methylene blue as a function of time, and Figure 1.4b shows the equilibrium adsorption capacity (q_e, mg/g) after 5 h. The unmodified starch (non-porous) showed a very low adsorption rate (20.5%) towards methylene blue, which is due to its low surface-to-volume ratio providing few available reactive sites for adsorption. The adsorption efficiency of the fully porous starch (control), both in terms of the adsorption rate and the amount of methylene blue adsorbed per unit weight of the samples (*i.e.*, the adsorption capacity) was higher than the half-porous Janus starch. Methylene blue was completely removed after 5 h by the fully porous starch, while only 72.1% of methylene blue was adsorbed by the half-

porous Janus starch. The higher adsorption efficiency of fully porous starch could be due to its higher surface-to-volume ratio, which provides more available reactive sites for adsorption. The adsorption capacity for the non-porous, half-porous Janus, and fully porous starch samples after 5 h were 0.82, 2.88, and 3.96 mg/g, respectively. These results indicate that the Janus granules produced by the spin-coating spray approach have a porosity midway between the non-porous and fully porous starch.

3.5 Verification of OSA modification by ATR-FTIR Spectroscopy

The ATR-FTIR spectra of the unmodified, half-hydrophobic Janus, and fully hydrophobic amaranth starch granules are shown in Figure 1.5. For the unmodified starch, we observed the following characteristic bands that have been assigned to starch from the literature: a broad peak at 3400 cm^{-1} corresponding to O-H vibration; 2915 cm^{-1} for C-H stretching vibration; 1640 cm^{-1} for adsorbed water bending vibration; peaks at 1360–1420 cm^{-1} for C-H deformation; and the fingerprint region at 1000–1200 cm^{-1} for C-O stretching (Ye, et al., 2014). For the half-hydrophobic Janus starch granules—i.e., the granules whose one side was modified with OSA—a small peak (shoulder) appears at 1715 cm^{-1}, which can be attributed to the C=O stretching vibration of the ester peak formed during OSA reaction. Another small peak that appears at 1552 cm^{-1} confirms that the OSA group was indeed attached, because the asymmetric stretching vibration of its carboxylate group is present. For the fully hydrophobic starch granules—i.e., the granules homogeneously modified by OSA over its entire surface—the same peaks at 1715 and 1552 cm^{-1} appear, consistent with the literature (Ye, et al., 2014; Miao, et al., 2014). The peak at 1715 cm^{-1}, in particular, has a higher intensity for the

fully hydrophobic starch than the half-hydrophobic Janus starch, suggesting a higher degree of substitution due to the homogeneous distribution of the OSA group attached to the entire starch granule. This result supports the idea that the half-hydrophobic Janus granules produced via the spin-coating spray approach have a lower number of octenyl groups attached than the fully hydrophobic granules, suggesting that the material is less hydrophobic, which is consistent with Figure 1.3d demonstrating that only crescent- or half-shaped sections of these granules could be dyed by the hydrophobic Nile Red solution.

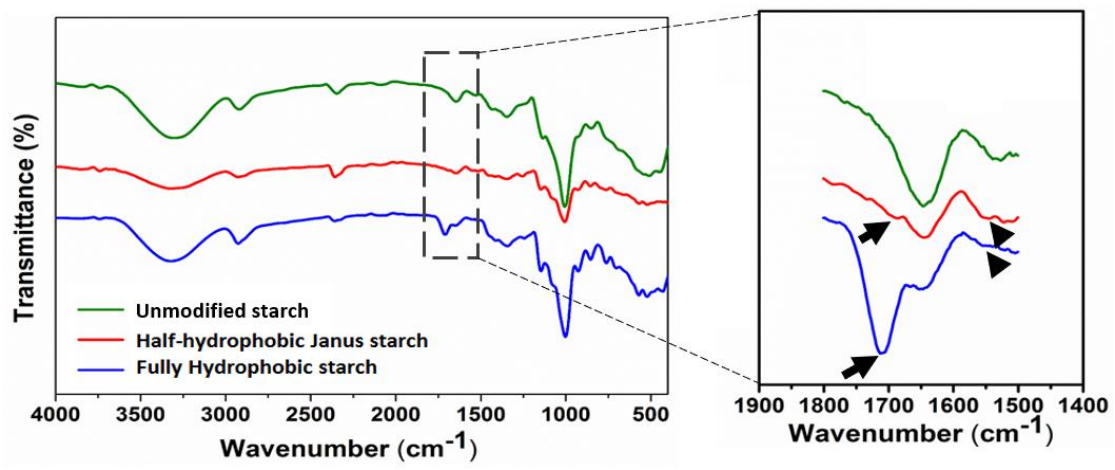

Fig. 1.5. ATR-FTIR Spectra of unmodified, half-hydrophobic Janus, and fully hydrophobic amaranth starch.

3.6 Self-assembly of half-hydrophobic Janus vs. fully hydrophobic amaranth starch

Modeling studies have shown that Janus particles, depending on the nature of their Janus balance (e.g., ~50/50, 60/40, 90/10 hydrophobic/hydrophilic) and their resultant attractive/repulsive forces (among other factors), can self-assemble into different superstructures in dilute solutions (Li, Lu, Sun, & An, 2012; Poggi & Gohy,

2017). In this study, unmodified amaranth starch granules in water appear as separate granules due to a lack of attraction between them (Figs. 1.6a-c). The control (fully hydrophobic granules), on the other hand, formed large aggregates in water (Figs. 1.6d-f) due to the strong hydrophobic attraction. There is some agreement between this result and a modeling study conducted by Zhan-Wei Li *et al.* that showed that particles that are fully or nearly-fully hydrophobic on their surface (> 88%) indeed form "complex supermicelles" or large, spherical aggregates (see inset photo of Fig. 1.6f) (Li, Lu, Sun, & An, 2012).

Incidentally, this result also sheds new light on another aspect of fully hydrophobic OSA-modified starch—its increased viscosity (Sweedman, Tizzotti, Schafer, & Gilbert, 2013; Bhosale & Singhal, 2007; Hui, Qi-he, Ming-liang, Qiong, & Guo-qing, 2009; Altuna, Herrera, & Foresti, 2018; Ovando-Martinez, Whitney, Ozsisli, & Simsek, 2017). Typically, when starch is modified homogeneously or fully with OSA, its peak pasting viscosity in water increases, which the literature explains by stating that the bulky octenyl group attached by OSA disrupts the intermolecular hydrogen bonding between glucose chains through steric hindrance, thus weakening the granule's internal structure and allowing more water to penetrate, which in turn makes the granule swell and results in a 2–4-times increase in viscosity (Sweedman, Tizzotti, Schafer, & Gilbert, 2013; Bhosale & Singhal, 2007; Hui, Qi-he, Ming-liang, Qiong, & Guo-qing, 2009; Altuna, Herrera, & Foresti, 2018; Ovando-Martinez, Whitney, Ozsisli, & Simsek, 2017). However, it is possible that the observed self-assembly of the fully hydrophobic (fully OSA-modified) starch into supermicelles is another, additional explanation for the increased viscosity.

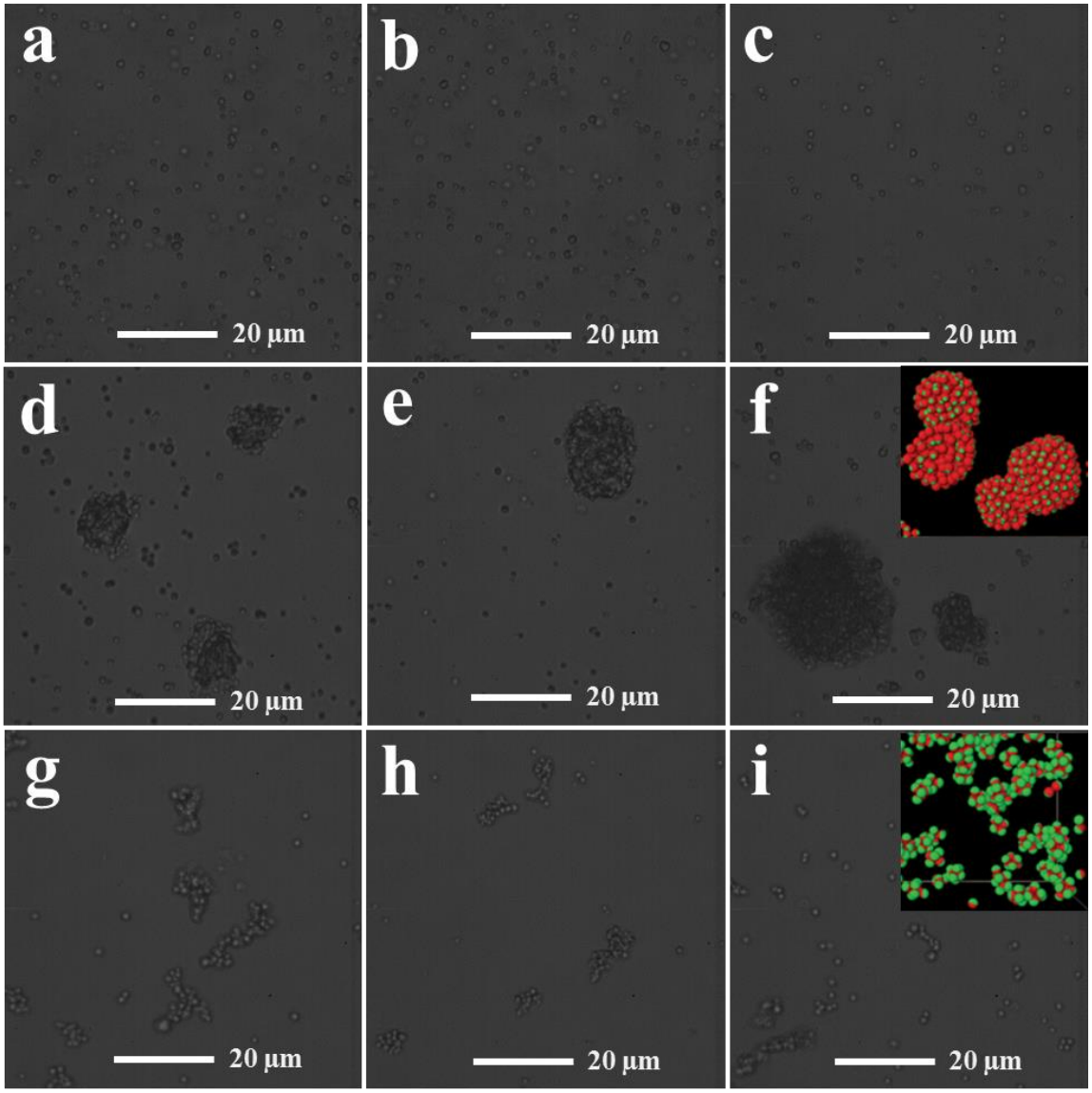

Fig. 1.6. (a-c) Microscope images at 100x magnification showing no self-assembly of the unmodified amaranth starch granules in water, (d-f) aggregation into "supermicelles" of fully hydrophobic amaranth starch granules, (g-i) and self-assembly into wormlike strings or irregular micelles of half-hydrophobic amaranth starch Janus granules, all after sonication. The inset photos for 6f and 6i are reproduced in part from a modeling study conducted by Zhan-Wei Li *et al.* (Li, Lu, Sun, & An, 2012), with permission from the corresponding author and the Royal Society of Chemistry. The 6f inset photo shows that particles with > 88% attractive patches (red color) are expected to self-assemble into "complex supermicelles" or large aggregates, while the 6i inset photo shows that the Janus particles with 50-60% attractive patches are expected to self-assemble into wormlike strings.

Given the same number of particles, flocculated particles (such as supermicelles) have a higher combined volume fraction than the sum of the volume fractions of their individual component particles due to some liquid being trapped between them (McClements, 2016). This higher volume fraction will increase resistance to flow when shear stress is applied, which may help explain why fully hydrophobic (fully OSA-modified) starch has a higher viscosity than unmodified starch during gelatinization.

In contrast, the half-hydrophobic amaranth Janus granules produced by the spin-coating spray approach appear to form irregular wormlike clusters in water, with some two- or three-particle clusters occasionally observed (Figs. 1.6g-i). This result agrees with the same modeling study conducted by Zhan-Wei Li *et al.*, which showed that half-hydrophobic particles (~50–60% surface patch coverage) form irregularly shaped micelles or wormlike strings (see inset photo of Fig. 1.6i) (Li, Lu, Sun, & An, 2012). In fact, another modeling paper has shown that the actual shape or configuration of these wormlike strings will depend on how big a hydrophobic patch was attached to the particle—if the hydrophobic patch is very small, then at most a four-particle cluster is formed (Chen, et al., 2011), with the hydrophobic patches at the center of the formation. If the hydrophobic patch takes up half of the particle, then given that the particles are near enough to interact with each other, they begin to form two-particle clusters. If their orientation is such that part of their attractive patch is accessible to a third Janus particle, then a three-particle cluster is formed; and if the third particle is itself oriented such that its attractive patch is accessible to a fourth, then a four particle-cluster is formed, and so on and so forth, until they grow into bigger wormlike clusters (Chen, et al., 2011). Evidence for the formation of these small and larger clusters can be seen in Figure 1.6i.

It is reasonable to assume—given that the spin-coating process allows us to modulate the film thickness—that we can also fine-tune the size of the hydrophobic patch on the Janus granule, and perhaps also the degree of OSA substitution. Therefore, the spin-coating spray approach gives us some measure of control on the superstructures formed by the resulting Janus granules. Indeed, by changing the attractive force strength and the size of the attractive patch, Zhan-Wei Li *et al.* (2012) predicted that other superstructures are also possible, such as double helices, single helices, and bilayers—structures which could be useful in nano- and biotechnology.

We estimated the size distribution of these self-assembled aggregates using ImageJ by calculating the relative area they consume compared to the overall total area of all aggregates. By comparing the size distribution between the unmodified, half-hydrophobic Janus, and fully hydrophobic starch granules, we can quantify differences in their self-assembly behavior. Figure 1.7 shows that for unmodified starch, 85% exist as separate granules (no aggregates), 15% as two- or three-granule clusters, and no wormlike clusters or supermicelles were formed. This distribution can be explained by the fact that no hydrophobic patches are present to generate any inter-granule interactions. The two- or three-granule clusters observed may be due to random positioning on the microscope slide or interactions due to residual proteins remaining on the granule surface after isolation from the grain. For the half-hydrophobic Janus starch, only 19% and 13% exist as separate granules and clusters; the majority (68%) appear as wormlike strings or micelles. However, no supermicelles were formed. Again, the hydrophobic patch covering half of the granule gives it enough hydrophobic interaction to self-assemble into micelles or wormlike strings, but not strong enough to

form spherical supermicelles. And lastly, for the fully hydrophobic starch, only 17% and 9% exist as separate granules or clusters, while about 8% form irregular micelles and the majority (66%) form near-spherical supermicelles. It is important to note that because we are using the area instead of the volume to determine the size distribution, our values are necessarily skewed to favor the smaller aggregates. The proportions of the granules actually aggregating into wormlike strings or supermicelles are thus expected to be much higher than the estimates presented here, which serve as a minimum.

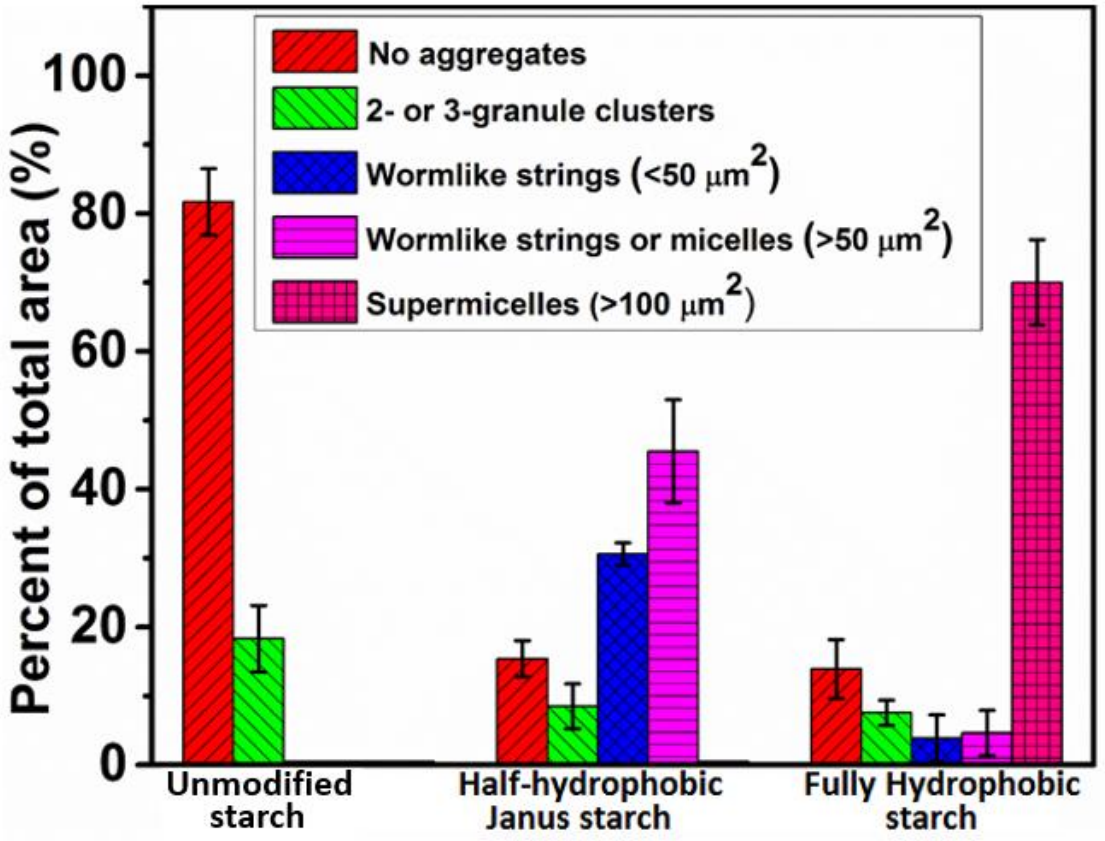

Fig. 1.7. Size distribution of the self-assembled aggregates of unmodified, half-hydrophobic Janus, and fully hydrophobic amaranth starch granules. The μm^2 values noted in the legend refer to the cross-sectional area of each discrete element belonging to that category.

4. Conclusions

The use of natural biopolymers like starch to make Janus particles in the food industry and other related fields has not yet been fully explored. Given that Janus particles made from synthetic polymers and inorganic materials have already been shown to have unique anisotropic properties and interesting self-assembly behaviors, it stands to reason that bringing these potential advantages to the food industry using only food-grade ingredients may produce surprising results. In this work, we demonstrated that a spin-coating spray approach can be used to form large half-porous waxy cornstarch Janus granules and small half-hydrophobic amaranth starch Janus granules. Although the low yield typical of Janus preparation methods prevents a more detailed characterization of these particles (Vries, Nikiforidis, & Scholten, 2014), the differences in the porosity (i.e., adsorption rate and adsorption capacity) between the half-porous and fully porous waxy cornstarch, and differences in self-assembly between the half-hydrophobic (which form micelles or wormlike strings) and fully hydrophobic amaranth starch particles (which aggregate into spherical supermicelles) likewise portend differences in their physicochemical, colloidal, and rheological properties, which could lead to new applications as texturants or surface-active agents. Half-hydrophobic starch products in food, due to their unique self-assembly different from that of fully hydrophobic starch products, could provide unique textures to the tongue and mouth that have not yet been investigated. In fact, if we can make starch granules half-porous or half-hydrophobic, the possibilities of other binary combinations present themselves. For example, a starch-based, biodegradable Janus particle with one side porous and the

other side coated with titanium dioxide could self-mix and remove organic pollutants under light irradiation more efficiently than static systems. The possibility of adding other functional groups or a positive or negative charge to one side of a starch granule and another functional group to the other side, is an interesting opportunity that may open new ideas for food research and applications.

References

Abiddin, Z., Yusoff, N., & Ahmad, N. (2015). Optimisation of reaction conditions of octenyl succinic anhydride (OSA) modified sago starch using response surface methodology (RSM). *International Food Research Journal, 22*(3), 930-935.

Ai, L., Yue, H., & Jiang, J. (2012). Sacrificial template-directed synthesis of mesoporous manganese oxide architectures with superior performance for organic dye adsorption. *Nanoscale, 4*, 5401-5408.

Altuna, L., Herrera, M. L., & Foresti, M. L. (2018). Synthesis and characterization of octenyl succinic anhydride modified starches for food applications: A review of recent literature. *Food Hydrocolloids, 80*, 97-110.

Asensio, J. L., Arda, A., Canada, F. J., & Jimenez-Barbero, J. (2013). Carbohydrate-Aromatic interactions. *Accounts of Chemical Research, 46*(4), 946-954.

Bahrami, R. L., Groschel, A., Schmalz, H., Muller, A., & Altstadt, V. (2014). The impact of Janus nanoparticles on the compatibilization of immiscible polymer blends under technologically relevant conditions. *ACS Nano*, 10048-10056.

Bao, Z., Chen, L., Weldon, M., Chandross, E., Cherniavskaya, O., Dai, Y., & Tok, J. (2002). Toward controllable self-assembly of microstructures: selective functionalization and fabrication of patterned spheres. *Chemistry of Materials, 14*, 24-26.

Bechtel, D., Zayas, I., Kaleikau, L., & Pomeranz, Y. (1990). Size distribution of wheat starch granules during endosperm development. *Cereal Chemistry , 1*, 67.

Benavent-Gil, Y., & Rosell, C. M. (2017). Comparison of porous starches obtained from different enzyme types and levels. *Carbohydrate Polymers, 157*, 533-540.

Bertolini, A. (2009). *Starches: Characterization, Properties, and Applications.* Boca Raton, FL: CRC Press.

Bhosale, R., & Singhal, R. (2007). Effect of octenylsuccinylation on physicochemical and functional properties of waxy maize and amaranth starches. *Carbohydrate Polymers, 68*, 447-456.

Chen, Q., Whitmer, J., Jiang, S., Bae, S. C., Luijten, E., & Granick, S. (2011). Supracolloidal reaction kinetics of Janus spheres. *Science, 14*, 199-201.

de Gennes, P. (1992). Soft Matter. *Reviews of Modern Physics, 64*(3).

Dhital, S., Warren, F., Butterworth, P., Ellis, P., & Gidley, M. (2017). Mechanisms of starch digestion by alpha-amylase-Structural basis for kinetic properties. *Critical Reviews in Food Science and Nutrition, 57*(5), 875-892.

Dura, A., Blaszczak, & Rosell, C. (2014). Functionality of porous starch obtained by amylase or amyloglucosidase treatments. *Carbohydrate Polymers, 101*, 837-845.

Eltaboni, F., Imragaa, A., Edbey, K. E., & Mousa, N. (2015). Adsorption and conformations of starch at solid-liquid interfaces using spectrophotometry and turbidity techniques. *American Chemical Science Journal, 9*(1), 1-11.

Eskandarloo, H., Kierulf, A., & Abbaspourrad, A. (2017). Light-harvesting synthetic nano- and micromotors: a review. *Nanoscale, 9*, 12218–12230.

Eskandarloo, H., Kierulf, A., & Abbaspourrad, A. (2017). Nano- and micromotors for cleaning polluted waters: Focused review on pollutant removal mechanisms. *Nanoscale, 9*(37), 13850-13863.

Gao, F., Li, D., Bi, C.-h., Mao, Z.-h., & Adhikari, B. (2014). Preparation and characterization of starch crosslinked with sodium trimetaphosphate and hydrolyzed by enzymes. *Carbohydrate Polymers , 103*, 310-318.

Groschel, A., Walther, A., Lobling, T., Schmelz, J., Hanisch, A., Schmalz, H., & Muller, A. (2012). Facile, solution-based synthesis of soft, nanoscale Janus particles with tunable balance. *Journal of the American Chemical Society*, 13850-13860.

Guo, L., Li, G., Liu, J., Meng, Y., & Tang, Y. (2013). Adsorptive decolorization of methylene blue by crosslinked porous starch. *Carbohydrate Polymers, 93*, 374-379.

Hong, L., Cacciuto, A., Luijten, E., & Granick, S. (2008). Clusters of amphiphilic colloidal spheres. *Langmuir, 24*, 621-625.

Hu, J., Zhou, S., Sun, Y., Fang, X., & Wu, L. (2012). Fabrication,properties and applications of Janus particles. *Chemical Society Reviews, 41*, 4356-4378.

Hui, R., Qi-he, C., Ming-liang, F., Qiong, X., & Guo-qing, H. (2009). Preparation and properties of octenyl succinic anhydride modified potato starch. *Food Chemistry, 114*, 81-86.

Jia, R., Jiang, H., Jin, M., Wang, X., & Huang, J. (2015). Silver/chitosan-based Janus particles: Synthesis, characterization, and assessment of antimicrobial activity in vivo and vitro. *Food Research International, 78*, 433-441.

Khlestkin, V., Peltek, S., & Kolchanov, N. (2018). Review of direct chemical and biochemical transformations of starch. *Carbohydrate Polymers, 181*, 460-476.

Kim, J., Santiano, B., Kim, H., & Kan, E. (2013). Heterogeneous oxidation of methylene blue with surface-modified iron-amended cativated carbon. *American Journal of Analytical CHemistry, 4*, 115-122.

Li, Z.-W., Lu, Z.-Y., Sun, Z.-Y., & An, L.-J. (2012). Model, self-assembly structures, and phase diagram of soft Janus particles. *Soft Matter, 8*, 6693-6697.

McClements, D. J. (2016). *Food Emulsions: Principles, Practices, and Techniques.* Boca Raton, FL: CRC Press.

Miao, M., Li, R., Jiang, B., Cui, S., Zhang, T., & Jin, Z. (2014). Structure and physicochemical properties of octenyl succinic esters of sugary maize soluble starch and waxy maize starch. *Food Chemistry, 151*, 154-160.

Orozco, J., Mercante, L., Pola, R., & Merkoci, A. (2016). Graphene-based Janus micromotors for the drynamic removal of pollutants. *Journal of Materials Chemistry A, 4*, 3371-3378.

Ovando-Martinez, M., Whitney, K., Ozsisli, B., & Simsek, S. (2017). Physicochemical properties of octenyl succinic esters of cereal, tuber, and root starches. *Journal of Food Processing and Preservation, 41*, e12872.

Pei, X., Zhai, K., Liang, X., Deng, Y., Xu, K., Tan, Y., . . . Pixin, W. (2018). Fabricaiton of shape-tunable macroparticles by seeded polymerization of styrene using non-crosslinked starch-based seed. *Journal of Colloid and Interface Science, 512*, 600-608.

Poggi, E., & Gohy, J.-F. (2017). Janus particles: from synthesis to application. *Colloid & Polymer Science, 295*, 2083-2108.

Qiu, C., Yang, J., Ge, S., Chang, R., & Xiong, L. S. (2016). Preparation and characterization of size-controlled starch nanoparticles based on short linear chains from debranched waxy corn starch. *LWT Food Science and Technology, 74*, 303-310.

Simkovic, I. (2008). What could be greener than composites made from polysaccharides? *Carbohydrate Polymers, 74*, 759-762.

Sweedman, M., Tizzotti, M., Schafer, C., & Gilbert, R. (2013). Structure and physicochemical properties of octenyl succinic anhydride modified starches: a review. *Carbohydrate Polymers, 92*, 905-920.

Tanaka, T., Okayama, M., Minami, H., & Okubo, M. (2010). Dual stimuli-responsive "mushroom-like" Janus Polymer particles as Particulate Surfactants. *Langmuir, 26*(14), 11732-11736.

Thangawng, A., Ruoff, R., Swartz, M., & Glucksberg, M. (2007). An ultra-thin PDMS membrane as a bio/micro-nano interface: fabrication and characterization. *Biomedical Microdevices, 9*, 587-595.

Vries, A., Nikiforidis, C., & Scholten, E. (2014). Natural amphiphilic proteins as tri-block Janus particles: Self-sorting into thermo-responsive gels. *A letters journal exploring the frontiers of physics, 107*(58003), 1-6.

Walther, A., & Muller, A. (2013). Janus particles: Synthesis, self-assembly, physical properties, and applications. *Chemical Reviews*, 5194-5261.

Wang, F., Pauletti, G., Wang, J., Zhang, J., Ewing, R. W., & Shi, D. (2013). Dual surface-functionalized Janus nanocomposites of polystyrene/Fe3O4@SiO2 for simultaneous tumor cell targeting and stimulus-induced drug release. *Advanced Materials, 25*, 3485-3489.

Wang, H., Lv, J., Jiang, S., Niu, B., Pang, M., & Jiang, S. (2016). Preparation and characterization of porous corn starch and its adsorption toward grape seed proanthocyanidins. *Starch/Starke, 68*, 1254-1263.

Xia, X., Li, G., Liao, F., Zhang, F., Zheng, J., & Kan, J. (2015). Granular structure and physicochemical properties of starches from Amaranth grains. *International Journal of Food Properties, 18*, 1029-1037.

Yamada, H., Kayama, M., Saito, K., & Hara, M. (1986). A fundamental research on phosphate removal by using slag. *Water Research, 20*(5), 547-557.

Ye, F., Miao, M., Huang, C., Lu, K., Jiang, B., & Zhang, T. (2014). Elucidation of substituted ester group position in octenylsuccinic anhydride modified sugary maize soluble starch. *Agricultural and Food Chemistry, 62*, 11696-11705.

Zhang, B., Cui, D., Liu, M., Gong, H., Huang, Y., & Han, F. (2012). Corn porous starch: Preparation, characterization, and adsorption property. *International Journal of Biological Macromolecules, 50*, 250-256.

Zhang, J., Grzybowski, B., & Granick, S. (2017). Janus particle synthesis, assembly, application. *Langmuir, 33*, 6964-6977.

Zhu, F. (2017). Encapsulation and delivery of food ingredients using starch based systems. *Food Chemistry, 229*, 542-552.

Zhu, F. (2017). Structures, physicochemical properties, and applications of amaranth starch. *Critical Review in Food Science and Nutrition, 57*(2), 313-325.

CHAPTER 2

Protein content of amaranth and quinoa starch plays a key role in their ability as Pickering emulsifiers

Abstract

Growing concerns about the safety of using synthetic surfactants to stabilize food emulsions have inspired a trend towards the use of natural ingredients like starch as alternative food stabilizers in what are called Pickering emulsions. The hydrophilicity of commercially available starches, however, necessitates further chemical treatment to increase their hydrophobicity and emulsifying ability. Here we demonstrate an alkaline isolation method to extract amaranth and quinoa starch from flour while retaining a high protein content, which gives these materials an emulsifying ability comparable to octenyl succinylated starches. We highlight the key role played by protein by showing that a serial reduction of the protein content leads to a parallel reduction in emulsifying ability, and that pH affects this ability. Our method of retaining proteins naturally present in amaranth and quinoa not only bolsters the nutritional profile of the food but also takes advantage of the proteins' native hydrophobicity for improved emulsification.

1. Introduction

The use of emulsifiers to form stable emulsions and foams has afforded many incredible applications for the food, pharmaceutical, cosmetic, and drug industries (Berton-Carabin & Schroen, 2015; Dickinson, 2010). The thick texture of a common

food like mayonnaise, for example, can be attributed not to its oil content or water content alone, but to how emulsifiers are able to structure the oil and water together as an oil-in-water emulsion, which resists flow and gives a higher viscosity. Typical emulsifiers used today are small, amphiphilic molecules (~1 nm) that orient themselves at the oil/water interface to impart stability (see Fig. 2.1a). They can be categorized as either synthetic surfactants (e.g., polysorbates, monoacylglycerols) or biopolymers (e.g., proteins like casein or soy, and carbohydrates like gum arabic or carrageenan) (Berton-Carabin et al., 2015; McClements, 2016). Concerns over the biocompatibility, biodegradability, and carcinogenicity of synthetic surfactants, however, have led to a growing trend towards the use of natural emulsifiers in "clean label" food products. In the food and pharmaceutical industries, in particular, there has been increasing interest in what are called Pickering emulsifiers. These are large, solid particles (~10 nm–10μm) that possess the ability to stabilize emulsions due to their moderate hydrophobicity and larger size (see Fig. 2.1b) (Bon, 2015; Aveyard, Binks, & Clint, 2003; Timgren, Rayner, Sjoo, & Dejmek, 2011; Yang, et al., 2017). Plant-based solid particles like starch granules are especially good candidates for this application because they are cheap, widely available, biodegradable, non-allergenic, and GRAS (Timgren et al., 2011; Xiao, Li, & Huang, 2016; Zhu, 2019).

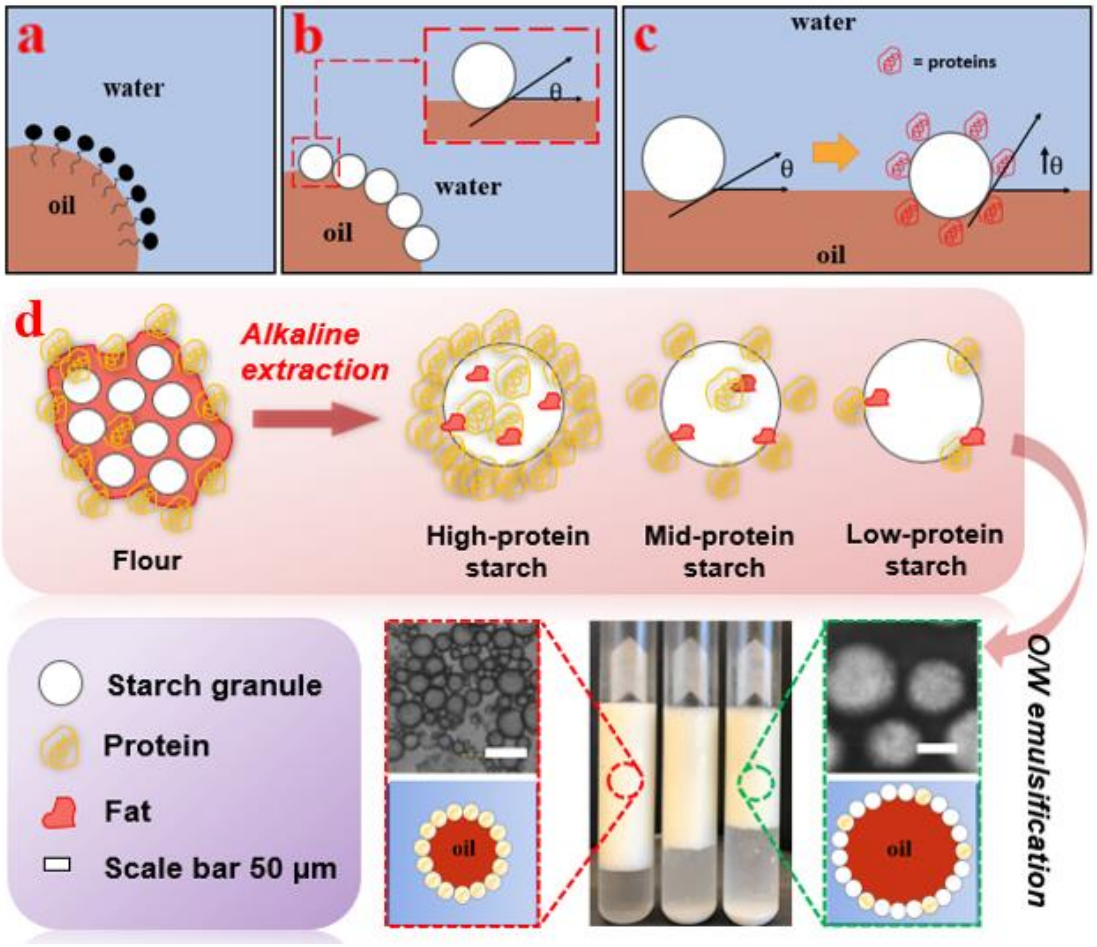

Figure 2.1. Schematic diagrams of (a) amphiphilic, small-molecule surfactants at the oil/water interface, (b) solid starch granules adsorbed at the oil/water interface at a contact angle θ, (c) proteins on the starch surface increasing its hydrophobicity and thus helping it adsorb deeper into the oil phase, increasing θ, and (d) how reducing the protein content of starch is expected to reduce its emulsifying ability. Note: Protein and fat are not drawn to scale; they have been enlarged to illustrate their influence on emulsification.

The problem with starch granules as Pickering emulsifiers is that in their commercial, purified, native form, they are very hydrophilic, making it difficult for them to adsorb onto the oil/water interface and thus making them poor emulsifiers in general (Aveyard et al., 2003). To resolve this issue, chemical treatment with octenyl succinic anhydride (OSA) has been typically employed to increase their hydrophobicity and thus improve emulsifying ability (Zhu, 2019). It is in this OSA-modified form that starches in general are used in food emulsions, although the high amount needed relative to the oil content (~0.4-1:1 w/w) still presents a disadvantage compared to small-molecule surfactants (~0.05:1 w/w) (McClements, 2016). Another problem is that it is not yet clearly understood why certain kinds of native starches (e.g., quinoa, rice, barley) appear to have at least some ability to form emulsions while some others do not (e.g., maize, waxy maize, amaranth) (Timgren, Rayner, Dejmek, Marku, & Sjoo, 2013; Marefati, Wiege, Haase, Matos, & Rayner, 2017). Variations in source grain, isolation method, native granule hydrophobicity, granule particle size, and shape have all been hypothesized to play a role. However, since all these factors can confound each other when comparing starches of different sizes and shapes extracted from a myriad of botanical sources using different methods, it is difficult to ascertain exactly what role each factor plays (Marefati et al., 2017).

Recent papers have highlighted the important role that protein content may play in starch's hydrophobicity and emulsifying ability. For example, dry heating quinoa, rice, barley, and wheat starches at 100–160 ºC has been shown to improve their emulsifying ability and oil-binding ability. Heating is believed to lipophilize the residual proteins on the surface of the starch granules, changing their character from hydrophilic to

hydrophobic and thus improving their emulsifying ability (Timgren et al., 2013; Seguchi, 1984; Baldwin, 2001). The protein contents were not quantified, however, and dry heating other kinds of starches (e.g., maize and waxy maize) did not produce the same improvement in emulsifying ability, making it difficult to make clear conclusions. In another recent paper, Marefati et al. (2017) have shown that quinoa starch with 0.69% protein were able to form emulsions, while amaranth starch with a lower 0.11% protein content could not form emulsions, leading them to conclude that a higher protein content may be responsible for improved emulsification properties (Marefati et al., 2017; Marefati, Matos, Wiege, & Rayner, 2018). Differences in particle size and shape between quinoa and amaranth starches, however, again presented a confounding factor that prevented a direct comparison. A direct relationship between protein content and starch's emulsifying ability has therefore not yet been established.

In this study we seek to establish a direct relationship between the protein contents of two kinds of starches, amaranth and quinoa, and their respective Pickering emulsifying abilities. We chose these two pseudo-cereals because of their small granule size and their naturally high protein contents (with excellent amino acid profiles), and because they have not been as well studied as other cereals (Janssen, Pauly, Rombouts, Jansens, & Delcour, 2017; Bressani & Garcia-Vela, 1990; Gurbuz, Kauntola, Diaz, & Jouppila, 2018). We speculate that their proteins are adsorbed on the granule surface, serve to increase their hydrophobicity, and thus improve their emulsifying abilities (Figs. 2.1c and 2.1d). We first isolated amaranth and quinoa starches from flour using a NaOH-based method that retained a high protein content (> 2%), measured their respective emulsifying capabilities, then serially reduced the protein contents down to

~1% by NaOH extraction, and again studied their respective emulsifications in terms of emulsion index (EI), droplet size, rheology, surface charge, and 4-week stability. Our aim was to highlight the key role that proteins may play in the emulsification properties of starches, so we showed, in addition, how these emulsions were sensitive to changes in pH. Having established that a high protein content was key to starch's ability to form Pickering emulsions, we argued that the isolation method presented here could produce naturally high-protein starches that can successfully be used to make Pickering emulsions without any further chemical treatment.

2. Materials and Methods

2.1 Materials

Amaranth and quinoa starches were isolated from commercially available flours (see Section *2.2* for the isolation method). Corn oil was purchased from Healthy Brand Oil Corporation (Long Island City, NY, USA). Sodium hydroxide (NaOH, 95–100%) beads were purchased from Fisher Scientific (NJ, USA). ACS-grade hydrochloric acid (HCl, 36.5–38%) was purchased from VWR Chemicals (PA, USA). Denatured ethanol (<92%) was purchased from Thermo Fisher Scientific (MI, USA). Citric acid monohydrate (100.4%), sodium carbonate (100%), sodium bicarbonate (100.3%), and sodium phosphate dibasic were purchased from Fisher Scientific (NJ, USA). Monobasic sodium phosphate was purchased from VWR Life Science (Ohio, USA). Trisodium citrate dihydrate (>99%) was purchased from Sigma-Aldrich (MO, USA). All prepared emulsions were stored in Kimble KIMAX disposable culture tubes (15 mL) (NJ, USA).

2.2 Isolation of amaranth and quinoa starches from flours

Amaranth and quinoa starches were isolated from commercially available flours using an alkaline isolation method. First, 100 g of flour was dispersed in a 500-mL 0.15% NaOH solution and mixed using an overhead stirrer at ambient temperature for 1 h. The slurry was then filtered for 10 min using a laboratory test sieve vibrator (Derrick Mfg. Co., Buffalo, NY, USA) with a 270-mesh sieve (53-μm pore size). The remaining residue that did not pass through the sieve was collected, and then dispersed in 100 mL of a 0.15% NaOH solution, which was then stirred for a further 10 min, filtered again through the 270-mesh sieve, and washed with another 100 mL of the 0.15% NaOH solution. The filtrates from both filtrations were combined and centrifuged at 3000 g for 20 min. The supernatant was discarded, and the top yellow-brownish layer of protein was removed using a spatula. The white starch layer was then re-suspended in deionized water, adjusted to pH 6.0 ± 0.1 using a 1 N HCl solution, and centrifuged at 3000 g for 20 min, again removing the top yellow-brown layer. It was then freeze-dried for 24 h and ground ultra-fine using a conical burr grinder. The starches isolated using this method had protein contents of 2.43% (amaranth) and 2.70% (quinoa). For the purposes of this study, we labelled these as "high-protein starches," to differentiate them from lower-protein starches to be produced in the next section (see Section *2.3*). By comparison, these high-protein starches (2.4-2.7%) have protein contents much higher than those of commercially available starches (typically ~0.05%-0.6%) (Baldwin, 2001). The starch extraction yields from the amaranth and quinoa flours were approximately 12% and 30%, respectively.

2.3 Protein extraction from starch

Protein extraction was done to further reduce the protein contents of the high-protein amaranth and quinoa starches isolated from Section *2.2* by using a modified alkaline extraction method (Lim, Kyonggi-do, Shin, & Lim, 1999). 8 g of starch was dispersed in 30 mL of a 0.20% NaOH solution and mixed at 80 rpm for 1h using a vertical rotating mixer (BT Lab Systems, MO, USA). The slurry was then centrifuged at 3000 g for 10 minutes, removing the top yellow-brown protein layer. The white starch was then re-suspended in deionized water, adjusted to pH 6.0 ± 0.1 using a 1 N HCl solution, and centrifuged, followed by removal of the top yellow-brown layer. The white starch was then washed further sequentially with ethanol then deionized water, each time centrifuging at 3000 g for 10 min and removing any remaining yellow-brown top layer. The sample was then freeze-dried for 24 h. This reduced the protein contents of the amaranth and quinoa starches down to 0.87% and 1.4%, respectively. For the purposes of this study, we labelled these "mid-protein starches," to differentiate them from the high-protein starches produced previously in Section *2.2*.

To even further reduce the protein content, the starches isolated from Section *2.2* were mixed with a 0.20% NaOH solution for 4 h instead of 1 h, replacing the NaOH solution every hour with a fresh solution, and performing the centrifugation, removal of the top protein layer, pH adjustment, washing, and freeze-drying steps in the same way as above. This further reduced the protein contents of the amaranth and quinoa starches down to 0.67% and 1.17%, respectively. For the purposes of this study, we labelled these "low-protein starches," to differentiate them from the mid-protein and high-protein starches produced previously.

2.4 Crude protein and crude fat analysis

Amaranth and quinoa flours, together with the high-protein starches isolated from them in Section *2.2* and the protein-reduced starches in Section *2.3* (mid-protein and low-protein) were tested in triplicate for crude protein using AOAC 992.23 (combustion method) and a nitrogen-to-protein conversion factor of 6.25, and tested for crude fat using AOAC 2003.05 (Randall-modified Soxhlet extraction), both on a % dry basis.

2.5 Scanning electron microscopy (SEM)

The amaranth and quinoa commercial flours were mounted on an SEM stub with conductive carbon tape. They were then sputter-coated with gold then imaged using a JCM-6000 Benchtop SEM (JEOL Ltd., Japan) at an accelerating voltage of 15 kV using a secondary electron detector at x1000 and x5000 magnifications.

The high-protein amaranth and quinoa starches isolated in Section *2.2*, together with the low-protein starches from Section *2.3*, were both mounted on a stub and sputter-coated with indium then imaged using a Zeis Gemini 500 Field Emission SEM.

2.6 Particle size of starch granules

The high-protein amaranth and quinoa starches isolated from flour in Section *2.2* were imaged using a JCM-6000 Benchtop SEM at x5000 magnification. The granule size and distribution were measured using ImageJ 1.51w software for over 200 granules. The surface mean diameter (d_{32}), volume mean diameter (d_{43}), and polydispersity index

(PDI) were calculated based on the following equations, respectively (Li, Li, Sun, & Yang, 2013):

$$d_{32} = \frac{\sum di^3}{\sum di^2} \quad (2.1)$$

$$d_{43} = \frac{\sum di^4}{\sum di^3} \quad (2.2)$$

$$\text{PDI} = \frac{d_{43}}{\sum di/N} \quad (2.3)$$

where d_i is the diameter of the particle to be measured, and N is the total number of particles.

2.7 Preparation of emulsions

Pickering emulsions were prepared using the high-protein, mid-protein, and low-protein amaranth and quinoa starches produced in Sections *2.2* and *2.3*. These emulsions were prepared with 30% v/v corn oil/water using a pH 7 buffer and a starch concentration of 0.15 g/mL oil. These were then homogenized at 11,000 rpm for 4 min using a high-speed homogenizer (IKA T25 digital Ultra Turrax, Germany) with S25N-18G dispersing tool. Six 10 mL replicates at each protein level were prepared in total—3 for measuring the EI and the 4-week stability, and another 3 for measuring both the emulsion droplet size and rheology. They were stored in 15 mL culture tubes, covered with a cap, sealed with parafilm, and stored at ambient temperature.

Pickering emulsions were also prepared using the high-protein amaranth and quinoa starches using different aqueous pH buffers (pH 3, 5.7, 7.0, 7.5, 8.5, 9.5, 10), again using 30% v/v corn oil/buffer, and a starch concentration of 0.15 g/mL oil. These

were then homogenized at 11,000 rpm for 4 min. Six 10 mL replicates at each pH level were prepared in total—3 for measuring the EI and the 4-week stability, and another 3 for measuring both emulsion droplet size and rheology. They were also stored in culture tubes, covered with a cap, sealed with parafilm, and stored at ambient temperature.

The buffers used above were prepared as follows: The pH 3 and pH 5.7 buffers were prepared using 0.1M citric acid monohydrate and 0.1M trisodium citrate dihydrate at 82:18 and 18:82 volume ratios, respectively. The pH 7, 7.5, and 8 buffers were prepared using 0.2M sodium phosphate dibasic and 0.2M monobasic sodium phosphate at 61:39, 84:16, and 94.6:5.4 volume ratios, respectively. The pH 9.2 and pH 10.0 buffers were prepared using 0.1M sodium carbonate and 0.1M sodium bicarbonate at 10:90 and 55:45 volume ratios, respectively.

2.8 Emulsion droplet size by optical microscopy

The Pickering emulsions prepared in Section *2.7* were placed on a microscope cover slip 1 day after preparation and imaged using a Leica Model DMIL LED Inverted Phase Contrast Microscope at 10x or 4x magnification, depending on their size. The emulsion droplet size was measured using ImageJ 1.51w software for over 200 droplets. The surface mean diameter (d_{32}), volume mean diameter (d_{43}), and polydispersity index (PDI) of the droplets were calculated using equations 2.1-2.3 from Section *2.6*.

2.9 Emulsion index and 4-week stability

To monitor emulsifying ability and emulsion stability over a 4-week period, the emulsion indices (EI) of the Pickering emulsions prepared in Section *2.7* were measured 1d, 7d, 2 weeks, and 4 weeks after preparation using the following equation:

$$Emulsion\ index = \frac{V_E}{V_T} \qquad (2.4)$$

where V_E is the volume of the emulsion (upper cream layer) and V_T is the total volume of the whole sample (including all layers or phases) (Saari, Heravifar, Rayner, Wahlgren, & Sjoo, 2016). Three replicates were prepared.

2.10 Rheology

Two days after the preparation of the Pickering emulsions in Section *2.7*, oscillation frequency sweep and flow sweep experiments were performed using an AR 1000-N Rheometer (TA Instruments, USA) with a 40-mm-diameter parallel plate, a 1000-μm gap height, and a 2-min equilibration time between runs (Song, Pei, Qiao, Ma, Ren, & Zhao, 2015). An oscillation frequency sweep was first performed at 25 ºC using a frequency range of 0.01–10 Hz and a strain of 0.1%. Then, a flow sweep was performed at 25 ºC using a shear rate range of 0.02–100 s^{-1}. The viscosity, storage modulus G', loss modulus G", and tan δ were plotted logarithmically and investigated.

2.11 Zeta potential

The Zeta potential values of the emulsions prepared in Section *2.7* were measured 4 weeks after preparation by diluting them by a factor of 0.1 and determining

their Zeta potential (mV) using a Malvern Zetasizer Nano Series. This was performed after the 4-week stability study.

3. Results and Discussion

3.1 Crude protein and crude fat analysis of flours and starches

The crude protein and crude fat analytical results are shown in Figures 2.2a and 2.2b. The commercial flours used in this study had crude protein contents of 17.37% (amaranth) and 14.93% (quinoa), and crude fat contents of 7.1% (amaranth) and 6.1% (quinoa), on a dry basis. Using the NaOH isolation procedure outlined in Section *2.2*, high-protein starches obtained from these flours featured protein contents of 2.43% (high-protein amaranth) and 2.70% (high-protein quinoa), and fat contents of 2.2% (amaranth) and 0.6% (quinoa). The protein contents were further reduced using the NaOH method outlined in Section *2.3*, producing mid-protein starches (0.87% protein and 0.5% fat for amaranth, and 1.40% protein and 0.4% fat for quinoa), and low-protein starches (0.67% protein and 0.2% fat for amaranth, and 1.20% protein and 0.3% fat for quinoa).

Proteins extracted from amaranth and quinoa were not fractioned in this study, but the available literature states that pseudo-cereal protein fractions (i.e., amaranth and quinoa proteins) are predominantly composed of albumins and globulins, which are particularly high in glutamic acid, aspartic acid, lysine, and arginine (Janssen et al., 2017). Different cultivars have been shown to have different protein compositions, but in general, protein fractions from amaranth and quinoa grains using the Osborne fractionation scheme are composed mostly of water-soluble albumins and globulins

(~40–77%), while the remaining fraction is composed of alkaline-soluble glutelins and alcohol-soluble prolamines (Bressani et al., 1990; Osborne, 1907; Janssen et al., 2017; Fairbanks, Burgener, Robison, Anderson, & Ballon, 1990). It is important to note that the protein extractions performed in Sections *2.2* and *2.3* (alkaline, water, and alcohol) did not totally extract all the proteins, so residual proteins remained on the starch granules, which is supported by the crude protein results (Gurbuz et al., 2018). In addition, amaranth and quinoa proteins (albumins, globulins, glutelins, and prolamins) are all globular proteins, which means that they take a longer time than random-coil proteins like casein to unfold and adsorb onto the oil/water interface (Joshi, Adhikari, Aldred, Panozzo, Kasapis, & Barrow, 2012).

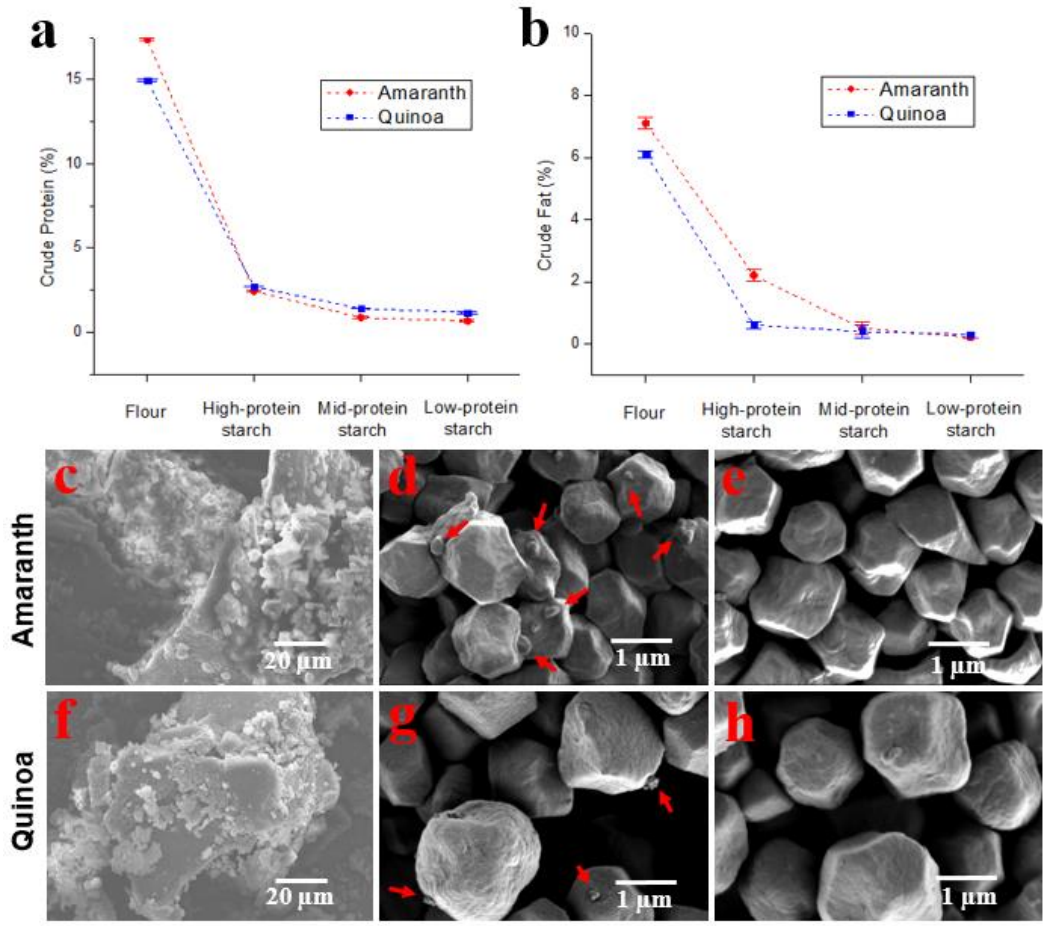

Figure 2.2. (a) Crude protein and (b) crude fat contents of amaranth and quinoa flours and their corresponding high-, mid-, and low-protein starches after isolation and further protein reduction. Error bars refer to standard deviation (SD). SEM images of (c) commercial amaranth flour, (d) isolated high-protein amaranth starch, and (e) low-protein amaranth starch at 1000x, 20,000x, and 20,000x magnifications, respectively. SEM images of (f) commercial quinoa flour, (g) isolated high-protein quinoa starch, (h) and low-protein quinoa starch at 1000x, 20,000x, and 20,000x magnifications, respectively.

3.2 Particle size of high-protein amaranth and quinoa starch granules

The high-protein amaranth starch isolated from flour in Section *2.2* featured a surface mean diameter, volume mean diameter, and a polydispersity index of 1.1µm (d_{32}), 1.2 µm (d_{43}), and 1.08, respectively. The high-protein quinoa starch had a slightly

larger size with 1.4 μm (d_{32}), 1.5 μm (d_{43}), and 1.12 (PDI). These values agree with the literature (Timgren et al., 2013; Xia, Li, Liao, Zhang, Zheng, & Kan, 2015).

3.3 SEM of flours and starches

The SEM images of amaranth flour, high-protein amaranth starch, and low-protein amaranth starch are shown in Figures 2.2c, 2.2d, and 2.2e, respectively. Amaranth flour (Fig. 2.2c) is composed of aggregates of starch granules attached to each other by protein and fat. High-protein amaranth starch (Fig. 2.2d) is composed of well-separated polygonal granules 1.2 μm in diameter with sharp edges, with some small residual particles on the surfaces (red arrows), which could perhaps be residual protein or fat. Low-protein amaranth starch (Fig. 2.2e) appears the same, but with fewer small residual particles. SEM images of quinoa flour, high-protein quinoa starch, and low-protein quinoa starch are shown in Figures 2.2f, 2.2g, and 2.2h, respectively. Like amaranth flour, quinoa flour (Fig. 2.2f) is composed of aggregates of starch granules attached together with protein and fat. High-protein quinoa starch (Fig. 2.2g) is composed of well-separated polygonal granules 1.5 μm in diameter with rounded edges, again with some small residual particles on the surface (red arrows), which could be residual protein or fat. Low-protein quinoa starch (Fig. 2.2h) appears the same, but with fewer residual particles.

3.4 Emulsification properties

3.4.1 Effect of protein content on emulsion droplet size, emulsion index, and 4-week stability

While conventional, small-molecule surfactants can stabilize emulsions because they are amphiphilic (their hydrophobic tails orient themselves towards the oil phase and their hydrophilic heads orient towards the aqueous phase), solid Pickering emulsifiers can stabilize emulsions because they are moderately hydrophobic over their entire surface (i.e., they are not amphiphilic). The more hydrophobic they are over their entire surface (e.g., higher degree of OSA substitution), the more easily they will adsorb onto the oil/water interface, promoting the formation of smaller droplets, and also the more deeply they will embed into the oil phase (higher Θ), thus making them more stable over time (i.e., higher desorption energy, harder to remove). If our contention that residual protein content adds hydrophobicity to starch like OSA, then a higher starch native protein content will be expected to likewise enhance starch's emulsifying ability, and reducing the protein content will conversely reduce this ability (We provide a more thorough discussion of conventional vs. Pickering emulsifiers in Sections S1 and S2 under Supplementary Information).

We see exactly this trend in the results: High-protein amaranth starch (Fig. 2.3a) and quinoa starch (Fig. 2.3b) formed emulsions with small droplet sizes (27.9, 32.1μm) and high EIs (0.78, 0.62). As we reduced the protein content, the droplet sizes increased (91.3, 126.7 μm) and the EIs decreased (0.58, 0.32) (for tabular data, see Supplementary Tables S1 and S2 under Supplementary Information). We believe that reducing the protein content reduces starch's hydrophobicity, which in turn reduces starch's ability

to adhere to the oil/water interface, thus promoting the formation of larger emulsion droplets (Timgren et al., 2013). In addition, larger emulsions have a smaller effective volume than smaller emulsions. The reason being that the effective volume fraction is $(1+\delta_x/r)^3$ times that of the actual volume fraction, where δ_x is the thickness of the adsorbed starch layer and r is the droplet radius (Chanamai & McClements, 2000). Thus, it follows that larger emulsions formed with low-protein, less hydrophobic starch will have lower emulsion volume, i.e., a lower EI, which is supported by Figs. 2.3a and 2.3b. Of course, larger emulsions are also more prone to creaming according to Stokes' law (McClements, 2016), thus further reducing the EI. The inverse of this relationship—increasing hydrophobicity leads to the formation of smaller emulsions and a higher EI—is supported by literature on OSA-modified starch (Timgren et al., 2013).

The larger emulsion droplets produced by lowering the starch protein content may also have been due to some of the low-protein granules (more hydrophilic) failing to adsorb onto the oil/water interface and settling down (Figs. 2.3a and 2.3b, see bottom of tubes). As a result, the effective concentration of starch that participates in the emulsification is lowered, which further contributes to the lower EI.

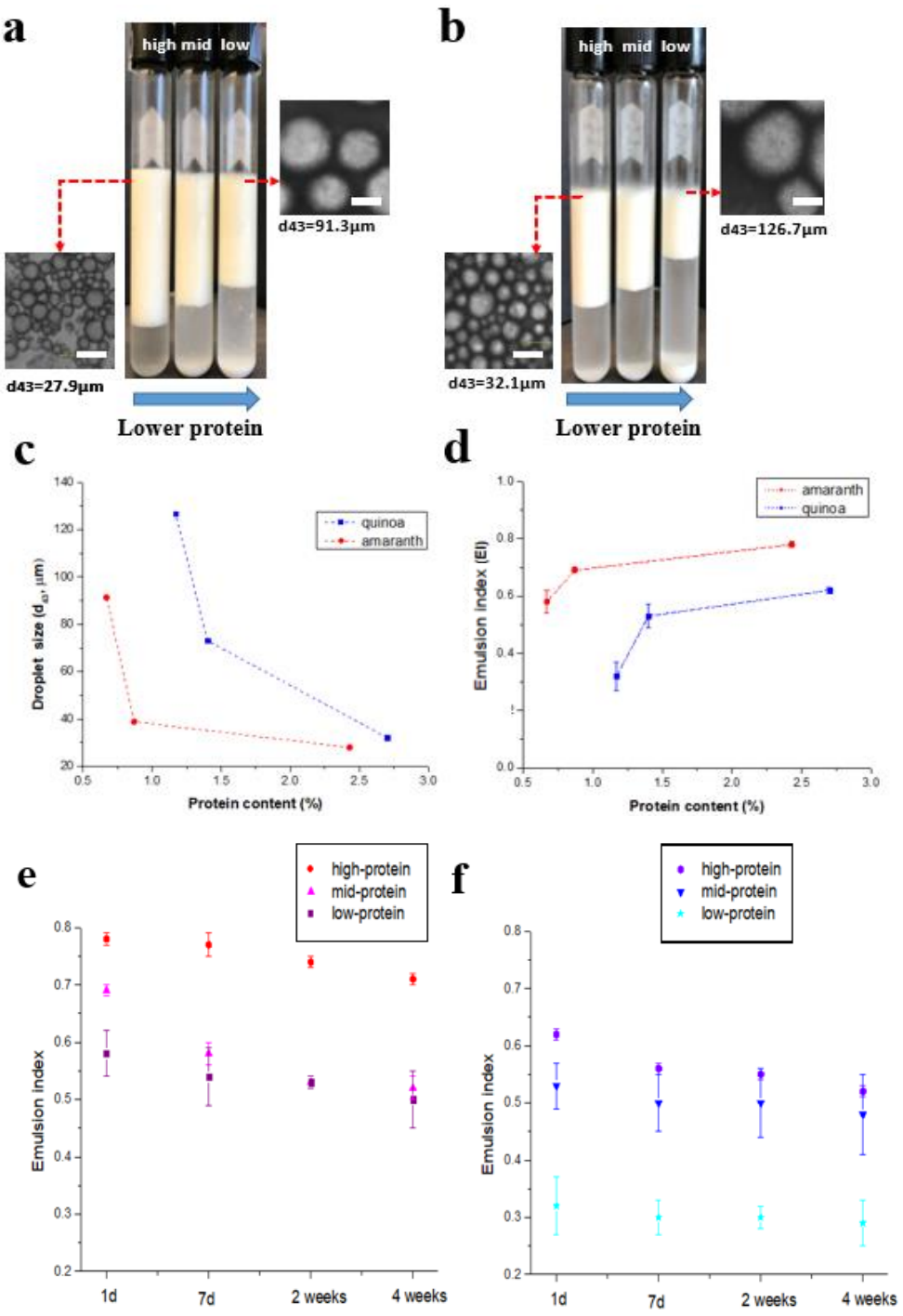

Figure 2.3. Effect of starch's protein content on emulsifying ability. Digital camera and optical microscope images of emulsions prepared at pH 7 using (a) amaranth and (b) quinoa starches with different protein contents ("low", "mid", and "high"), taken 1 day after preparation. Scale bar is 50 μm. Relationship of starch protein content *vs.* (c) emulsion droplet size and (d) EI of emulsions prepared using amaranth and quinoa starches at pH 7 and 1d after preparation. Four-week stability of Pickering emulsions prepared using (e) amaranth and (f) quinoa starches with different protein levels. Error bars refer to standard deviation (SD).

The effectiveness of amaranth and quinoa starches as Pickering emulsifiers appears to depend appreciably on their protein content (Figs. 2.3c and 2.3d). In particular, high-protein amaranth and quinoa starches formed 27.9μm and 32.1μm droplets, respectively, which appear comparable to, if not better than, traditional OSA-modified starches, which typically form larger droplets in the 38–48 μm range at similar conditions (Marefati et al., 2017; Saari et al., 2016). Of course, that protein generally plays a role in emulsification is not new; it has been shown by literature outside starch research. For example, the proteinaceous fractions of natural carbohydrate-protein conjugates like gum arabic or sugar beet pectin are believed to be the one responsible for making them bind to the oil/water interface. Their direct removal reduces their emulsification ability (Ozturk & McClements, 2016; Sweedman, Tizzotti, Schafer, & Gilbert, 2013; Evans, Ratcliffe, & Williams, 2013; Zhang, Wu, Lan, & Yang, 2014; Randall, Phillips, & Williams, 1988). Of course, the high amount of natural carbohydrate-protein conjugates required relative to the oil content (1:1) to form emulsions pose a disadvantage (Ozturk et al., 2016; Evans et al., 2013).

The role that the crude fat content of starch plays in its emulsifying ability has been hypothesized in the literature, but the verdict remains unclear (Tang, 2007). To shed some light on this matter, we compared the emulsifying ability of amaranth starch with high fat content versus low fat content while keeping the protein content relatively constant, and found that the crude fat content appears to have no significant effect on emulsifying ability (see Section S3 and Figure S1 under Supplementary Information).

Amaranth starch outperformed quinoa starch in terms of forming smaller droplet sizes and larger EIs, despite the fact that in this study our amaranth starch had a lower

protein content than quinoa at each protein level (at “low,” “mid,” “high”), which may be due to other factors. If we cut a vertical line across Fig. 2.3c or Fig. 2.3d to interpolate the droplet size at a particular protein level, it appears that for the same level of protein, amaranth worked as a better emulsifier than quinoa. This may be due to several factors. The main factor may be size: amaranth starch (1.2μm) is smaller than quinoa (1.5μm), which makes it easier for it to adsorb onto the oil/water interface, and should allow it to theoretically form smaller droplets (Destribats, Ravaine, Heroguez, Leal-Calderon, & Schmitt, 2010; Berton-Carabin et al., 2015). In general, a particle can form a Pickering emulsion with a droplet size one order of magnitude greater than the particle size, and smaller particles generally form smaller emulsions (Berton-Carabin et al., 2015; Xiao et al, 2016; Timgren et al., 2013). Another factor could be the fact that amaranth granules have sharper edges than quinoa (Fig. 2.2e vs. Fig. 2.2h), which has been theorized to help adsorption at the oil/water interface (Tcholakova, Denkov, & Lips, 2008).

Geometrically (approximating a granule as a sphere), as a particle increases in size, its cross-sectional area (the area it can use to cover and stabilize an emulsion droplet) increases by the square of the radius only, while its volume or mass increases by the cube of the radius. It follows that smaller granules have a higher total cross-sectional area and can thus sterically cover more emulsion droplet surface area than larger granules. Thus, given the same amount of oil and the same amount of starch, smaller starch granules can afford to stabilize smaller droplets (with a larger total surface area) while larger granules can only afford to stabilize larger droplets (with a lower total surface area). This may explain why amaranth granules can form emulsions

that are smaller than those formed by quinoa granules. Theoretical models elsewhere have confirmed this relationship (Destribats et al., 2010).

To check the stability of these emulsions, we also measured their EIs over 4 weeks. We found that all emulsions prepared using high-, mid-, and low-protein starches had a 10–20% reduction in EI (Figs 2.3e and 2.3f). High-protein and mid-protein amaranth starches retained the highest EIs after 4 weeks, while mid-protein and low-protein quinoa starches featured the lowest EIs. This may be due to both gravitational separation and coalescence. Stokes' law predicts that the gravitational phase separation rate of an emulsion increases by the square of the emulsion droplet size (Berton-Carabin et al., 2015; Joshi, et al., 2012). Thus, the larger quinoa-stabilized emulsion droplets should undergo phase separation (creaming) faster than smaller amaranth-stabilized emulsions, which explains why quinoa has smaller EIs over 4 weeks. Other factors that may have also affected the stability of these emulsions over time were their viscosity and Zeta potential, which will be discussed in Sections *3.5* and *3.6*.

3.4.2 *Effect of pH on emulsion droplet size, emulsion index, and 4-week stability*

To highlight the role that protein plays in starch's emulsifying ability, we also investigated the effect of pH on the emulsions formed by high-protein amaranth and quinoa starches. As we increased the pH from 3 to 10, the emulsion droplet sizes appeared to increase slightly for both amaranth- (Fig. 2.4a top) and quinoa-stabilized emulsions (Fig. 2.4b top). As expected, this slight increase in droplet sizes led to a reduction of the EIs for both amaranth- (Fig. 2.4a bottom) and quinoa-stabilized emulsions (Fig. 2.4b bottom). These relationships are summarized in Figs. 2.4c and 2.4d (see also Supplementary Tables S3 and S4).

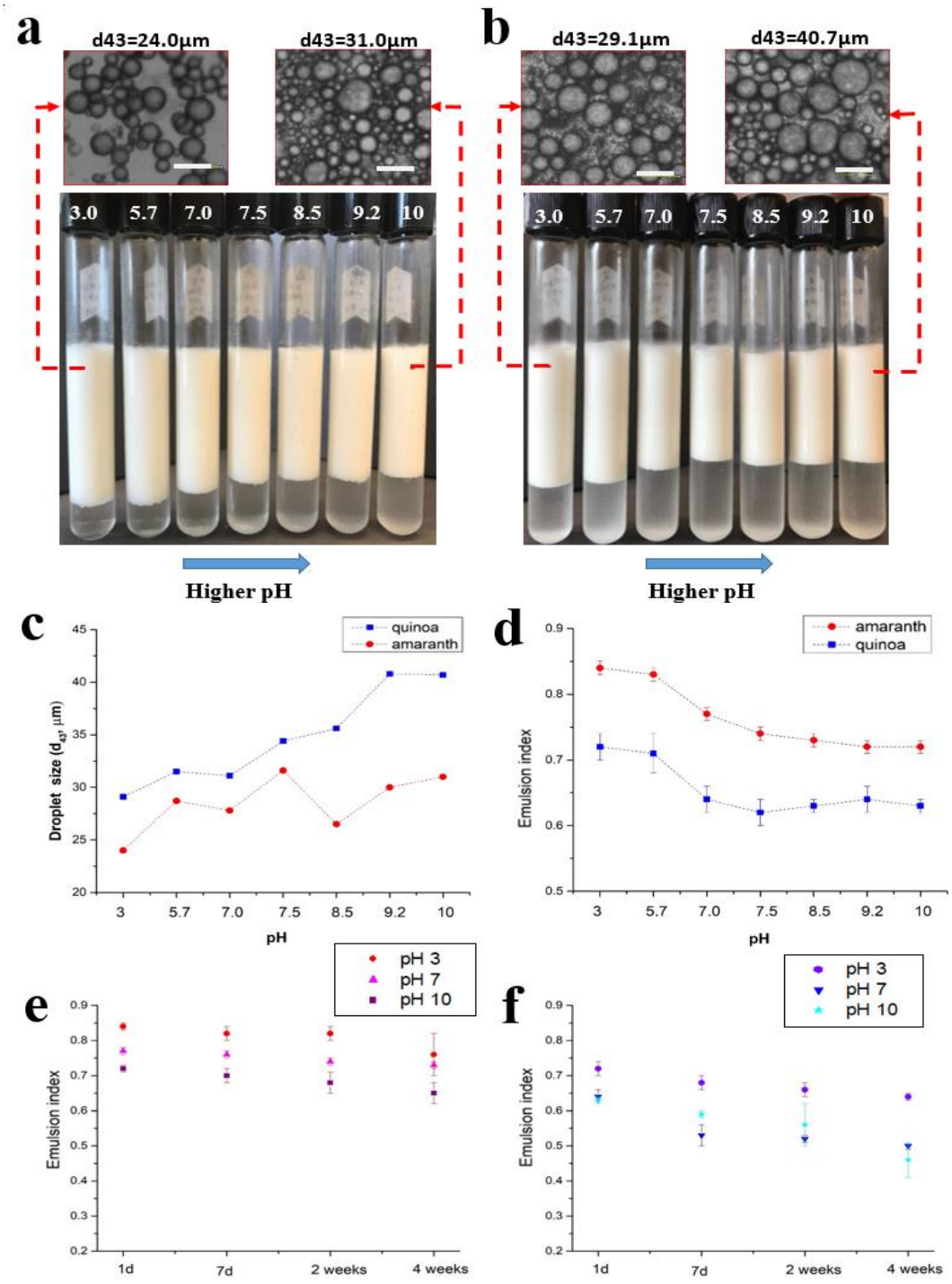

Figure 2.4. Effect of pH on starch's emulsifying ability. Digital camera and optical microscope images of emulsions prepared with high-protein (a) amaranth and (b) quinoa starches at different pHs (3.0, 5.7, 7.0, 7.5, 8.5, 9.2, 10) 1d after preparation. Scale bar is 50 µm. Relationship of the pH vs. (c) the emulsion droplet size and (d) the EI of emulsions prepared using high-protein amaranth and quinoa starches, 1 day after preparation. Four-week stability of Pickering emulsions prepared using high-protein (e) amaranth and (f) quinoa starches at pH 3, pH 7, and pH 10. Error bars refer to standard deviation (SD).

Emulsions formed using small-molecule surfactants and proteins are generally affected by pH due to the deprotonation or protonation of certain functional groups, which can change the surface charge and affect the stabilizing mechanism of repulsion between droplets. Pickering emulsions prepared using OSA-modified starch granules may show some slight variation when the pH is changed—Song et al. (2015), for example, saw a slight decrease in the EI of OSA-modified starch-stabilized emulsions when the pH was increased. However, in general, starch-stabilized Pickering emulsions are known to be otherwise resistant to pH variations because of the lack of sensitive functional groups, and because their main stabilizing mechanism is steric hindrance rather than electrostatic repulsion (McClements, 2016). In contrast, our results show that Pickering emulsions stabilized by high-protein starches are actually affected by pH. This suggests that the ability of starch granules to form Pickering emulsions depends heavily on their protein content, because we can expect the protein to change starch's surface charge when pH is altered.

The literature shows that the proteins from amaranth starch granules have an isoelectric point (pI) at approximately pH 4–6 (Bolontrade & Scilingo, 2013). More specifically, the different protein fractions composing amaranth proteins have pIs at different pHs—7.5 (albumins); 5.6, 9.2, 5.2-5.8 (globulins); and 5.7-6.3 (glutelins), with the pIs for prolamins still unknown. Similarly, the proteins on quinoa starch granules have a pI at the following pHs: 5.0–6.5 (globulins), with the pIs for albumins, glutelins, and prolamins still unknown (Janssen et al., 2017). Thus, in general, at a pH of 4–6.5, both amaranth proteins and quinoa proteins will display a relatively neutral charge, and

as we increase the pH farther away from the isoelectric point up to pH 10, we expect a more negative charge (Joshi, et al., 2012). Amaranth and quinoa protein extracts generally have been found to display poor solubility at low pH values of 3.0–5.0 (2–35% solubility), and good solubility at higher pHs of 5.0–11.0 (50–90% solubility) (Janssen et al., 2017). Lower solubility at low pHs indicates that these proteins are more hydrophobic under these conditions. Thus, we argue that at low pH, the relatively neutral charge of the residual proteins on the surface of both amaranth and quinoa starches makes them more hydrophobic and thus more effective as emulsifiers, which is why they form smaller emulsion droplets and higher emulsion indices at low pH. On the other hand, at higher pHs, the negative charge of these proteins makes these starches less hydrophobic and thus less effective emulsifiers, resulting in larger emulsion droplets and lower EIs. (See Section *3.6.2* for supporting Zeta potential data showing that the surface charge indeed becomes more negative at higher pH.) Improved emulsifying ability at low pH could also be due to the extensive uncoiling of amaranth proteins that can be induced by low pH, which can further improve the emulsifying ability (Janssen et al., 2017). Furthermore, studies have shown that at very low pH (near pH 2), amaranth proteins may actually become denatured, dissociated, or partially hydrolyzed into smaller fragments by an endogenous peptidase, which will allow it to diffuse faster into an air/water interface to make a more flexible or viscoelastic film, thus forming more stable foams at low pH than at high pH (Janssen et al., 2017; Bolontrade et al., 2013).

To check whether pH also affected emulsion stability, we measured the EI over a 4-week period (Figs 2.4e and 2.4f; see also Supplementary Tables S3 and S4). We

found that all the Pickering emulsions showed a 10–20% decrease in their EI after this period. And as expected, emulsions prepared at pH 3 retained higher EIs than those prepared at pH 10 after 4 weeks. Emulsions stabilized with amaranth starch (Fig. 2.4e) also appeared, again, to outperform those stabilized with quinoa starch (Fig. 2.4f), having higher EIs at all pH levels tested. Other factors that may have also affected the stability of these emulsions over time were their viscosity and Zeta potential, which will be discussed in the following sections.

3.5 Rheology

3.5.1 Effect of protein content on viscosity and elasticity

As the protein content of starch granules were increased, we saw in Fig. 2.3c that the droplet size of the Pickering emulsions decreased. Our rheology results demonstrate that a higher starch protein content (and smaller emulsion droplet size) also led to a higher viscosity for both amaranth-stabilized emulsions (Fig. 2.5a) and quinoa-stabilized emulsions (Fig. 2.5b). Smaller emulsions had a higher viscosity than larger emulsions across almost the entire range of shear rates tested (0.02–100 s^{-1}). Several papers have shown the same relationship using surfactant-stabilized oil/water emulsions, citing several possible reasons for the trend (Pal, 1996; Chanamai et al., 2000).

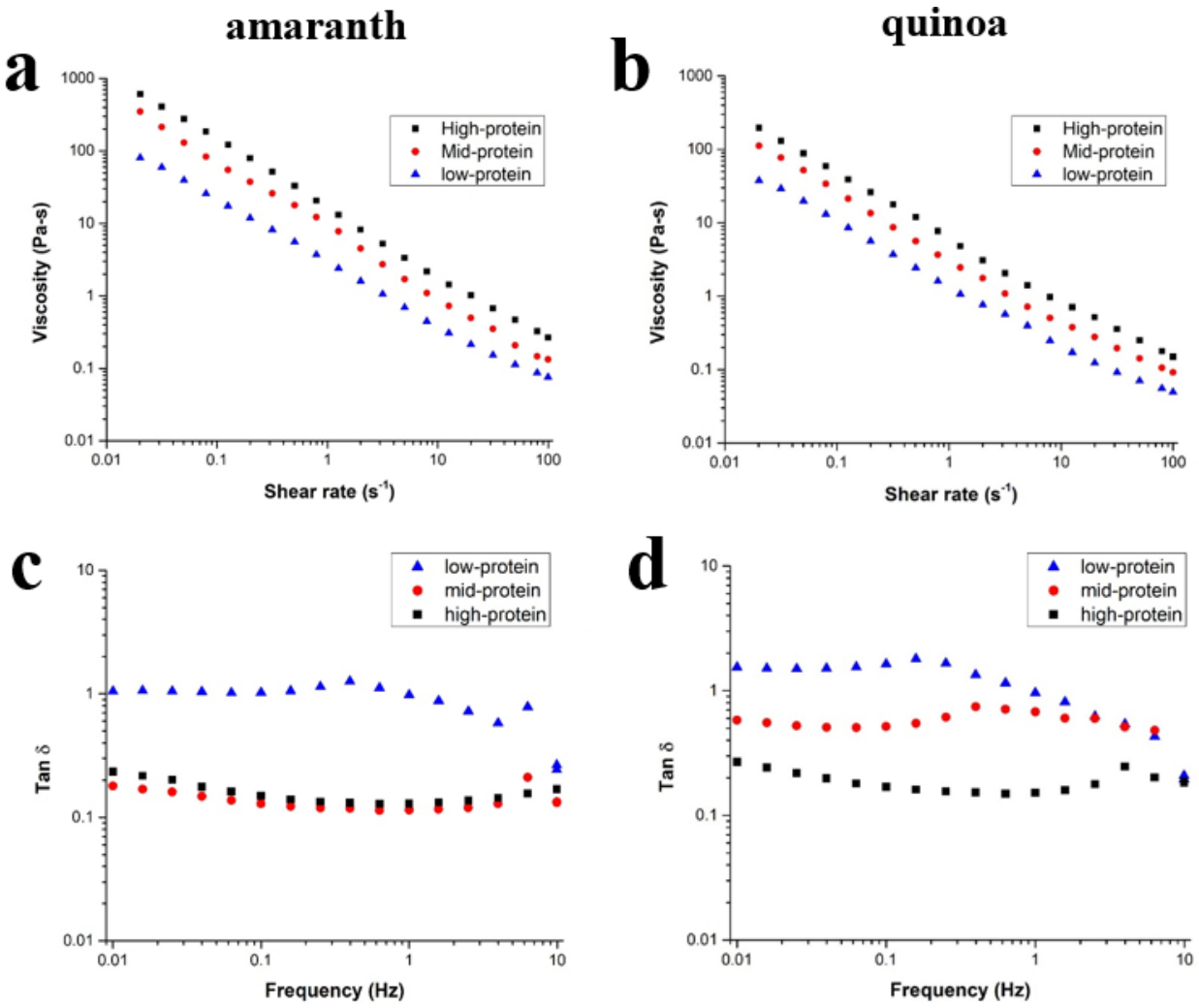

Figure 2.5. Effect of starch's protein content and the pH on the rheology of starch-stabilized Pickering emulsions. Viscosity vs. shear rate graphs of (a) amaranth- and (b) quinoa-stabilized Pickering emulsions at different protein levels using a log-log scale, measured 2 days after preparation at pH 7. Tan δ vs. frequency graphs of (c) amaranth- and (d) quinoa-stabilized Pickering emulsions at different protein levels using a log-log scale, also measured 2 days after preparation at pH 7 (continued…)

First, smaller droplets have a smaller mean distance of separation between them, leading to greater hydrodynamic interaction and collision frequency, and thus a higher viscosity. Second, as the droplet size decreases, the ratio between the thickness of the adsorbed starch layer and the droplet size increases, which leads to a higher effective volume fraction or a higher effective dispersed phase concentration. As we noted in the previous section, the effective volume fraction is $(1+\delta_x/r)^3$ times that of the actual volume fraction, where δ_x is the thickness of the adsorbed layer and r is the droplet radius (Chanamai et al., 2000). Thus, at smaller droplet sizes (lower r), the effective volume fraction of the dispersed phase is higher, leading to a higher viscosity. A recent modeling study on the rheology of Pickering emulsions has also shown that a smaller droplet size leads to higher viscosity (Pal, 2018). Lastly, smaller droplets tend to be more monodisperse, and this also leads to higher viscosity (Pal, 1996). This higher viscosity can further help explain why emulsions stabilized by high-protein starches retained the highest EI over 4 weeks (Figs. 2.3e and 2.3f), as compared to those stabilized by low-protein starches, because a higher viscosity delayed phase separation. Notice also that across all protein levels (high, mid, low), amaranth-stabilized emulsions (Fig. 2.5a) showed higher viscosity than quinoa-stabilized emulsions (Fig. 2.5b), which again may be due to the smaller size of amaranth granules and thus the smaller emulsion droplets that they tend to form, and thus the greater 4-week stability.

Both amaranth- and quinoa-stabilized emulsions also exhibited shear-thinning behavior. As the shear stress was increased, the randomly distributed emulsions may have begun to align themselves with the flow into strings or layers, which reduced resistance to the flow of the fluid, thus decreasing viscosity (McClements, 2016). We note here that any excess amount of granules in the continuous phase may have also formed a 3D network to stabilize these emulsions, and in addition could have increased the viscosity of the aqueous phase and thus also delayed phase separation according to Stokes' law (Aveyard et al., 2003; Binks & Lumsdon, 2000).

In addition, we also found that these emulsions exhibited viscoelastic behavior, measured by **tan δ** (tan $\delta = G''/G'$), where G'' is the loss modulus or a measure of energy lost due to viscous dissipation in the material, and G' is the storage modulus, or a measure of the energy stored in the material. For both amaranth-stabilized (Fig. 2.5c) and quinoa-stabilized emulsions (Fig. 2.5d), low-protein starches formed less elastic Pickering emulsions, generally with tan $\delta > 1$, while mid- and high-protein starches produced more elastic Pickering emulsions with tan $\delta < 1$.

This gel-like behavior may be attributed to inter-droplet network formation that resists flow (Song et al., 2015). In general, Pickering emulsions show gel-like elasticity in frequency sweep tests, which is ascribed to the rigid interface created by the solid particles, which leads to surface elasticity (Xiao et al., 2016). Compressing a Pickering emulsion causes the solid interface to be slightly deformed, but strong adhesion between the solid particles produces a kind of scaffold that can cause it to revert back, thus exhibiting elasticity (Xiao et al., 2016). And because a higher protein content leads to the formation of smaller emulsion droplets, and smaller emulsion droplets in turn have

a more packed structure with more granules rubbing against each other in a scaffold, it follows that a higher protein content leads to more elastic Pickering emulsions.

3.5.2 *Effect of pH on viscosity and elasticity*

As the pH was increased, we saw that emulsion viscosity decreased (Fig. 2.5e for amaranth, and Fig. 2.5f for quinoa) across the shear rates tested. We expect the protein on the starch granule surface to become more negative as the pH goes up, and this can reduce the emulsion viscosity in two ways: first, a more negative charge makes the starch more hydrophilic overall, and thus reduces its emulsifying ability, causing it to form bigger emulsion droplets with lower effective volume and thus lower viscosity. Second, a more negative charge at high pH also causes the droplets to repel each other more, which allows them to slide across each other more easily when shear is applied, which translates again to a lower viscosity. Thus, both amaranth and quinoa starches had better emulsifying abilities at low pH and the resultant higher viscosity at low pH further helped the emulsions retain a high EI over a 4-week period. Amaranth, in particular, formed more viscous emulsions than quinoa across all pH levels tested, which again may be due to the smaller emulsions it formed.

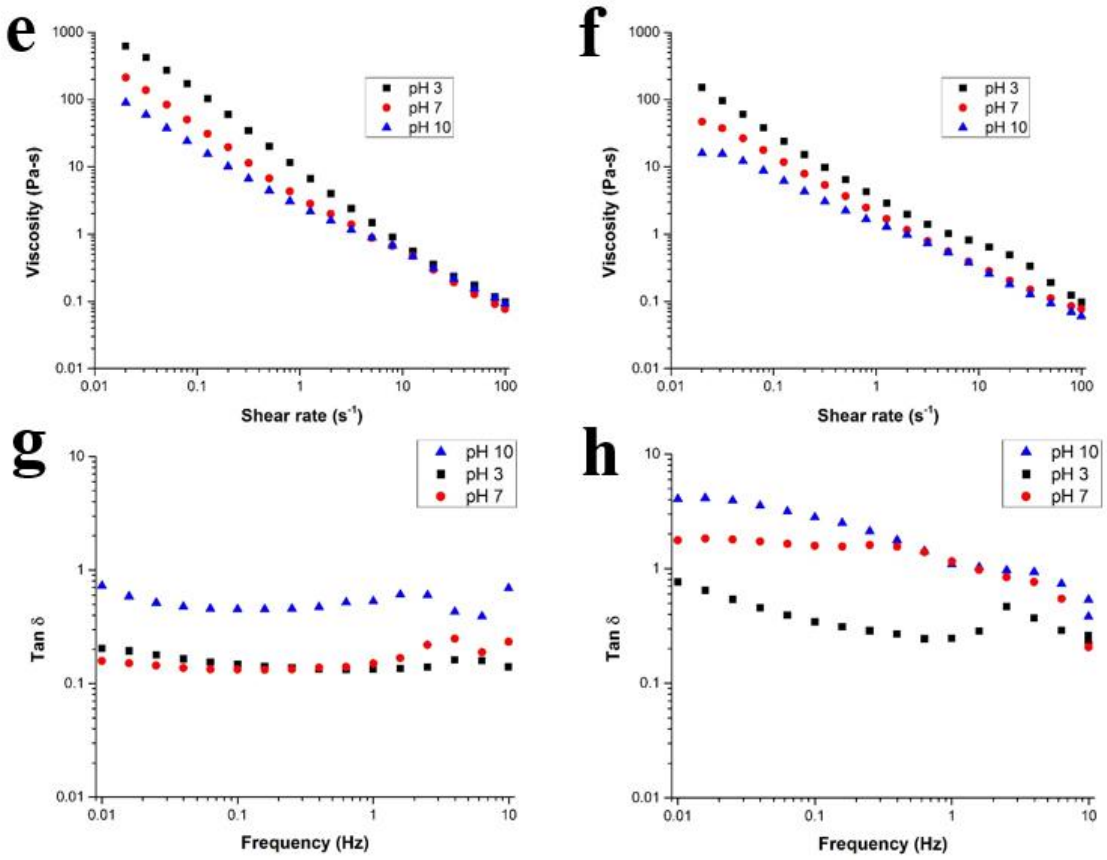

Figure 2.5 (continuation). Viscosity vs. shear rate graphs of (e) amaranth- and (f) quinoa-stabilized Pickering emulsions at pH 3.0, 7.0, and 10.0, using a log-log scale and measured 2 days after preparation. Tan δ vs. frequency graphs of (g) amaranth- and (h) quinoa-stabilized Pickering emulsions at pH 3.0, 7.0, and 10.0, using a log-log scale and also measured 2 days after preparation.

These Pickering emulsions also exhibited, in addition, viscoelastic behavior due to the solid granule scaffolds created between droplets. In general, these Pickering emulsions showed more elasticity at low pH than at high pH (Fig. 2.5g for amaranth and Fig. 2.5h for quinoa), likely because the smaller emulsion droplets formed at low pH allowed more starch granules to rub against each other when shear was applied, which deformed the droplet and, when the shear was removed, caused the granules to be pulled back into the oil/water interface, thus exhibiting better elasticity.

3.6 Zeta potential

3.6.1 Effect of protein content on Zeta potential

Zeta potential gives the net surface charge of an emulsion, and the higher the magnitude of this charge, the higher the repulsion between emulsion droplets and therefore the more stable they are over time (Joshi et al., 2012). As the protein content of starch was increased, we found that the Zeta potential of the Pickering emulsions formed also became more negative (measured after the 4-week stability study) (Fig. 2.6a). A higher protein content thus not only makes the starch more hydrophobic to form more stable, smaller emulsions, it also lends these emulsions at the same time a more negative net surface charge due to the presence of more COO^- groups that can help further stabilize the droplets by electrostatic repulsion. This supports our previous results showing that emulsions stabilized by high-protein starches have better 4-week stability (higher EIs) than those stabilized by low-protein starches (Figs. 2.3e for amaranth and 2.3f for quinoa).

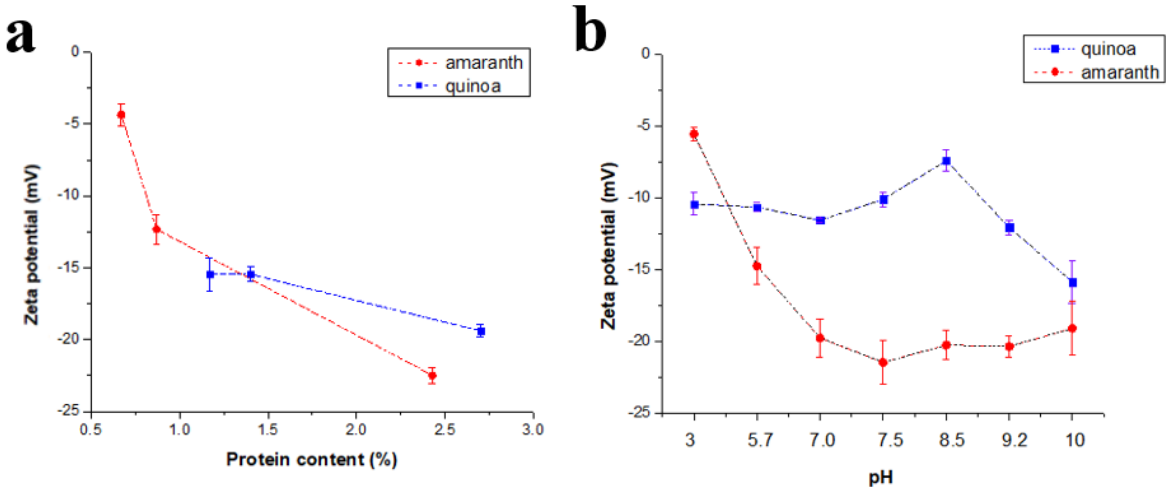

Figure 2.6. Effect of (a) starch's protein content and (b) pH on the Zeta potential of starch-stabilized Pickering emulsions. For (a), emulsions were prepared at pH 7. All Zeta potential values were measured 4 weeks after preparation, after a 4-week stability study. Error bars refer to standard deviation (SD).

3.6.2 Effect of pH on Zeta potential

As the pH was increased from 3 to 10, the Zeta potential of the Pickering emulsions prepared using high-protein amaranth and quinoa starches became more negative (measured after the 4-week stability study) (Fig. 2.6b). This trend confirms our expectation that as we increase the pH farther away from the isoelectric point (pH 4–6) of the residual proteins on the starch, the charge of these residual proteins should become more negative. This more negative charge at high pH (at the same protein content and the same amount of hydrophobic moieties) makes starch more hydrophilic overall (i.e., less hydrophobic), and reduces its emulsifying ability. This helps explain why we found that high-protein starches had better emulsifying abilities at lower pH than at high pH (Figs. 2.4a for amaranth and 2.4b for quinoa) and why they are also

more stable at lower pH over a 4-week period (Figs. 2.4e for amaranth and 2.4f for quinoa).

4. Conclusions

In the growing trend towards the use of natural, clean-label emulsifiers in food, we hope that the alkaline isolation method presented here can be used to produce high-protein amaranth and quinoa starches that take advantage of their protein's native hydrophobicity for improved emulsification without further chemical treatment. High-protein starches appear to have emulsifying abilities comparable to, if not better than, that of OSA-modified starches in the literature. Amaranth starch, in particular, exhibits a better emulsifying ability than quinoa starch at all the protein and pH levels tested, which may be due to its smaller particle size or more angular shape. We highlighted the main function that the protein contents of amaranth and quinoa starches play in their emulsifying abilities by performing a serial reduction of the protein content—from high-protein (> 2%) to low-protein levels (~1%)—and showing that this directly reduced their respective abilities to form emulsions. High-protein starches, being more hydrophobic than low-protein starches, formed smaller emulsion droplets with higher EIs, higher viscosity and elasticity, and better 4-week stability. Reduction of starch's crude fat content, on the other hand, did not have a significant effect. In addition, decreasing the pH from pH 10 to pH 3 improved these starches' emulsifying abilities, a trend that can be attributed to the less negative charge of proteins at lower pH, making these starches more hydrophobic, and thus resulting in smaller emulsion droplets with higher EIs, higher viscosity and elasticity, and better 4-week stability. This variation of

emulsifying ability with pH further underscores the key role that protein content plays in starch's emulsifying ability.

References

Aveyard, R., Binks, B. P., & Clint, J. H. (2003). Emulsions stabilized solely by colloidal particles. *Advances in Colloid and Interface Science, 100-102*, 503-546.

Baldwin, P. M. (2001). Starch-granule-associated proteins: A review. *Starch/Starke, 53*, 475-503.

Berton-Carabin, C., & Schroen, K. (2015). Pickering emulsions for food applications: Background, trends, and challenges. *Annual Review of Food Science and Technology, 6*, 263-97.

Binks, B., & Lumsdon, S. (2000). Catastrophic phase inversion of water-in-oil emulsions stabilized by hydrophobic silica. *Langmuir, 16*(6), 2539-2547.

Bolontrade, A., & Scilingo, A. A. (2013). Amaranth proteins foaming properties: adsorption kinetics and foam formation--part 1. *Colloids and Surfaces B: Biointerfaces, 105*, 319-327.

Bon, S. A. (2015). The phenomenon of Pickering stabilization: A basic introduction. In S. B. To Ngai, *Particle-stabilized emulsions and colloids: Formation and applications* (p. 1). Cambridge, UK: The Royal Society of Chemistry.

Bressani, R., & Garcia-Vela, L. A. (1990). Protein fractions in Amaranth grain and their chemical characterization. *Journal of Agricultural and Food Chemistry, 38*(5), 1205-1209.

Chanamai, R., & McClements, D. J. (2000). Dependence of creaming and rheology of monodisperse oil-in-water emulsions on droplet size and concentration. *Colloids and Surfaces A, 172*, 79-86.

Destribats, M., Ravaine, S., Heroguez, V., Leal-Calderon, F., & Schmitt, V. (2010). Outstanding stability of poorly-protected Pickering emulsions. In *Trends in colloid and interface science XXIII. Progress in colloid and polymer science vol 137* (pp. 13-18). Berlin, Heidelberg: Springer.

Dickinson, E. (2010). Food emulsions and foams: stabilization by particle. *Current Opinion in Colloid and Interface Science, 15*, 40-49.

Evans, M., Ratcliffe, I., & Williams, P. A. (2013). Emulsion stabilisation using polysaccharide-protein complexes. *Current Opinion in Colloid & Interface Science, 18,* 272-282.

Fairbanks, D., Burgener, K., Robison, L., Anderson, W., & Ballon, E. (1990). Electrophoretic characterization of quinoa seed proteins. *Plant breeding, 104,* 190-195.

Gurbuz, G., Kauntola, V., Diaz, J. M., & Jouppila, K. (2018). Oxidative and physical stability of oil-in-waer emulsions prepapred with quinoa and amaranth proteins. *European Food Research and Technology, 244,* 469-479.

Janssen, F., Pauly, A., Rombouts, I., Jansens, K. J., & Delcour, J. (2017). Proteins of Amaranth, Buckwheat, and Quinoa: A Food science and technology perspective. *Comprehensive Reviews in Food Science and Food Safety, 16,* 39-58.

Joshi, M., Adhikari, B., Aldred, P., Panozzo, J., Kasapis, S., & Barrow, C. (2012). Interfacial and emulsifying properties of lentil protein isolate. *Food Chemistry, 134,* 1343-1353.

Li, C., Li, Y., Sun, P., & Yang, C. (2013). Pickering emulsions stabilized by native starch granules. *Colloids and Surfaces A: Physicochemical and Engineering Aspects, 431,* 142-149.

Lim, S.-T., Kyonggi-do, J.-H. L., Shin, D.-H., & Lim, H. S. (1999). Comparison of protein extraction solutions for rice starch isolation and effects of residual protein content on starch pasting properties. *Starch, 51*(4), 120-125.

Marefati, A., Matos, M., Wiege, B. H., & Rayner, M. (2018). Pickering emulsifiers based on hydrophobically modified small granular starches Part II-Effects of modification on emulsifying ability. *Carbohydrate Polymers, 201,* 416-424.

Marefati, A., Wiege, B., Haase, N., Matos, M., & Rayner, M. (2017). Pickering emulsifiers based on hydrophobically modified small granular starches: Part 1: manufacturing and physico-chemical characterization. *Carbohydrate Polymers, 175,* 473-483.

McClements, D. J. (2016). *Food Emulsions 3rd ed.* Boca Raton, FL: CRC Press.

Osborne, T. B. (1907). *The proteins of the wheat kernel.* Washington, DC: University of Caliifornia Libraries.

Ozturk, B., & McClements, D. J. (2016). Progress in natural emulsifiers for utilization in food emulsions. *Current Opinion in Food Science, 7,* 1-6.

Pal, R. (1996). Effect of droplet size on the rheology of emulsions. *AIChE Journal, 42*(11), 3181-3190.

Pal, R. (2018). A Simple Model for the viscosity of Pickering emulsions. *Fluids, 3*(2).

Randall, R. C., Phillips, G. O., & Williams, P. A. (1988). The role of th proteinaceous component on the emulsifying properties of gum arabic. *Food Hydrocolloids, 2*(2), 131-140.

Saari, H., Heravifar, K., Rayner, M., Wahlgren, M., & Sjoo, M. (2016). Preparation and characterization of starch particles for use in Pickering emulsions. *Cereal Chemistry, 93*(2), 116-124.

Seguchi, M. (1984). Oil-binding ability of heat-treated wheat starch. *Cereal Chemistry, 61*(3), 248-250.

Song, X., Pei, Y., Qiao, M., Ma, F., Ren, H., & Zhao, Q. (2015). Preparation and characterization of Pickering emulsions stabilized by hydrophobic starch particles. *Food Hydrocolloids, 45*, 256-263.

Sweedman, M. C., Tizzotti, M. J., Schafer, C., & Gilbert, R. G. (2013). Structure and physicochemical properties of octenyl succinic anhydride modified starches: a review. *Carbohydrate Polymers, 92*, 905-920.

Tang, C. (2007). Thermal properties of buckwheat proteins as related to their lipid contents. *Food Research International, 40*(3), 381-387.

Tcholakova, S., Denkov, N., & Lips, A. (2008). Comparison of solid particles, globular proteins, and surfactants as emulsifiers. *Physical Chemistry Chemical Physics, 10*, 1608-1627.

Timgren, A., Rayner, M., Dejmek, P., Marku, D., & Sjoo, M. (2013). Emulsion stabilizing capacity of intact starch granules modified by heat treatment or octenyl succinic anhydride. *Food Science and Nutrition, 1*(2), 157-171.

Timgren, A., Rayner, M., Sjoo, M., & Dejmek, P. (2011). Starch particles for food based Pickering emulsions. *Procedia Food Science , 1*, 95-103.

Xia, X., Li, G., Liao, F., Zhang, F., Zheng, J., & Kan, J. (2015). General structure and physicochemical properties of starches from amaranth grain. *International Journal of Food Properties, 18*, 1029-1037.

Xiao, J., Li, Y., & Huang, Q. (2016). Recent advances on food-grade particles stabilized Pickering emulsions: Fabrication, characterization, and research trends. *Trends in Food Science and Technology, 55*, 48-60.

Yang, Y., Fang, Z., Chen, X., Zhang, W., Xie, Y., Chen, Y.; Liu, Z.; Yuan, W. (2017). An overview of Pickering emulsions: Solid-particle materials, classification, morphology, and applications. *Frontiers in Pharmacology, 8*(287), 1-20.

Zhang, J., Wu, N., Lan, T., & Yang, X. (2014). Improvement in emulsifying properties of soy protein isolate by conjugation with maltodextrin using high-temperature, short-time dry-heating Maillard reaction. *International Journal of Food Science an Technology, 49,* 460-467.

Zhu, F. (2019). Starch-based Pickering emulsions: Fabrication, properties, and applications. *Trends in Food Science & Technology, 85*, 129-137.

Supplementary Information

S1. Brief review of conventional surfactants

Here we provide a brief review of conventional small-molecule surfactants to aid in understanding their difference from Pickering emulsifiers and aid in this study's discussion of its results. Generally, when two immiscible liquids like oil and water are poured together, they experience an interfacial tension γ (N/m) that the system spontaneously tries to minimize by undergoing phase separation, which reduces the total contact area A (m^2) between them and lowers the free energy G (Berton-Carabin & Schroen, 2015):

$$\Delta G = \gamma \Delta A \qquad (2.5)$$

Thus, to successfully disperse one immiscible phase into another as fine droplets (which increases the contact area and makes the system thermodynamically unstable), mechanical energy must be added (e.g., by applying a high shear or mixing), and then to prevent separation back into the two phases, a conventional emulsifier is added—typically a small-molecule, soluble surfactant (< 1nm, 250–1,200 g/mol) or a biopolymer, like casein protein. These amphiphilic emulsifiers, having both a hydrophilic part and a hydrophobic part, will adsorb onto the oil/water interface of the droplets as they form (Fig. 2.1a), and do two things: 1) they will lower the interfacial tension due to the emulsifier's amphiphilicity, making it easier to actually disperse one liquid into the other by facilitating droplet breakup and making smaller droplets, and also delay phase separation; and 2) after the emulsions are formed, they can provide

steric hindrance (a few nanometers in thickness) and/or electrostatic repulsion between droplets, thereby kinetically stabilizing them against coalescence for a certain period of time, thus extending their shelf life (Marefati, Wiege, Haase, Matos, & Rayner, 2017; Yang, et al., 2017; Xiao, Li, & Huang, 2016; Pichot, Duffus, Zafeiri, Spyropoulos, & Norton, 2015; Joshi, et al., 2012; Timgren, Rayner, Dejmek, Marku, & Sjoo, 2013; Berton-Carabin et al., 2015).

We can predict how a particular surfactant will behave and how effectively it can stabilize an emulsion using two parameters: 1) its hydrophile-lipophile balance (HLB) number and 2) its geometry, which will determine how well it will pack at the oil/water interface. A hydrophilic surfactant (high HLB, 10–18) with a large area at its hydrophilic head and a small area at its hydrophobic tail will tend to curve around an oil droplet, thus forming an oil-in-water emulsion. Conversely, a hydrophobic surfactant (low HLB, 3–6) with a larger area at its hydrophobic chain would tend to form a water-in-oil emulsion (Aveyard, Binks, & Clint, 2003; McClements, 2016). Extremely low (<3) or extremely high (>18) HLB numbers mean that they would rather dissolve in oil or water rather than stabilize emulsions, and intermediate HLB numbers (7–9) are considered to be good "wetting agents."

In general, small amphiphilic surfactants are required only at low concentrations (<1%) in the formulation to form small, stable ~100–200-nm-size emulsions, while larger biopolymers like proteins are required at higher concentrations (>2%) to form relatively larger emulsions (0.5–2 μm) (Ozturk & McClements, 2016). Proteins can act as emulsifiers because they have polypeptide chains with both hydrophobic and hydrophilic amino acids and they can also stabilize the emulsions against aggregation

through electrostatic repulsion via either negative (—COO^-) or positive (—NH_3^+) charges (Ozturk et al., 2016). There is also some evidence that the protein layer may inhibit lipid oxidation via free-radical scavenging and metal chelation (Gurbuz, Kauntola, Diaz, & Jouppila, 2018). Currently, animal-based proteins, such as casein and whey, are already being used in the food industry as emulsion stabilizers, while plant-based proteins, such as soy, pea, and corn germ proteins have shown promise (Ozturk et al., 2016). While these small-molecule surfactants and proteins can indeed facilitate the formation of small and stable emulsions with an interfacial layer thickness of a few nanometers and a surface load of 1–3 mg/m^2 (amount of surfactant adsorbed per surface area), they can be easily detached from the interface with an energy of only 0.5–1 *kT* (surfactants) or 1–20 *kT* (proteins), where *k* is the Bolztmann's constant and *T* is the absolute temperature (Saari, Fuentes, Sjoo, Rayner, & Wahlgren, 2017; Berton-Carabin et al., 2015). By comparison, as will be discussed in the next section, Pickering emulsions require about 10^6–10^8 *kT* before solid particles can be detached from the interface.

S2. Brief review of Pickering emulsifiers

Solid particles are believed to work in a different way than conventional small emulsifiers (Berton-Carabin et al., 2015; Levine, Bowen, & Partridge, 1989). First of all, unlike small surfactants (< 1 nm), which diffuse easily and adsorb to the interface spontaneously, large solid particles (> 10 nm) require a sizable addition of kinetic energy for them to adsorb to the interface (Kaz, McGorty, Mani, Brenner, & Manoharan, 2012). Additionally, surfactants work because the self-orientation of their hydrophobic part to the oil phase and the hydrophilic part to the aqueous phase lowers the oil/water

interfacial tension. Solid particles, on the other hand, are not amphiphilic. Rather, they possess moderate hydrophobicity over their entire surface, making them partially wettable by both the oil and water phases, which allows them to adsorb at the interface (Fig. 2.1b). Solid particles lower the total oil/water tension by physically reducing the oil/water contact area by their physical presence at the interface (Levine et al., 1989), and once adsorbed they require a larger amount of energy (10^6–10^8 kT) to be desorbed than conventional, small-molecule emulsifiers, much higher than the thermal energy due to Brownian motion, unlike surfactants and proteins, which are easily detached (0.5–20 kT) (Marefati et al., 2017; Saari et al., 2017). Levine *et al*. (1989) have theorized that the stability of Pickering emulsions can be predicted by the magnitude of this desorption energy:

$$\Delta G_d = \pi r^2 \gamma_{oil/water}(1 - |cos\theta|)^2 \qquad (2.6)$$

in which $\gamma_{oil/water}$ is the oil/water interfacial tension, r is the radius of the solid particle (particle size), and θ is the contact angle that the solid particle makes at the oil/water interface, which reflects the particle's moderate hydrophobicity or partial wettability in both the oil and water phases but solubility in neither (Fig. 2.1b) (Tang, Quinlan, & Tam, 2015; Levine et al., 1989; Aveyard et al., 2003; Matos et al., 2017; Xiao et al., 2016). Both the contact angle and the particle size have an impact during and after emulsification. Particles that are more partially wettable by both oil and water ($30° < \Theta < 150°$) or are of a smaller size will diffuse faster and adsorb more easily to the oil/water interface, promoting the formation of smaller droplets (Timgren et al., 2013; Matos et al., 2017; Tcholakova, Denkov, & Lips, 2008). Likewise, after adsorption, more partially wettable particles ($30° < \Theta < 150°$) or larger particles will be harder to dislodge

from the interface because of the larger desorption energy required to do so, assuming negligible effects from gravity (Aveyard et al., 2003). Very small particles (~1 nm), even if they are moderately hydrophobic, are quite easy to detach, while larger particles (~1 μm) are effectively irreversibly adsorbed, even if they are less hydrophobic to begin with (Aveyard et al., 2003; Berton-Carabi et al., 2015). This is why even millimeter-sized Pickering emulsions can be stabilized effectively by large solid particles, due to the large desorption energy (Zhai & Efrima, 1996). Extremely hydrophilic ($0° < \Theta < 30°$) or extremely hydrophobic particles ($150° < \Theta < 180°$) would not form stable emulsions, however, because they would remain either in the water or oil phase only during mixing or they would be easily detached after emulsion formation (Aveyard et al., 2003; Xiao et al., 2016). In addition, it has also been theorized that particles with sharper edges may form emulsions more easily (Tcholakova et al., 2008), while particles with smoother surfaces adhere better to the interface (Bon, 2015; Ballard & Bon, 2011).

And lastly, small surfactants provide only a thin barrier against coalescence (a few nanometers), while large solid particles provide a thicker steric barrier (~10 nm to 1 μm, depending on the particle size) against coalescence and Ostwald ripening (Matos et al., 2017; Aveyard et al., 2003; Tang et al., 2015; Berton-Carabin et al., 2015; Marefati et al., 2017; Zhu, 2019). Of course, the surface load (mg emulsifier/m^2) needed to make these Pickering emulsions will also be higher than that for small surfactants, so a higher emulsifier concentration is needed (Berton-Carabin et al., 2015).

S3. Effect of crude fat content on starch's emulsifying ability

We studied the effect of the crude fat content of amaranth starch on its emulsifying ability by using hexane extraction to preferentially remove fat and keep the protein content relatively constant (Thiex, Anderson, & Gildemeister, 2003). Afterwards, we prepared emulsions from these starches then compared the emulsion index (EI) and droplet size distribution before and after hexane extraction. The hexane extraction was performed using a 1:4 starch:hexane w/w ratio, mixing at room temperature for 3h, replacing the solvent after every hour, then washing 1x acetone, 2x deionized water, then freeze-drying. This extraction method decreased the crude fat content from 1.6% down to 0.1%. By contrast, the protein content was only slightly reduced from 2.3% to 1.9%.

Emulsions were prepared at pH 7 buffer in triplicate. The amaranth samples containing 1.6% fat and 0.1% fat gave the same emulsion indices (0.73±0.01 vs. 0.73±0.01, respectively) and similar droplet size distributions (d_{43}=27.4μm, PDI=1.2 vs. d_{43}=27.1μm, PDI=1.3, respectively). The crude fat content of starch appears to have no significant effect on its Pickering emulsifying ability (see Supplementary Figure S1).

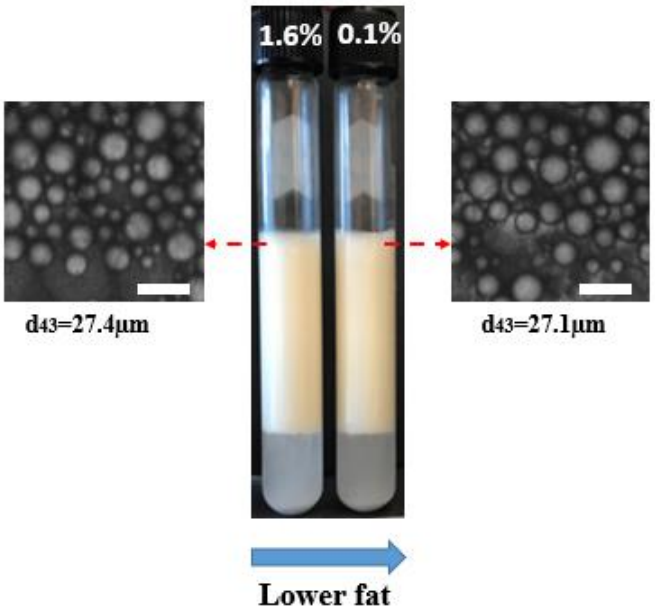

Supplementary Figure S1. Effect of crude fat content on the emulsion index (EI) and droplet size (1d) of emulsions stabilized by amaranth starch. Scale bar is 50 μm.

Supplementary Table S1. Effect of starch's protein content on the emulsion index (EI) and initial droplet size (1d) of emulsions stabilized by amaranth starch.

Protein (%)	Emulsion index				Droplet size distribution		
	1d	7d	2 weeks	4 weeks	d_{32}	d_{43}	PDI
0.67 ± 0.06 (low)	0.58 ± 0.04	0.54 ± 0.05	0.53±0.01	0.50±0.05	85.2	91.3	1.23
0.87 ± 0.06 (mid)	0.69 ± 0.01	0.58 ± 0.02	0.53±0.01	0.52±0.02	35.8	38.8	1.35
2.43 ± 0.06 (high)	0.78 ± 0.01	0.77 ± 0.02	0.74±0.01	0.71±0.01	25.8	27.9	1.35

Supplementary Table S2. Effect of starch's protein content on the emulsion index (EI) and initial droplet size (1d) of emulsions stabilized by quinoa starch.

Protein (%)	Emulsion index				Droplet size distribution		
	1d	7d	2 weeks	4 weeks	d_{32}	d_{43}	PDI
1.17 ± 0.06 (low)	0.32 ± 0.05	0.30 ± 0.03	0.30 ± 0.02	0.29 ± 0.03	120.2	126.7	1.19
1.40 ± 0.00 (mid)	0.53 ± 0.04	0.50 ± 0.05	0.50 ± 0.06	0.48 ± 0.07	69.2	73.1	1.20
2.70 ± 0.00 (high)	0.62 ± 0.01	0.56 ± 0.01	0.55 ± 0.01	0.52 ± 0.01	29.8	32.1	1.38

Supplementary Table S3. Effect of pH on the emulsion index (EI) and initial droplet size (1d) of emulsions stabilized by amaranth starch.

pH	Emulsion index				Droplet size distribution		
	1d	7d	2 weeks	4 weeks	d_{32}	d_{43}	PDI
3.0	0.84 ± 0.01	0.82 ± 0.02	0.82 ± 0.02	0.76 ± 0.06	22.5	24.0	1.27
5.7	0.83 ± 0.01	0.82 ± 0.02	0.80 ± 0.01	0.79 ± 0.02	26.5	28.7	1.38
7.0	0.77 ± 0.01	0.76 ± 0.01	0.74 ± 0.01	0.73 ± 0.01	24.4	27.8	1.59
7.5	0.74 ± 0.01	0.71 ± 0.03	0.68 ± 0.01	0.66 ± 0.02	27.9	31.6	1.53
8.5	0.73 ± 0.01	0.72 ± 0.02	0.72 ± 0.02	0.66 ± 0.02	23.6	26.5	1.49
9.2	0.72 ± 0.01	0.70 ± 0.02	0.70 ± 0.01	0.66 ± 0.02	24.8	30.0	1.73
10.0	0.72 ± 0.01	0.70 ± 0.02	0.68 ± 0.03	0.65 ± 0.03	25.3	31.0	1.90

Supplementary Table S4 Effect of pH on the emulsion index (EI) and initial droplet size (1d) of emulsions stabilized by quinoa starch.

pH	Emulsion index				Droplet size distribution		
	1d	7d	2 weeks	4 weeks	d_{32}	d_{43}	PDI
3.0	0.72 ± 0.02	0.68 ± 0.02	0.66 ± 0.02	0.64 ± 0.01	27.0	29.1	1.31
5.7	0.71 ± 0.03	0.66 ± 0.03	0.63 ± 0.03	0.62 ± 0.03	28.5	31.5	1.41
7.0	0.64 ± 0.02	0.53 ± 0.03	0.52 ± 0.01	0.50 ± 0.01	28.4	31.1	1.36
7.5	0.62 ± 0.02	0.53 ± 0.02	0.51 ± 0.03	0.50 ± 0.03	31.5	34.4	1.39
8.5	0.63 ± 0.01	0.58 ± 0.03	0.57 ± 0.04	0.56 ± 0.05	32.1	35.6	1.43
9.2	0.64 ± 0.02	0.57 ± 0.02	0.56 ± 0.04	0.55 ± 0.05	36.4	40.8	1.48
10.0	0.63 ± 0.01	0.59 ± 0.01	0.56 ± 0.06	0.46 ± 0.05	35.8	40.7	1.60

References

Aveyard, R., Binks, B. P., & Clint, J. H. (2003). Emulsions stabilized solely by colloidal particles. *Advances in colloid and interface science, 100-102*, 503-546.

Ballard, N., & Bon, S. A. (2011). Hybrid Biological Spores wrapped in a mesh composed of interpenetrating polymer nanoparticles as "patchy" Pickering stabilizers. *Polymer Chemistry, 2*(4), 823-827.

Berton-Carabin, C., & Schroen, K. (2015). Pickering emulsions for food applications: Background, trends, and challenges. *Annual review of food science and technology, 6*, 263-97.

Bon, S. A. (2015). The Phenomenon of Pickering Stabilization: A Basic Introduction. In S. B. To Ngai, *Particle-Stabilized Emulsions and Colloids: Formation and Applications* (p. 1). Cambridge, UK: The Royal Society of Chemistry.

Gurbuz, G., Kauntola, V., Diaz, J. M., & Jouppila, K. (2018). Oxidative and physical stability of oil-in-waer emulsions prepapred with quinoa and amaranth proteins. *European Food Research and Technology, 244*, 469-479.

Joshi, M., Adhikari, B., Aldred, P., Panozzo, J., Kasapis, S., & Barrow, C. (2012). Interfacial and emulsifying properties of lentil protein isolate. *Food chemistry, 134*, 1343-1353.

Kaz, D. M., McGorty, R., Mani, M., Brenner, M. P., & Manoharan, V. (2012). Physical aging of the contact line on colloidal particles at liquid interfacecs. *Nature Materials, 11*(2), 138.

Levine, S., Bowen, B., & Partridge, S. (1989). Stabilization of emulsions by Fine Particles I. Partitioning of particles between continuous phase and oil/water interface. *Colloids and Surfaces, 38*, 325-343.

Marefati, A., Wiege, B., Haase, N., Matos, M., & Rayner, M. (2017). Pickering emulsifiers based on hydrophobically modified small granular starches: Part 1: manufacturing and physico-chemical characterization. *Carbohydrate Polymers, 175*, 473-483.

Matos, M., Marefati, A., Bordes, R., Gutierrez, G., & Rayner, M. (2017). Combined emulsifying capacity of polysaccharide particles of different size and shape. *Carbohydrate polymers, 169*, 127-138.

McClements, D. J. (2016). *Food Emulsions 3rd ed.* Boca Raton, FL: CRC Press.

Ozturk, B., & McClements, D. J. (2016). Progress in natural emulsifiers for utilization in food emulsions. *Current Opinion in Food Science, 7*, 1-6.

Pichot, R., Duffus, L., Zafeiri, I., Spyropoulos, F., & Norton, I. T. (2015). Particle-stabilized Food Emulsions. In *Particle-Stabilized Emulsions and Colloids: Formation and Applications* (pp. 247-282). Royal Society of Chemistry.

Saari, H., Fuentes, C., Sjoo, M., Rayner, M., & Wahlgren, M. (2017). Production of starch nanoparticles by dissolution and non-solvent precipitation for use in food-grade Pickering emulsions . *Carbohydrate Polymers, 157*, 558-566.

Tang, J., Quinlan, P. J., & Tam, K. (2015). Stimuli-responsive Pickering emulsions:recent advances and potential applications. *Soft matter, 11*, 3512-3529.

Tcholakova, S., Denkov, N., & Lips, A. (2008). Comparison of solid particles, globular proteins, and surfactants as emulsifiers. *Physical chemistry chemical physics, 10*, 1608-1627.

Thiex, N., Anderson, S., & Gildemeister, B. (2003). Crude fat, hexanes extraction, in feed, cereal grain, and forage (Randall/Soxtec/submersion method): Collaborative study. *Journal of AOAC International, 86*(5), 899-908.

Timgren, A., Rayner, M., Dejmek, P., Marku, D., & Sjoo, M. (2013). Emulsion stabilizing capacity of intact starch granules modified by heat treatment or octenyl succinic anhydride. *Food Science and Nutrition, 1*(2), 157-171.

Xiao, J., Li, Y., & Huang, Q. (2016). Recent advances on food-grade particles stabilized Pickering emulsions: Fabrication, characterization, and research trends. *Trends in Food Science and Technology, 55*, 48-60.

Yang, Y., Fang, Z., Chen, X., Zhang, W., Xie, Y., Chen, Y., . . . Yuan, W. (2017). An overview of Pickering emulsions: Solid-particle Materials, Classification, morphology, and applications. *Frontiers in Pharmacology, 8*(287), 1-20.

Zhai, X., & Efrima, S. (1996). Chemical and physical aspects of macroemulsions stabilized by interfacial colloids. *The Journal of physical chemistry, 100*(26), 11019-11028.

Zhu, F. (2019). Starch based Pickering emulsions: Fabrication, properties, and applications. *Trends in Food Science & Technology, 85*, 129-137.

CHAPTER 3

Janus starch particles: Scalable 3D mask approach via a wax Pickering emulsion method

Abstract

Incredible progress in the field of Janus particles over the last three decades—while tempered by challenges of scalability, method difficulty, and concerns over toxicity—has nevertheless delivered many promising smart-material prototypes, from cancer-targeting drug delivery vehicles to self-motile nanobots. We aim to demonstrate in this study that we can assimilate the technology of Janus particles into the food space, in order to take advantage of these particles' extraordinary flexibility and functionality for the rational design of smart food ingredients for the future. To this end, employing a scalable 3D mask approach, we developed a wax Pickering emulsion method for the bulk synthesis of Janus particles using a natural and safe ingredient like starch as the base material. Using this method, we found that we could make Janus particles with 49% Janus balance, and that Janus starch granules with one half side modified with octenyl succinic anhydride self-assembled into worm-like strings in water, unlike the unmodified and homogeneously modified controls. These Janus starch granules outperformed the control as thickening and gelling agents, as evidenced by their fourfold increase in water-holding capacity, a 30% lower critical caking concentration, a viscosity greater by orders of magnitude, and their formation of gels that were stiffer and stronger also by orders of magnitude. No improvements in surface activity, however, were observed. Overall, in line with consumer trends, we believe that these Janus particles may be used as low-calorie, plant-based texturizers in food products, and

that the emerging field of food-based Janus particles in general may bring exciting, smart applications into the food space.

1. Introduction

Janus particles—i.e., particles with two different sides or halves—have attracted a lot of attention in the last three decades due to their unique anisotropic properties, making them prime candidates as smart materials. They have now been synthesized via many different techniques using different starting materials, and intended for a wide array of applications (Loget & Kuhn, 2012; Liang, Zhang, & Yang, 2014; Zhang, Grzybowski, & Granick, 2017; Walther & Müller, 2013). When the starting materials are solid particles such as silica or polymer spheres, the major methods of synthesis can be categorized as 2D masking (Takein & Shimizu, 1997), 3D masking (Hong, Jiang, & Granick, 2006), or seeded polymerization (Kim, Larsen, & Weitz, 2006). When the starting materials are in the liquid phase such as monomers or polymers, the major methods of synthesis can be categorized as phase separation (Tanaka, Okayama, Kitayama, Kagawa, & Okubo, 2010; Kim, Abbaspourrad, & Weitz, 2011) or the self-assembly of block copolymers (Gröschel, et al., 2012). Due to their unique asymmetry, Janus particles have found wide use as surfactants, sensors/probes, targeted drug delivery vehicles, micro- or nano-motors, and materials for electronics and coatings applications (Loget & Kuhn, 2012; Liang, Zhang, & Yang, 2014; Zhang, Grzybowski, & Granick, 2017; Walther & Müller, 2013; Zhang, et al., 2016).

Our aim here is to demonstrate that we can bring the field of Janus particles, together with their potential applications as smart materials, into the food space. Two

challenges make this aim difficult: 1) Most Janus particles produced until now, together with their methods of synthesis, have been designed for synthetic polymers or inorganic materials; thus, we cannot easily appropriate them into the food industry due to concerns over toxicity, either from the starting materials or reagents used; and 2) Most methods for Janus synthesis are complex, give poor control, and offer low yield, making them difficult to scale up for potential application in the food industry (Zhang, et al., 2016).

Although very little work has been done in bringing the advantages of these extraordinary Janus particles into the food space, some recent efforts have shown that this direction shows great promise. For example, Janus particles have been produced to protect blueberries from microbes—with one side of the Janus particle containing positively charged chitosan, which binds well to negatively charged bacterial cell walls, and the other side containing silver, which kills bacteria (Jia, Jiang, Jin, Wang, & Huang, 2015). Janus particles have also been designed for the ultrafast detection of Salmonella in milk and mayonnaise—one side of the Janus particle contains platinum, which self-propels the particle like a motor, and the other side contains quantum dots, which screen for toxins via fluorescence (Pacheco, Jurado-Sanchez, & Escarpa, 2018). In fact, starch-polystyrene composites of different shapes—Janus/snowman, raspberry, or octahedron—have been shown to be possible to synthesize using a seeded polymerization technique (Pei, et al., 2018).

Our lab has demonstrated previously that we can make Janus particles using cornstarch and amaranth starch as starting materials via a 2D mask approach (Kierulf, et al., 2019). We showed that these Janus starch granules self-assemble in solution into wormlike strings, in contrast to non-Janus particles that self-assemble into

supermicelles, which suggests that Janus particles made from starch may find use as surface-active agents or texturizers in the food space. The yield, however, was very low, making it challenging to further test their potential use. In this study, we aim to move to a 3D mask approach, in order to improve the yield and allow for the bulk synthesis of these Janus particles and their thorough characterization for the food space.

The principle behind our 3D mask approach is based on the work of Granick et al., with some modifications (Hong, Jiang, & Granick, 2006). Melted wax droplets are first made in water by high-shear homogenization and stabilized using high-protein amaranth granules as Pickering emulsifiers. Due to the native hydrophobicity of high-protein amaranth starch (Kierulf, et al., 2020), these starch granules will half-embed into the wax droplets, which serve as our 3D substrate or mask as soon as the wax solidifies. Once the starch granules are half-embedded and trapped in the solid wax, the embedded halves are considered "masked", while the other halves are free and can then be modified with a reagent such as octenyl succinic anhydride (OSA) to make them hydrophobic. After treatment, we can dissolve the wax using a solvent, and isolate the Janus starch granule, which will give us a Janus particle that is hydrophilic on its unmodified or masked side and hydrophobic on the OSA-modified side. Using this 3D approach to produce Janus particles from starch by bulk, we then proceed to study their morphology and Janus balance by Scanning Electron Microscopy (SEM) and X-Ray Dispersive Spectroscopy (EDX); crystallinity by X-Ray Diffraction (XRD); degree of substitution and purity by Nuclear Magnetic Resonance Spectroscopy (NMR), Fourier Transform Infrared Spectroscopy with Attenuated Total Reflectance (FTIR-ATR), and Differential Scanning Calorimetry (DSC); self-assembly by optical microscopy;

physicochemical properties by the water-holding capacity test, the critical caking concentration test, and texture by rotational rheology; and surface activity by emulsification and measurement of interfacial tension.

2. Materials and Methods

2.1 Materials

Amaranth starch was extracted from a commercially available flour (see Section 2.2 for isolation method). Low-melting-point Paraffin wax (IGI 4630 Harmony Blend Wax, MP 48°C) was purchased from Candle Science (Durham, NC, USA). Sodium hydroxide (NaOH, 95–100%) beads were purchased from Fisher Scientific (NJ, USA). ACS-grade hydrochloric acid (HCl, 36.5–38%) was purchased from VWR Chemicals (PA, USA). *n*-Octenyl succinic anhydride (OSA) was provided by Dixie Chemical Company (Pasadena, Texas, USA). High-purity glass microfiber extraction thimbles (30x100mm, 0.8 µm particle retention) were purchased from GE Life Sciences (PA, USA). ACS-grade chloroform was purchased from Midland Scientific Inc. (NE, USA). 3-acrylamidopropyl trimethylammonium chloride (APTMAC) aqueous solution (75 wt%, Santa Cruz Biotechnology), tris[2-(dimethylamino)ethyl]amine (Me6-TREN, Sigma-Aldrich), copper nanopowder (25nm, Sigma-Aldrich), 2-bromopropionyl bromide (97%, Alfa Aesar), acetone (99.8% Certified ACS, Fisher), NEt3 (99.91%, Chem-Impex), and acetonitrile (99.5+% EMD Chemicals Inc.) were all used as received. Chloroform-D (99.8%) and Deuterium oxide (99.9%) were purchased from Cambridge Isotope Laboratories, Inc. (MA, USA), and acetone-d6 (99.9%) was purchased from Aldrich (MO, USA).

2.2 Isolation of amaranth starch from flour

High-protein amaranth starch was isolated from a commercially available flour using an alkaline method we developed previously elsewhere (Kierulf, et al., 2020). Briefly, 2L of 0.15% NaOH was added to 400g flour and then stirred for 1h at 500 rpm using an overhead stirrer at room temperature. The slurry was filtered through a 270-mesh sieve (53-µm pore size) using a laboratory test sieve vibrator (Houghton Manufacturing Co., MI, USA) for 10 min. The unfiltered residue was collected, re-dispersed in 400 mL 0.15% NaOH, stirred for 10 min, then filtered again through the 270-mesh sieve, and washed with 200 mL 0.15% NaOH. The filtrates were combined then centrifuged for 20 min at 3000 g. After discarding the supernatant, the top yellow-brown layer of the pellet was removed using a spatula. The white pellet was then reconstituted in water, adjusted to pH 6.0 ± 0.1 using 1N HCl, and re-centrifuged, again removing the supernatant and the pellet's top yellow-brown layer. The isolated starch was then freeze-dried for 24h and ground using an ultra-fine conical burr grinder. The yield was approximately 12.5%, or 50g of **high-protein amaranth starch**, which was labelled as **unmodified amaranth starch.**

2.3 Bulk synthesis of Janus particles via the wax Pickering emulsion method

A schematic of the Wax Pickering approach we developed is shown in Figure 3.1a, which was based on a method first proposed by Hong and Granick (Hong, Jiang, & Granick, 2006). A reaction vessel (Figs. 3.1b and 3.1c) was designed to facilitate the method, with a bottom compartment where the emulsion would be formed, and a top

compartment that can be attached, to which a reagent can later be added, controlling the reagent flow through the emulsion by adjusting the stopcock at the bottom.

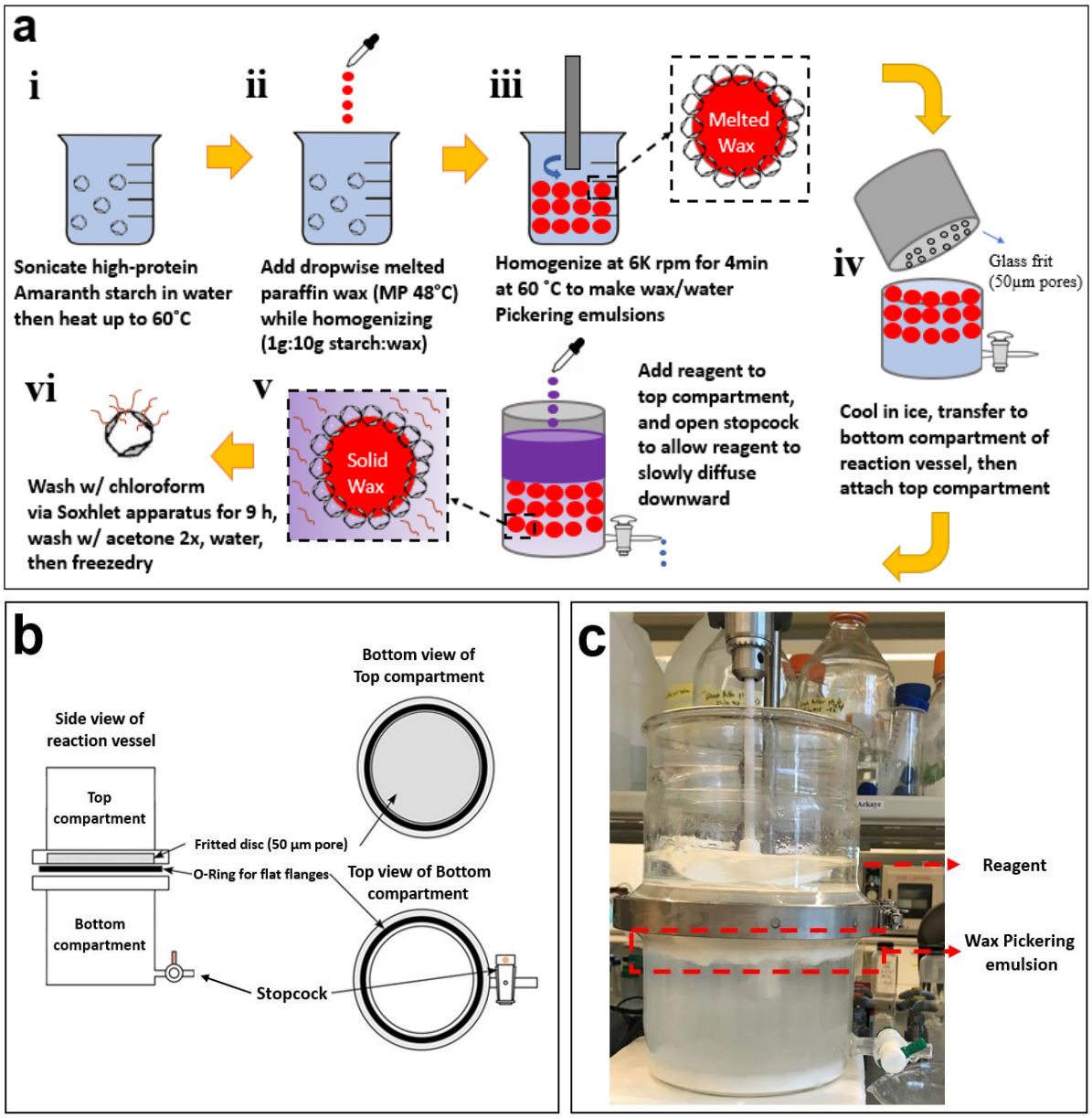

Figure 3.1. 3D mask approach via a wax Pickering emulsion method to make Janus particles. (a) Schematic of this method. (b) Schematic and (c) image of the reaction vessel used in this method, where the bottom compartment holds the wax Pickering emulsion containing the starch granules to be modified, and also has a bottom stopcock to control reagent flow; and the top compartment holds the reagent and has a fritted disc through which the reagent flows into the bottom compartment.

a. Treatment with OSA

First, 4g unmodified amaranth starch was dispersed in 100 mL deionized water inside a 200 mL beaker and sonicated for 15 min. Then, it was heated in a water bath set at 60°C (Fig. 3.1a-i). As soon as the starch dispersion reached 59-60°C, melted paraffin wax (1:10 w/w starch:wax) was added dropwise, homogenizing the mixture at 6k rpm for 4 min using a high-speed homogenizer (IKA T25 digital Ultra Turrax, Germany) with a S25N-18G dispersing tool (Fig. 3.1a-ii-iii). The beaker was then immediately submerged in ice and allowed to cool for 30 min. It was then removed from the ice, placed in a water bath at room temperature, and allowed to stabilize to room temperature for 1h. Four batches of these wax emulsions were prepared. After cooling to room temperature, the four batches were then all transferred to the bottom compartment of the reaction vessel, and the top compartment was attached (Fig. 3.1a-iv). An overhead stirrer was placed on the top compartment to make sure all reagents added will be mixing well during elution. Because the starch granules were now half-submerged into solid wax, the free half could now be modified with OSA.

We then added 400 mL of 1.5 mM NaOH into the top compartment of the reaction vessel, turned on the overhead stirrer, and opened the stopcock to allow a flow of about 2-3 drops per second (This will elute 400 mL of reagent in 15-20 minutes) (Fig. 3.1a-v). After the NaOH solution has completely eluted from the top compartment to the bottom compartment, we added 400 mL of a 0.12% (v/v) OSA solution in 30:70 etOH: DI water into the top compartment and allowed it to elute. In the same manner, we added the following in this order afterwards: 400 mL of 1.5 mM NaOH, 400 mL of 1.5 mM NaOH, 400 mL of 0.12% v/v OSA, 400 mL of 2.0 mM NaOH, 400 mL of 2.0

mM NaOH, 400 mL 0.12% v/v OSA, 400 mL of 2.5 mM NaOH, 400 mL of 2.0 mM NaOH, 400 mL of 0.12% v/v OSA, 400 mL of 2.0 mM NaOH, and 400 mL of 1.5 M NaOH. Afterwards, the sample was neutralized by eluting 400 mL of 0.01% HCl. The sample was then washed by eluting 2x 400 mL of 30% EtOH:water, followed by 400 mL DI water. The wax emulsions were then transferred into extraction thimbles and washed with chloroform for 9h using a Soxhlet apparatus with an oil bath set at 105ºC. The resultant residue was then washed with 2x acetone then with water, centrifuging at 5000g for 5 min each time to remove the supernatant, then freeze-dried (Fig 3.1a-vi). The Janus particles produced using this method was labelled as **Janus OSA amaranth starch**. The yield was approximately 25% or 4 g of Janus OSA starch.

The control was prepared in parallel by placing 4 g amaranth starch in a beaker and adding the NaOH and OSA reagents in the same order as above while stirring, removing the reagents every after OSA addition using a centrifuge at 5,000g for 5 min, then reconstituting the pellet with the next NaOH solution to be added. The control was then also neutralized with HCl solution and washed with 30% etOH twice and then water in the same way, then freeze-dried. The control produced using this method, which produced homogeneously OSA-modified starch, was labelled as **control OSA amaranth starch.**

b. Treatment with polymer

First, 1g unmodified amaranth starch was dispersed in 100 mL acetonitrile inside a beaker and sonicated for 15 min. Then, it was heated in a water bath set at 60°C (Fig. 3.1a-i). As soon as the starch solution reached 59-60°C, melted paraffin wax (1:10 w/w starch:wax) was added dropwise, homogenizing the mixture at 6k rpm for 4 min using

a high-speed homogenizer (IKA T25 digital Ultra Turrax, Germany) with a S25N-18G dispersing tool (Figs. 3.1a-ii and 3.1a-iii). The beaker was then immediately submerged in ice and allowed to cool for 30 min. It was then removed from the ice, and poured into the top compartment of the reaction vessel carefully (Note: Before this step, make sure that the top compartment has already been attached to the bottom compartment and the stopcock has been closed). Because the starch granules were now half-submerged into solid wax, the other free half could now be modified with 3-acrylamidopropyl trimethylammonium chloride (APTMAC, a nitrogen-rich polymer) (Fig. 3.1a-v).

First, we attached the initiator in this way: The reaction vessel and all reagents to be used were placed in a cold room at 4°C for 1h, then to the top compartment we added a solution of bromopropionyl bromide (174 μL, 1.66 mmol) in acetonitrile (35.0 mL) containing NEt3 (232 μL, 1.66 mmol), which was allowed to elute by opening the stopcock. After the solution has completely immersed the wax emulsion, we closed the stopcock and allowed the reaction to run for 1 h at 4 °C and after that for an additional 2 h at room temperature. Then excess water was added into the top compartment and the stopcock was opened to allow the water to wash the emulsion.

After the initiator has been attached, we then proceeded with surface-initiated Cu (0)-mediated reversible radical polymerization (RDRP) via a "grafting from" approach. A solution of 75.0 w% APTMAC (9.24 mL) in water (27.7 mL) containing Me_6-TREN (44.4 μL) was deoxygenated for 30 min at 20 °C by N_2 bubbling. Nanosize Cu(0) (25 nm, 10.56 mg) was added and the mixture was sonicated for 1 min to disperse the copper. This mixture was then added to the reaction vessel and allowed to elute through the wax emulsion containing 1.0 g of previously initiator-functionalized

amaranth starch. The stopcock was then closed, then the reaction was allowed to run for 4h at room temperature. Afterwards, the wax emulsions were transferred into an extraction thimble and washed with chloroform for 9h using a Soxhlet apparatus with an oil bath set at 105ºC. The resultant residue was then washed with 2x acetone then with water, centrifuging at 5000g for 5 min each time to remove the supernatant, then freeze-dried (Fig. 3.1a-vi). The Janus particles produced here was labelled as **Janus polymer amaranth starch.**

The polymer control was prepared in parallel by placing 1g amaranth starch in a beaker in a cold room, adding the reagents for initiator attachment in the same amount, then stirring for 1h at 4°C, then 2h at room temperature. It was then washed 3x with water, removing the supernatant each time after centrifugation at 5000g for 5 min. After washing, it was then transferred to a round bottom flask, and then the reagents for polymerization were added in the same amount. The reaction was allowed to run for 4h with stirring at room temperature. Afterwards, it was washed with water 3x, centrifuging at 5,000g for 5 min each time to remove the supernatant, then freeze-dried. The control prepared using this method was labelled as **control polymer amaranth starch.**

2.4 Crude protein analysis

The unmodified amaranth starch isolated from Section *2.2,* and the Janus OSA and control OSA amaranth starches produced from Section *2.3* were tested in triplicate for crude protein content using AOAC 992.23 (combustion method) and a nitrogen-to-protein conversion factor of 6.25 on a % dry basis (Latimer, 2016).

2.5 Scanning electron microscopy (SEM) and X-Ray dispersive spectroscopy (EDX)

We used SEM to verify the working principle behind the wax Pickering emulsion method—i.e., that we can indeed half-embed high-protein amaranth starch granules into wax droplets. The wax droplets produced in Fig. 3.1a-iii (solid wax droplets with half-embedded amaranth starch on their surface before OSA treatment) and Fig. 3.1a-v (solid wax droplets after OSA treatment) were mounted on an SEM stub with conductive carbon tape, then dried in a vacuum desiccator for 24h. A blade was used in some areas to slice through the solid wax droplets to look at their cross-section. These samples were then sputter-coated with gold then imaged using a JCM-6000 Benchtop SEM (JEOL Ltd., Japan) at an accelerating voltage of 15 kV using a secondary electron detector at x1000 and x5000 magnifications. In addition, to check that the paraffin wax had been removed during the washing step (Fig. 3.1a-vi), we took SEM images of samples washed via Soxhlet-chloroform at 3, 6, 9, and 24h durations.

To visualize the morphology of Janus particles produced via the wax Pickering emulsion method, we mounted the Janus polymer amaranth starch produced in section 2.3b on a silicon wafer atop an SEM stub and sputter-coated it with carbon then imaged it using a Zeis Gemini 500 Field Emission SEM to look at their morphology. In addition, we also produced nitrogen density maps via EDX, using an aperture size of 60 μm and electron beam of 7.5kV. We did the same for the unmodified amaranth starch and the control polymer amaranth starch for comparison.

To measure experimentally the Janus balance of the Janus polymer amaranth starch, or % coverage of polymer on the surface of the amaranth starch granule, we took nitrogen density maps by EDX of 20 random Janus-polymer amaranth starch particles,

measured their individual Janus balances by ImageJ 1.52p, and computed for average Janus balance and standard deviation (experimental value).

2.6 Random simulation of Janus particles

To understand the random nature of the method used in section *2.5* to measure the average Janus balance, we performed random simulations using Blender 2.79a software. We generated three simulations of 20 Janus particles each, all randomly oriented on top of a flat plane, with theoretical Janus balances from 0% to 100%. For simplicity, we modelled them as perfectly spherical particles, with all orientations having equal probability. We used the Hair type "Particle System modifier" with random initial orientation and different seed points to generate different sets of random locations for particles. "Rotation" box was checked and for each case random parameters were both set on maximum (1.0 for normal and 2.0 for phase). These simulations generated 3D images that were then processed as 2D images using Image J in order to compute for the average Janus balance of each 20-particle simulation. Graphs of average Janus balance and standard deviation vs. theoretical Janus balance were then produced, and compared against the experimental value calculated in section *2.5*.

2.7 Attenuated total reflectance-Fourier transform infrared spectroscopy (ATR-FTIR)

The ATR-FTIR spectra of the unmodified, Janus OSA amaranth starch, and control OSA amaranth starch were obtained using an ATR-FTIR Shimadzu Affinity-1S, to qualitatively assess the ester bonds formed due to reaction with OSA. The 400–4000 cm^{-1} region was scanned in transmittance mode with 2 cm^{-1} resolution and 60 scans.

In addition, to assess the effectiveness of the Soxhlet-chloroform washing step (Fig 3.1a-vi) in removing the Paraffin wax from the Janus particles, the FTIR spectra of samples washed for 3, 6, 9, and 24h were obtained as well.

2.8 Nuclear magnetic resonance microscopy (NMR)

To measure OSA degree of substitution (DS), ^{1}H NMR spectrograms of the unmodified, Janus OSA, and control OSA were generated at 50°C using a Bruker INOVA 500 NMR spectrometer. The starch samples were prepared by dissolving 50 mg in 1 mL D_2O, and heating at 90°C for 2h before analysis. The DS was estimated using the following equation:

$$Degree\ of\ substitution\ (DS) = \frac{A_{OSA}}{3\ x\ A_{STARCH}} \quad (3.1)$$

where A_{OSA} refers to the area of the peak assigned to the methyl protons of OSA (1.2 ppm) and A_{STARCH} refers to the area of the peak assigned to the equatorial proton of the anhydroglucose unit of starch (5.7 ppm) (Shih & Daigle, 2003). The DS was estimated in duplicate.

To check for residual wax and residual chloroform, 100 mg of Janus OSA starch were mixed in 1.5 mL deuterated chloroform and 1.5 mL of deuterated acetone, respectively, at 25°C for 24h. The solutions were then filtered and their respective ^{1}H NMR and ^{13}C NMR spectrograms were generated.

2.9 X-Ray diffraction (XRD)

X-ray diffraction (XRD) analyses of the unmodified, Janus OSA, and control OSA amaranth starch were performed using a Bruker D8 Advance ECO powder

diffractometer (Billerica, MA) to assess whether gelatinization occurred during the Wax Pickering emulsion method. The powder samples were run from 5 to 60° under continuous scan at a step size of 0.026 with 2θ min−1.

2.*10 Differential scanning calorimetry (DSC)*

The DSC profiles of the unmodified, Janus OSA, and control OSA amaranth starch were generated using a TA Q1000 Modulated Differential Scanning Calorimeter (Delaware, USA). The DSC profile of the wax-starch Pickering emulsion (taken after OSA treatment but before Soxhlet washing with chloroform) was also generated for comparison. A 1:5 w:w sample-to-water ratio was used, and the profile was taken from 30°C to 90°C at a heating rate of 10°C/min.

2.11 Self-assembly via optical microscopy

To study self-assembly, 2 mg each of the unmodified, Janus OSA, and control OSA amaranth starch were weighed, and 3 mL of DI water was added to each. They were then vortexed for 2 min, sonicated for 2-5 min, and mixed in a vertical rotator for 30 minutes. Using a blind experiment, a 20µL aliquot of each sample was then placed on a coverslip, allowed to settle for 1 min, then observed using a Leica Model DMIL LED microscope (Germany) with fast camera at 100x magnification. For each sample, twenty random images were taken in series from left to right and from top to bottom, covering approximately a 500x500 μm^2 area and approximately 1000+ discrete granules or aggregates.

All images were then processed using ImageJ 1.52p to automatically generate the corresponding areas of each discrete granule or discrete aggregate. These areas were then pooled into five different categories by size, namely: (a) no aggregate, where a granule appears discrete and separate (0.6-2 μm^2), (b) 2- or 3- granule clusters, where 2 or 3 granules appear to be bound together or touching (2-6 μm^2), (c) small wormlike strings, where multiple granules form irregular, string-like aggregates that take up less than 50 μm^2, (d) large wormlike strings, where multiple granules form irregular, string-like aggregates that take up more than 50 μm^2 but less than 100 μm^2, and lastly (e) supermicelles, where multiple granules form a large almost-spherical aggregate that generally takes up more than 100 μm^2. The relative distribution of each aggregate category in terms of total area were then plotted in a bar graph using Origin Pro 9.7.5.184 (2020b).

2.12 Critical caking concentration

The critical caking concentration (CCC) of the unmodified, Janus OSA, and control OSA amaranth starch were measured in triplicate using a Buchner funnel filtration method: 1g of sample was placed in a 15-mL tube, to which 9 mL of DI water was added. The tubes were vortexed for 2 min, sonicated for 2 minutes, and mixed in a vertical rotator for 30 min. They were then poured onto a 1.2-µm-pore-size microfiber filter inside a Buchner funnel, and a 50 kPa vacuum pressure was applied until a wet starch cake was formed on the filter and no un-adsorbed water remained on top of the cake (i.e., the Buchner funnel can be turned upside down and no water will flow down

the sides). The critical caking concentration was calculated using the following equation:

$$Critical\ caking\ concentration = \frac{wt\ of\ dry\ starch}{wt\ of\ wet\ cake} \times 100\% \quad (3.2)$$

2.13 Water-holding capacity

The water-holding capacity (WHC) of the unmodified, Janus OSA, and control OSA amaranth starch were measured in triplicate using a modified centrifugation method based from Singh et al. (Singh, Sandhu, & Kaur, 2004) and Azfaralariff et al. (Azfaralariff, Fazial, Sontanosamy, Nazar, & Lazim, 2020): 1g of sample was placed in a 15-mL centrifuge tube, to which 9 mL of DI water was added. The tubes were vortexed for 2 min, sonicated for 5 minutes, and mixed in a vertical rotator for 1h. They were then centrifuged at 3000g for 10 min, the supernatants were decanted, any remaining water drained for 10 min, and the sediment was weighed before and after freeze-drying for 24h. The water holding capacity was calculated using the following equation:

$$Water - holding\ capacity = \frac{wt\ of\ wet\ sediment - wt\ of\ dried\ sediment}{wt\ of\ dried\ sediment} \times 100\% \quad (3.3)$$

2.14 Rheology

a. Viscosity at one concentration

The viscosity of 20% (w/w) dispersions of the unmodified, Janus OSA, and control OSA amaranth starch were measured in triplicate using a TA DHR3 rotational

rheometer (Delaware, USA) and employing a 20-mm parallel plate and 500 μm gap size. The dispersions were vortexed for 2 min, sonicated for 5 min, and mixed in a vertical rotator for 30 min prior to measurement. Very viscous dispersions that could not be mixed by vortex were mixed manually prior to sonication. The viscosity was measured at 25℃ using a 0.02-100 1/s shear rate sweep.

b. Moduli and viscosity at different concentrations

The storage moduli, loss moduli, and viscosity at different concentrations of the unmodified, Janus OSA, and control OSA amaranth starch were measured in triplicate at 25°C using a TA DHR3 rotational rheometer and employing a 20-mm parallel plate and 500 μm gap size. For each sample, four different concentrations (w/w) were prepared at 2.5%, 5%, 7.5%, and 10% below the CCC for that sample as measured in section *2.12*. The dispersions were vortexed for 2 min, sonicated for 5 min, and mixed in a vertical rotator for 30 min prior to measurement. Very viscous dispersions that could not be mixed by vortex were mixed manually prior to sonication. The following tests were then performed: oscillation strain sweep at 1Hz frequency, at 0.1-10% strain; oscillation frequency sweep at 0.1% strain, at 0.01-100 Hz frequency; and shear rate sweep at 0.02-100 1/s shear rate. The yield point was estimated to be the point at which G' starts to decline by 5% or more, and the flow point as the point after which the G' and G" values intersect and G">G'.

2.15 Surface activity

a. Emulsifying ability via droplet size and emulsion index (EI)

The emulsifying abilities of unmodified, Janus OSA, and control OSA amaranth starch were studied by preparing in triplicate 30% v/v O/W emulsions using 0.67 g starch/mL corn oil and a pH 6.5 buffer. The emulsions were made by homogenization at 11k rpm for 4 min using a high-speed homogenizer (IKA T25 digital Ultra Turrax, Germany) with an S25N-18G dispersing tool. The emulsion index was measured using the following equation:

$$Emulsion\ index = \frac{V_E}{V_T} \qquad (3.4)$$

where V_E is the volume of the emulsion (upper cream layer) and V_T is the total volume of the whole sample (including all layers or phases) (Saari, Heravifar, Rayner, Wahlgren, & Sjoo, 2016). Likewise, the emulsion droplet size was measured by taking images of the emulsion droplets using an optical microscope at 4x magnification then using ImageJ to calculate the diameter *di* of *N* number of particles, where N>200, to compute for the volume mean diameter (d_{43}) and polydispersity index (PDI) using the following equations (Li, Li, Sun, & Yang, 2013):

$$d_{43} = \frac{\sum di^4}{\sum di^3} \qquad (3.5)$$

$$\text{PDI} = \frac{d_{43}}{\sum \frac{di}{N}} \qquad (3.6)$$

b. Interfacial tension

The interfacial tension between corn oil and water in the presence of unmodified, Janus OSA, and control OSA were measured using a pendant drop method based on Zhao et al. (Zhao, et al., 2018). A 30 µL droplet of a starch dispersion (1% w/w) in DI water was formed at the tip of a syringe and submerged into corn oil. The interfacial

tension was then measured using an advanced goniometer (model 500-U1, rame-hart instrument co., NJ, USA) at 10s intervals over 1000s.

2.16 Statistical analysis

Triplicate analyses were performed (unless otherwise stated), and analysis of variance (ANOVA) and t-tests ($P<0.05$) were performed where appropriate.

3. Results and Discussions

We will divide the discussion of the results into two parts: 1) method characterization and 2) Janus particle characterization. Under method characterization, we first evaluate the wax Pickering emulsion method we developed as a 3D mask approach to making Janus particles by using SEM, ATR-FTIR, DSC, and NMR. Then, having evaluated this method, we then proceed to characterize the Janus particles themselves that the method produces, via SEM-EDX, ATR-FTIR, XRD, DSC, NMR, optical microscopy, and physicochemical tests including CCC, WHC, and rheology.

3.1 Method characterization

3.1.1 SEM of 3D masking of starch granules

The working principle behind the wax Pickering emulsion approach is the 3D mask: the method can half-embed a starch granule into a solid 3D mask in the form of a wax droplet, such that one half of the granule is inside the wax droplet surface (or "masked" and immobilized) and the other half is outside and "free", which then allows for the other half to be modified by a reagent like OSA (or a polymer) to make a Janus particle (see Fig 3.1a). We found that we can indeed use this method to embed starch granules into a wax droplet's surface (Fig. 3.2a).

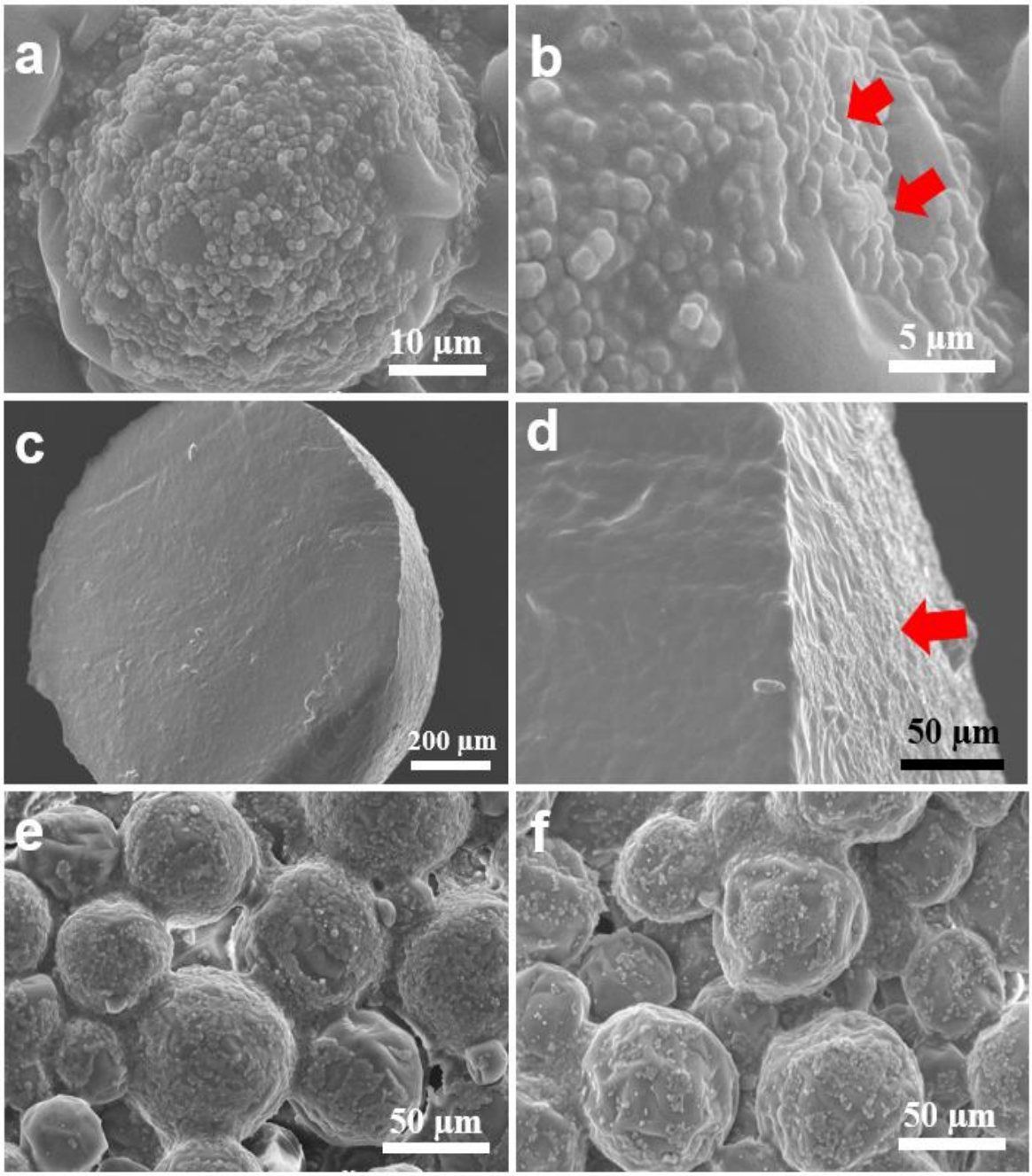

Figure 3.2. Method characterization: 3D mask working principle of the wax Pickering emulsion method for making Janus particles. SEM images of (a) a solid wax droplet with amaranth starch granules half-embedded on its surface; (b) close-up of wax droplet, with red arrows showing the granules half-embedded; (c) a sliced wax droplet showing its cross-section; (d) close-up of the sliced wax droplet with a red arrow showing that starch granules only embed on the surface but not the interior; wax droplets with starch granules on its surface (e) before OSA treatment and (f) after OSA treatment, showing that some granules get detached from the wax surface during treatment, but many remain embedded.

Zooming in, we see that the granules are about half-embedded into the wax, with the other half free, which makes it conducive to Janus modification (Fig. 3.2b). Furthermore, if we slice a large starch-stabilized wax droplet in half, we see that starch granules only embed at the droplet surface and do not go into the interior (Figs. 3.2c and 3.2d). SEM images of wax droplets before and after treatment with a reagent (e.g., OSA) (Figs. 3.2e and 3.2f, respectively) show that some granules get detached during reagent elution, but that majority of granules remain embedded at the surface. All these results suggest that the Wax Pickering emulsion approach is conducive for Janus modification.

3.1.2 Residual wax

a. Wax content decreases as washing time is increased (ATR-FTIR)

After the starch granules have been half-embedded into the solid wax droplets so that their free halves can be modified by a reagent, the solid wax then needs to be washed out using chloroform via a Soxhlet apparatus for 9h to isolate the Janus particles (See Fig 3.1a-vi). We obtained the FTIR spectra of samples prepared via the Wax Pickering emulsion approach then washed using Soxhlet-chloroform at different durations (3, 6, 9, and 24h) (Fig. 3.3a). The unwashed sample (wax droplets with starch embedded) (bottom, red line) has a large amount of paraffin wax, as evidenced by the intense peaks at 2916 and 2850 cm^{-1}, attributed to wax C-H stretching, and another strong peak at 1460 cm^{-1}, attributed to wax C-H deformation (Sharifah, ATBS, & Nor Khairusshima, 2017). As we increase the duration of Soxhlet-chloroform washing, from 3 to 24 h, the C-H peaks due to paraffin wax decrease in intensity substantially. A duration of 9h or above appears sufficient to remove paraffin wax.

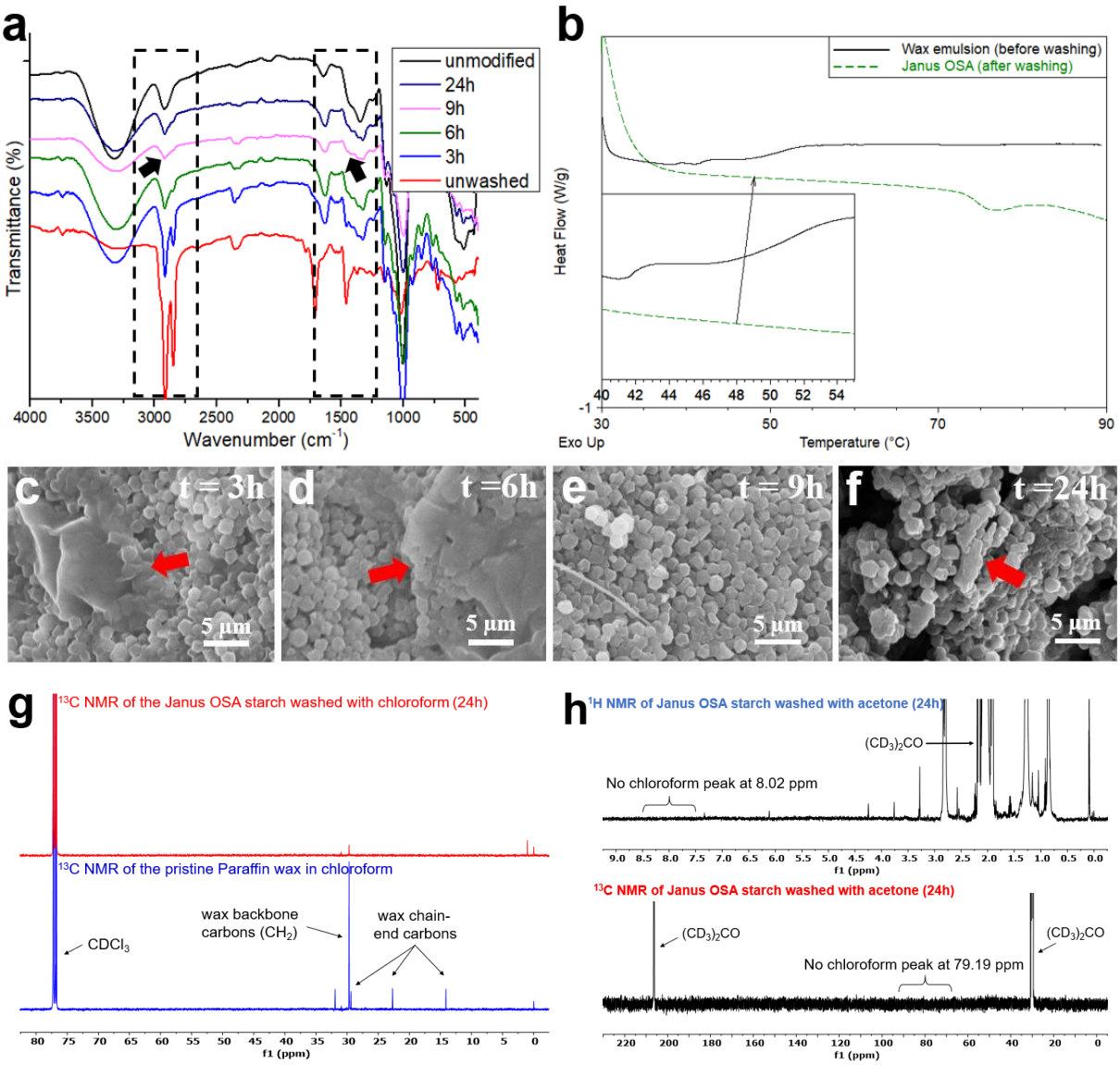

Figure 3.3. Method Characterization: Residual wax and residual chloroform. (a) ATR-FTIR spectra of starch samples at different Soxhlet-chloroform washing durations, (b) DSC profile of wax emulsion (before 9h Soxhlet-chloroform washing) and Janus OSA (after 9h washing), with inset showing no 48°C wax peak for Janus OSA; (c-f) SEM of starch samples after 3, 6, 9, and 24h Soxhlet-chloroform washing; ^{13}C and ^{1}H NMR chromatograms of washed Janus particles showing (g) only residual amounts of wax and (h) no chloroform left after washing.

b. No residual wax peak remains after a 9h wash (DSC)

To verify that any residual wax has been washed out using chloroform via a Soxhlet apparatus for 9h, we also generated the DSC profile of the isolated Janus OSA (after washing for 9h) vs. the wax-starch emulsion (before washing). The wax-starch emulsion before washing shows an endothermic peak at ~47°C, which indicates the melting point of the Paraffin wax (see Fig 3.3b). On the other hand, the Janus OSA amaranth starch washed for 9h in chloroform does not have a peak at ~47°C, as highlighted by the zoom-in inset image, indicating that the wax has been effectively removed.

c. *No residual wax is visible after a 9h wash (SEM)*

We also looked at the SEM images of Janus OSA samples washed with chloroform at different durations. Washing for 3 and 6 h does not fully remove the wax, as shown by the red arrows (Fig. 3.3c and 3.3d). At 9h, no wax can be seen (Fig. 3.3e). At 24h, no wax can be seen, but the starch has started to degrade (red arrow, Fig. 3.3f). These results provide further evidence that the 9h chloroform washing step of this method is sufficient for removing paraffin wax and isolating Janus particles.

d. Negligible wax peak remains after a 9h wash (NMR)

The 13C NMR spectra of Paraffin wax (see Fig. 3.3g bottom) shows a characteristic wax backbone methylene carbon (CH_2) peak at ~30 ppm, and chain-end saturated carbons at ~23 ppm and ~14 ppm. By contrast, the Janus OSA starch (see Fig. 3.3g top), which was washed with deuterated chloroform for 24h to detect any residual

wax, showed only a negligible peak ~30 ppm and no peaks at 14 and 24 ppm, indicating that wax has been effectively removed (Robertson, van Reenen, & Duveskog, 2020).

3.1.3 Residual chloroform

The 1H and 13C NMR spectra of Janus OSA starch, which was washed with deuterated acetone for 24h to detect any residual chloroform, showed no chloroform peaks at 8.02 ppm and 79.19 ppm, respectively, indicating that chloroform has effectively been removed.

3.2 Janus particle characterization

Having shown in the previous section that the working principle behind the wax Pickering emulsion method indeed allows for the synthesis of Janus particles via 3D masking, and that the washing step is sufficient to remove the wax afterwards, we then proceed to characterize the Janus particles thus produced in this section.

3.2.1 Verification of OSA modification by ATR-FTIR

We used the wax Pickering emulsion method to produce Janus particles from amaranth starch granules, employing OSA as a representative reagent. After half-embedding the starch granules in the wax droplet surface, we then modified the other free half with OSA. At basic conditions, alcoholate ions on the starch surface will attack the OSA's anhydride as a nucleophile, resulting in the attachment of a hydrophobic

octenyl group via an ester bond (see Fig. 3.4a) (Hui, Qi-he, Ming-liang, Qiong, & Guo-qing, 2009).

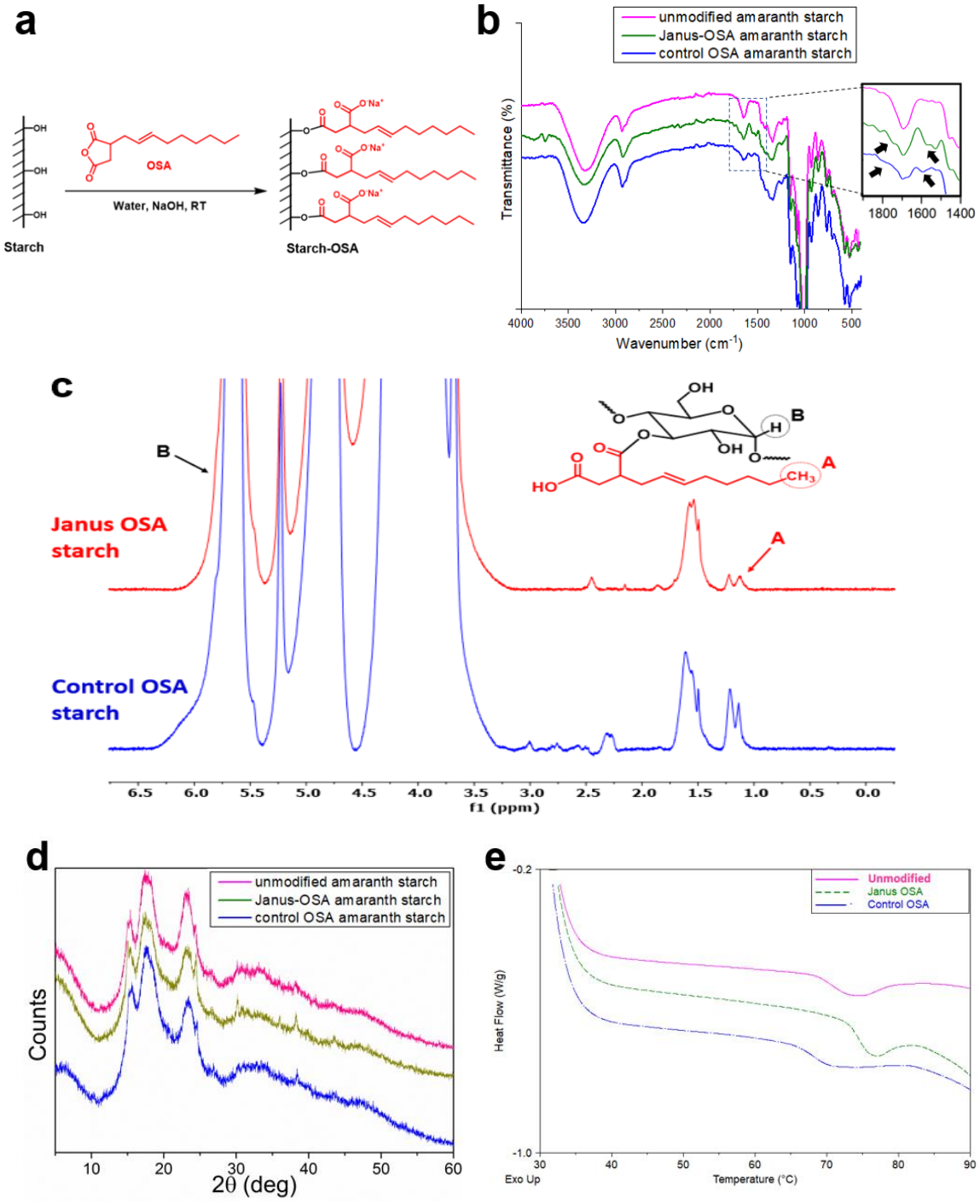

Figure 3.4. Janus particle characterization. (a) Reaction scheme of OSA reaction with starch. (b) ATR-FTIR spectra, (c) NMR chromatogram, (d) X-Ray Diffraction patterns, and (e) DSC profiles of unmodified, Janus OSA, and control OSA starch.

The spectra of the unmodified, Janus OSA, and control OSA amaranth starch are shown in Figure 3.4b. For the unmodified starch, we observe characteristic bands that have been assigned in the literature: a broad O-H vibration at 3400 cm^{-1}; C-H stretching at 2915 cm^{-1}; adsorbed water bending vibration at 1640 cm^{-1}; C-H deformation peaks at 1360–1420 cm^{-1}; and a fingerprint region at 1000–1200 cm^{-1} for C-O stretching (Ye, et al., 2014). For the OSA control, a strong peak appears at 1730 cm^{-1} for C=O stretching vibration, which confirms that an ester bond was formed between OSA and starch. Another small peak that appears at 1560 cm^{-1} for the asymmetric stretching vibration of the carboxylate group of OSA confirms the reaction (Ye, et al., 2014; Miao, et al., 2014). The Janus OSA starch also has the same peaks at 1730 (a small shoulder) and 1560 cm^{-1}, but much less intense (Ye, et al., 2014; Miao, et al., 2014). This suggests qualitatively that the control OSA has a higher degree of OSA substitution than Janus OSA, which is what we would expect if the Wax Pickering emulsion method indeed formed Janus particles.

3.2.2 OSA degree of substitution (DS) by NMR

The ^{1}H NMR method was used to estimate that the Janus OSA starch and control OSA starch have DS values of 0.0018±0.0001 and 0.0027±0.0001, respectively. Fig 3.4c (top image) shows the NMR spectra of Janus OSA starch, where peak A at ~1.1 ppm represents the OSA methyl protons and peak B at ~5.6 ppm represents the starch equatorial proton, from which the DS was estimated using eq. 3.1 (Shih & Daigle, 2003). The Janus OSA starch has a DS about 68% that of the control OSA starch (see Fig. 3.4c top vs. bottom), which corroborates the qualitative results from the FTIR-ATR spectra, and which is what we would expect more or less if the Wax Pickering emulsion

method indeed formed Janus OSA particles. Compared to the literature, where starches are modified with 3% OSA and have about DS=0.015, the DS values of the Janus OSA and control OSA starches produced in this study are lower, which can be explained by the fact that the method we used does not allow for the continual adjustment of the pH to the optimal pH for OSA reaction, which leads to a lower DS.

3.2.3 *Crystallinity of Janus OSA amaranth starch by XRD*

The wax Pickering emulsion method involves heating steps and a long washing step with chloroform, which could affect the crystallinity of the starch granules (see Fig 3.1a). To check, we obtained the XRD patterns of unmodified, Janus OSA, and control OSA amaranth starch (Fig. 3.4c). The unmodified amaranth starch has sharp peaks at 15º, 17.5º, and 23.5º, which indicates A-type crystallinity typical for amaranth starch (Xia, et al., 2014). The OSA control starch shows the same sharp peaks, but slightly broader due to OSA treatment. The Janus OSA starch feature the same sharp peaks as the control, which suggests that their crystallinity was not much affected by treatment via the wax Pickering emulsion method.

3.2.4 DSC profile of Janus OSA amaranth starch

The DSC profiles of the unmodified, Janus OSA, and control OSA amaranth starch shows endothermic peaks with peak gelatinization temperatures (T_p) at 73.7 (±0.0), 76.6 (±0.2), and 70.8 (±0.3) °C, with corresponding gelatinization enthalpies (ΔH_g) of 2.3 (±0.4), 1.8 (±0.04), and 2.0 (±0.1) J/g, respectively (see Fig. 3.4d). Homogeneous treatment of starch with OSA typically results in the reduction of both the peak gelatinization temperature and the gelatinization enthalpy, indicating that the hydrogen bonding between amylose and amylopectin strands in the granule have been

weakened due to the addition of bulky, hydrophobic octenyl groups, which allows the granules to swell at a lower temperature, requiring less energy to disrupt the crystalline structure (Bhosale & Singhal, 2007). Thus, in general agreement with the literature, we found that unmodified amaranth starch gelatinizes at 73.7°C, while control OSA gelatinizes at a lower temperature of 70.8°C, with a slightly lower enthalpy of gelatinization, as expected due to the OSA treatment (Bhosale & Singhal, 2007). On the other hand, the Janus OSA gelatinizes at a slightly higher temperature of 76.6°C, with a slightly lower enthalpy of gelatinization. It is clear that the synthesis of Janus OSA starch using the wax Pickering emulsion approach outlined here involved not only OSA treatment but also chloroform washing, both of which may have contributed to the reduction in gelatinization enthalpy. It is unclear, however, why the peak gelatinization temperature of Janus OSA appears to be higher than that of the unmodified amaranth starch, but may be due to the very high viscosity of the Janus OSA dispersion in water, as compared to the low viscosity of the unmodified amaranth starch dispersion, which may slow the diffusion of heat, and therefore shift the observed peak gelatinization temperature. Likewise, Janus OSA particles may self-assemble and trap water, lowering the amount of free water that can participate in gelatinization, which may also slightly shift the gelatinization temperature (Shih & Daigle, 2003).

3.2.5 Janus morphology by polymerization and SEM-EDX

A nitrogen-rich polymer (APTMAC) was grown on one half side of amaranth starch using the wax Pickering emulsion method to produce Janus polymer amaranth starch, in order to verify visually that the method can indeed produce Janus particles. After half-embedding the starch granules onto the wax surface, we first attached an

initiator to the free half using an acid bromide, then we attached APTMAC to them via "grafting from" radical polymerization (Fig. 3.5a). Under SEM, an unmodified amaranth starch granule appears polygonal with flat surfaces and sharp edges (Fig. 3.5b). Once we grow a polymer to one half side of the starch granule, we expect that polymer side to look more irregular and rounded, while the side without any polymer should look flat and sharp-edged, which is what we observe in our SEM images of Janus polymer starch (Fig. 3.5c). The control polymer amaranth starch, or the starch granule fully coated with polymer on its entire surface, looks more irregular and round over its entire surface, as expected (Figure 3.5d).

To further confirm the morphology of the Janus particles, we also obtained SEM-EDX nitrogen density maps of individual Janus polymer starch granules. Unmodified amaranth starch (Fig. 3.5e) does not show any appreciable nitrogen on its surface (Fig. 3.5i). The control polymer starch (Fig. 3.5f) shows an intense nitrogen density evenly distributed over its entire surface, which can be attributed to the nitrogen-rich polymer being evenly distributed over its entire surface (Fig. 3.5j). For comparison, we show two Janus polymer amaranth starch granules (Fig. 3.5g and 3.5h) with their respective nitrogen density maps (Fig. 3.5k and 3.5l). Unlike the control polymer, the Janus polymer particles have an intense nitrogen density on only one half side, which suggests that we were successful in producing Janus particles using the wax Pickering emulsion method. To show that this approach produces Janus particles in bulk, and not just in isolated instances, we show an SEM image of a group of Janus polymer particles (Fig. 3.5m), with their polymer halves highlighted in red (Fig. 3.5n).

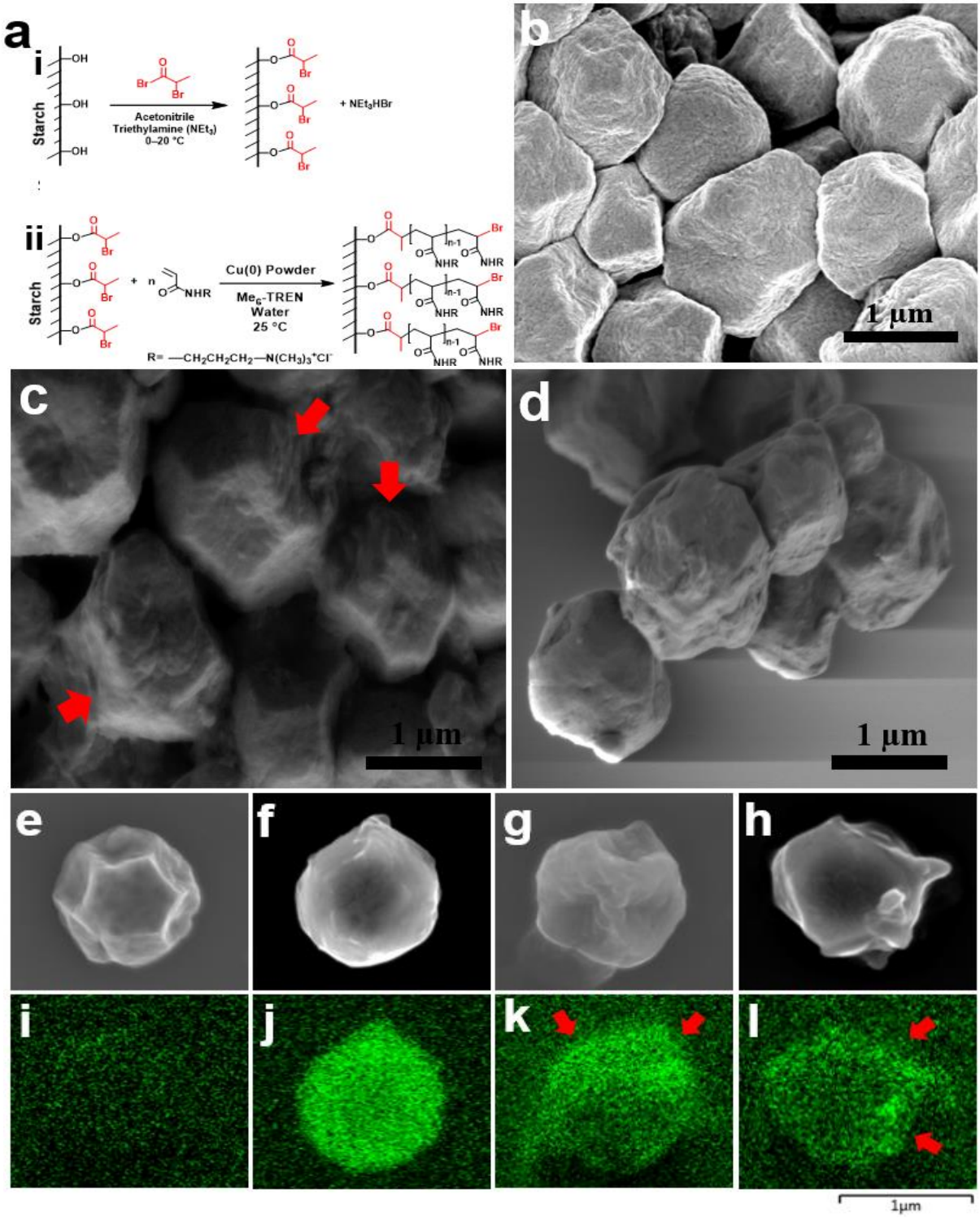

Figure 3.5. Janus morphology. (a) Reaction scheme of "grafting from" attachment of APTMAC onto starch. Field emission SEM images of (b) unmodified amaranth starch, (c) Janus polymer amaranth starch, with polymer patches highlighted with red arrows, and (d) control polymer amaranth starch. Field emission SEM images (upper panel) and SEM-EDX nitrogen density maps (lower panel) of a single granule of unmodified (e and i), control polymer (f and j), and two Janus polymer starch granules (g and k, h and l), respectively. The scale bar is 1µm for (e)-(l). (continued…)

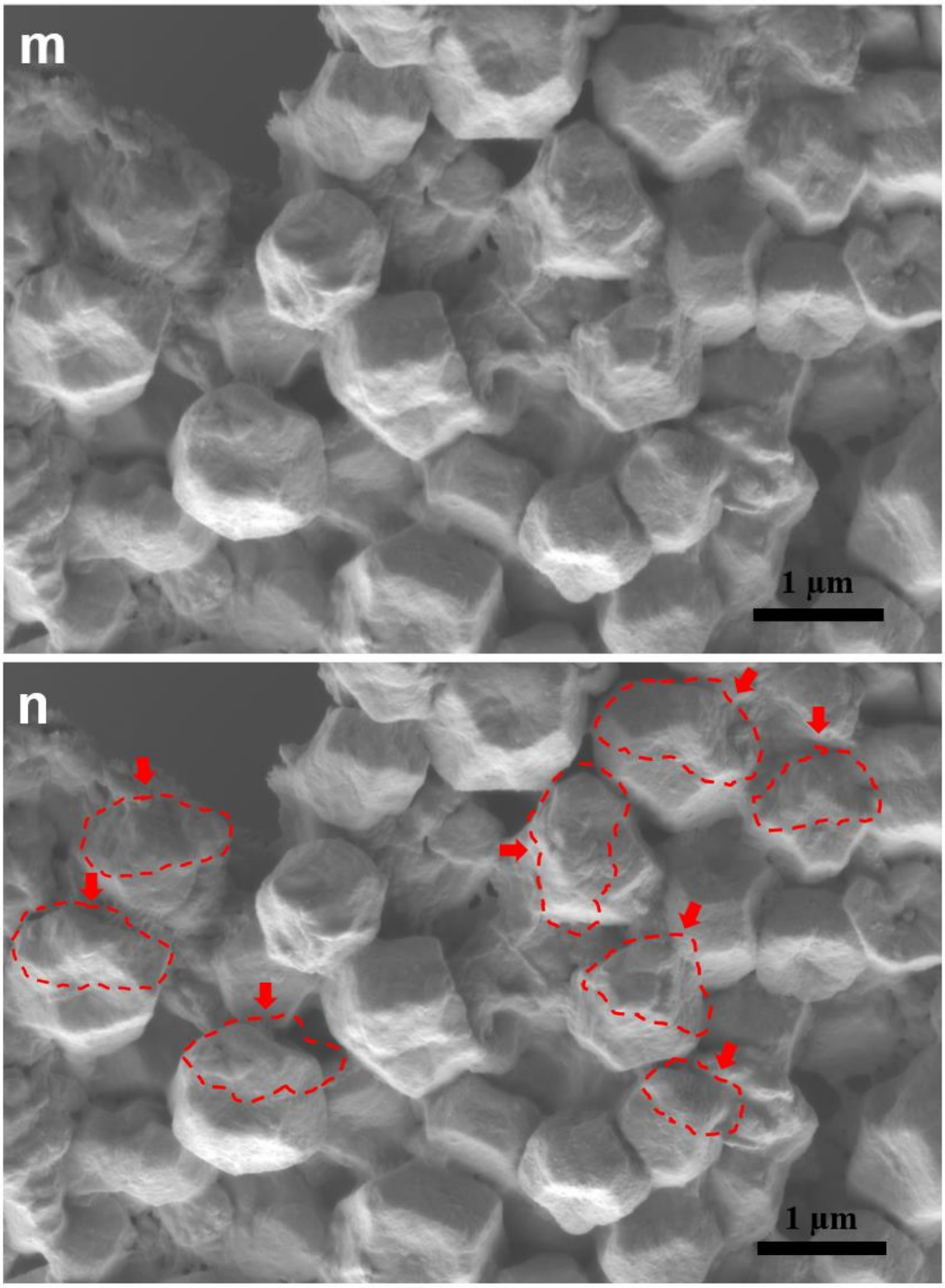

Figure 3.5. Janus morphology (continuation). (m) Field emission SEM image of a group of Janus polymer starch granules, (n) the same image, but with the polymer patches highlighted in red.

3.2.6 Janus balance by polymerization and SEM-EDX

Twenty random SEM-EDX images of Janus polymer amaranth starch granules were taken to compute for an experimental average Janus balance (or polymer coverage) of 49%, with a standard deviation of 21% (see Figs. 3.6a-e for 5 representative images out of the 20 images taken). To understand the significance of the experimental values generated, given the random nature of the measurement method, we also performed simulations. We performed 3 random 3D simulations of 20 Janus particles each, all randomly oriented on top of a flat surface, varying the theoretical Janus balance from 0% to 100% at each simulation (see Figs. 3.6f-h for simulations at 23%, 50%, and 77% Janus balance) and processed them as 2D images using Image J (see Figs. 3.6i-k) in order to compute for the simulated average Janus balance, which is plotted in Fig. 3.6l against theoretical Janus balance. These simulations confirm that when we take the average Janus balance out of 20 random Janus particles, the value we get is typically close to the theoretical Janus balance. This occurs because at each theoretical Janus balance from 0% to 100%, the distribution of polymer coverages we observe if we look at 20 random oriented particles on a flat surface from above should be symmetrical around the theoretical Janus balance. This result validates the randomized, SEM-EDX method we used to compute for the experimental average Janus balance of the Janus-polymer starch we synthesized.

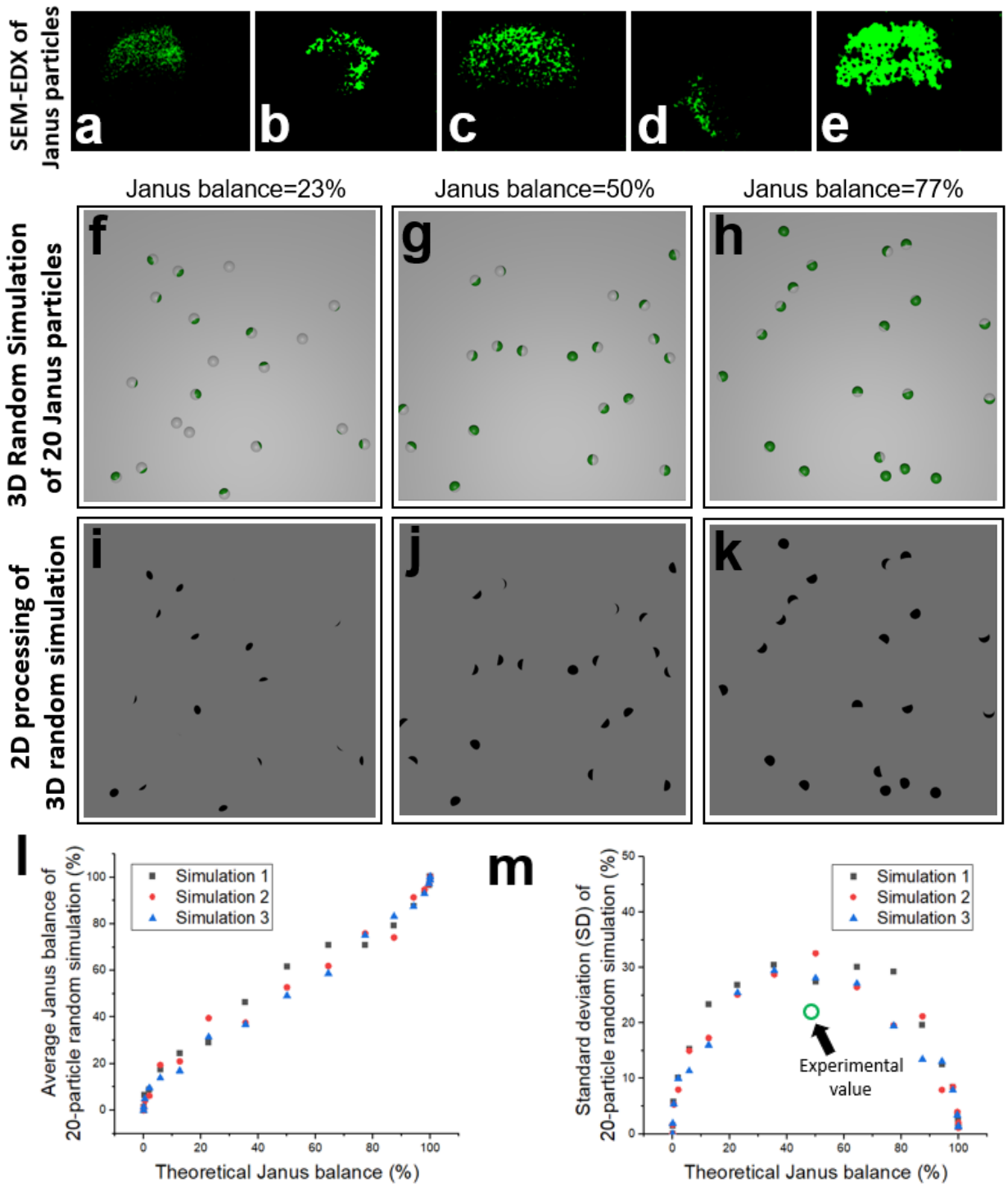

Figure 3.6. Janus balance. (a-b) Five representative SEM-EDX images of actual Janus-polymer particles made from starch (with noise removed), out of 20 random images taken to compute for the experimental average Janus balance. 3D random simulations of 20 Janus particles with a Janus balance of (f) 23%, (g) 50%, and (h) 77%, and their corresponding 2D processed images in ImageJ (i, j, and k, respectively) to compute for a simulated average Janus balance. (l) Simulated average Janus balance of 20-particle randomly simulated Janus particles vs. their theoretical Janus balance (3 simulations); (m) Standard deviation (SD) of the previous 3 simulations vs. theoretical Janus balance, with the experimental value generated from the 20 random SEM-EDX images of actual Janus polymer starch particles highlighted in green (open symbol).

In addition, the standard deviations of the simulations were also plotted against the theoretical Janus balance (see Fig. 3.6m), which shows that at both ends of the theoretical Janus balance, the standard deviations of the simulated average Janus balances are expected to be low, while near 50% theoretical Janus balance, the standard deviations are expected to be larger. This occurs because at a 50% theoretical Janus balance, all orientations can be reasonably assumed to have equal probability, so that the individual Janus balances of each of the 20 random particles generated will be spread out, thus giving a large standard deviation; on the other hand, as our theoretical Janus balance decreases down to near 0%, or increases up to near 100%, when we look at 20 random particles on a flat surface from above, we will see more particles with a narrower distribution of individual Janus balances, thus giving a smaller standard deviation. The experimental Janus balance of 49%, with an SD of 21%, was plugged into Fig 3.6m for comparison, which shows that the SD of the experimental value, while it appears high, is actually within expectation, given the random nature of the measurement method used. It is important to note here, however, that for the simulations, we modelled perfectly spherical particles, assumed that all orientations had equal probability across the 3D space, and assumed that all particles had the same Janus balance at each simulation.

3.2.7 Self-assembly of Janus OSA amaranth starch by optical microscopy

Representative or illustrative images that show the self-assembly in water of unmodified, control OSA, and Janus OSA amaranth starch are shown in Figs. 3.7a, b, and c, respectively. A total of 20 images were randomly captured for each sample and then processed using ImageJ to calculate for the corresponding areas of each discrete element (as shown outlined in Figs 3.7d, e, and f for unmodified, control OSA, and Janus OSA, respectively), and then tabulated in a bar graph to give the relative distribution of 1000+ discrete aggregates or elements of different sizes for each sample by cross-sectional area (see Figs. 3.7g, h, and i, respectively).

Unmodified amaranth starch in water exist mostly as discrete granules or 2- or 3-granule clusters (90% of all interactions) with no large aggregates because there is no strong attraction between granules to cause any significant interactions (see Figs. 3.7a and g). On the other hand, when we homogeneously attach hydrophobic groups over the entire surface of starch granules to produce control OSA, this leads to strong hydrophobic inter-granule interactions that bring about the formation of very large aggregates or supermicelles (>30% of all interactions) (see Figs. 3.7b. and h). For Janus OSA, where only one-half side of the granule was made hydrophobic, they mostly interact to form irregular, wormlike strings in water (>59% of all interactions) (see Figs. 3.7c and i). It is important to note here that the other “hydrophilic” side of the Janus OSA particle that was not modified by OSA may still contain residual proteins that may impart some level of hydrophobicity, although based on the self-assembly, they do not appear to be appreciable enough to mimic the behavior of the control OSA (see Figure 3.9d).

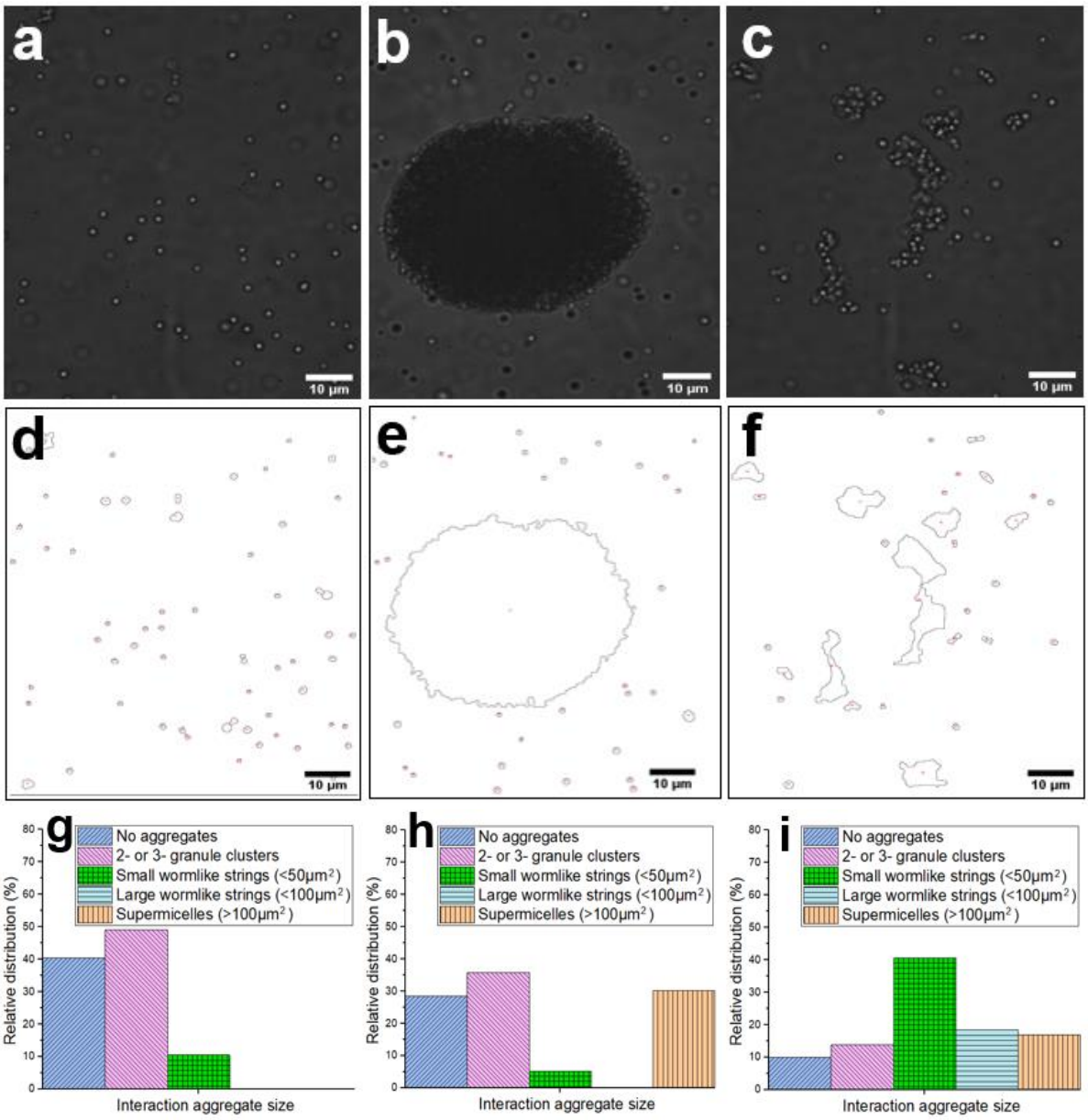

Figure 3.7. Self-assembly of Janus particles. Representative inter-granule self-assembly in water of (a) unmodified, (b) control OSA, and (c) Janus OSA amaranth starch, taken using an optical microscope at 100x magnification. Their corresponding aggregate area outlines after processing via ImageJ are shown for (d) unmodified, (e) control OSA, and (f) Janus OSA. The relative distributions of inter-particle aggregate sizes, taken out of 20 random images and 1000+ aggregates/particles each, are shown for (g) unmodified, (h) control OSA, and (i) Janus OSA.

A note on the size distribution graphs: Because we used the cross-sectional area and not the volume to generate them, the distributions will necessarily give more weight to smaller aggregates than to larger aggregates, and so the true distribution will probably consist of a larger percentage of larger aggregates than shown.

These results generally agree with our previous work on starch-based Janus particles produced via a 2D mask approach, where we saw that Janus OSA also formed wormlike strings and control OSA formed supermicelles in water (Kierulf, et al., 2019). In fact, a modeling study has shown that if a Janus particle has an attractive patch that covers 50-60% of the particle's surface, wormlike strings will indeed be formed, and that if the patch covers more than 89% – which closely resembles our control OSA – larger aggregates or supermicelles will be formed instead (Li, Lu, Sun, & An, 2012). It is believed that Janus particles self-assemble into these wormlike strings because one Janus particle will first attach to a second Janus particle if their attractive patches are aligned, and then this second particle will then attach to a third particle if their attractive patches are again available to each other, and then to a fourth particle, and so on and so forth, thus forming a wormlike string (Chen, et al., 2011). On the other hand, for the control OSA, because they are homogeneously hydrophobic over their entire surface, inter-granule attraction is non-directional, and so one granule can attract several granules surrounding it, and those in turn can attract many more granules around them, thus forming much larger aggregates or supermicelles.

3.2.8 Critical caking concentration of Janus OSA amaranth starch

The critical caking concentration (CCC) measures the concentration at which a starch solution starts to form a semi-solid cake. The unmodified, control OSA, and Janus OSA amaranth starch have critical caking concentrations of 38 ± 1, 33 ± 3, and 26 ± 2 %, respectively (see Fig. 3.8a). While the difference between the CCC of the unmodified starch and that of the control OSA is not statistically significant, the much lower CCC of the Janus OSA is, however, statistically different from both ($p<0.05$).

An effective thickener, or a material that even at low concentrations quickly thickens a solution, can be expected to have a lower critical caking concentration, while a less effective thickener that requires a high concentration before it can thicken a solution can be expected to have a higher critical caking concentration. The unmodified starch—because they largely do not self-assemble (see Fig. 3.7a)—will have more or less the same dispersed phase volume that their actual granular volume will dictate, and thus gives us a 38% critical caking concentration, which is typical for amaranth starch. On the other hand, control OSA—because many granules do not self-assemble but a good proportion form large supermicelles (see Fig. 3.7b and h)—can be expected to have a slightly larger effective dispersed phase volume than the unmodified starch, simply because the spaces between the OSA control granules forming the supermicelles can add to the effective dispersed phase, thus possibly giving it a slightly better thickening ability than the unmodified starch, and thus a lower critical caking concentration (33%), although in this case the difference was not statistically significant.

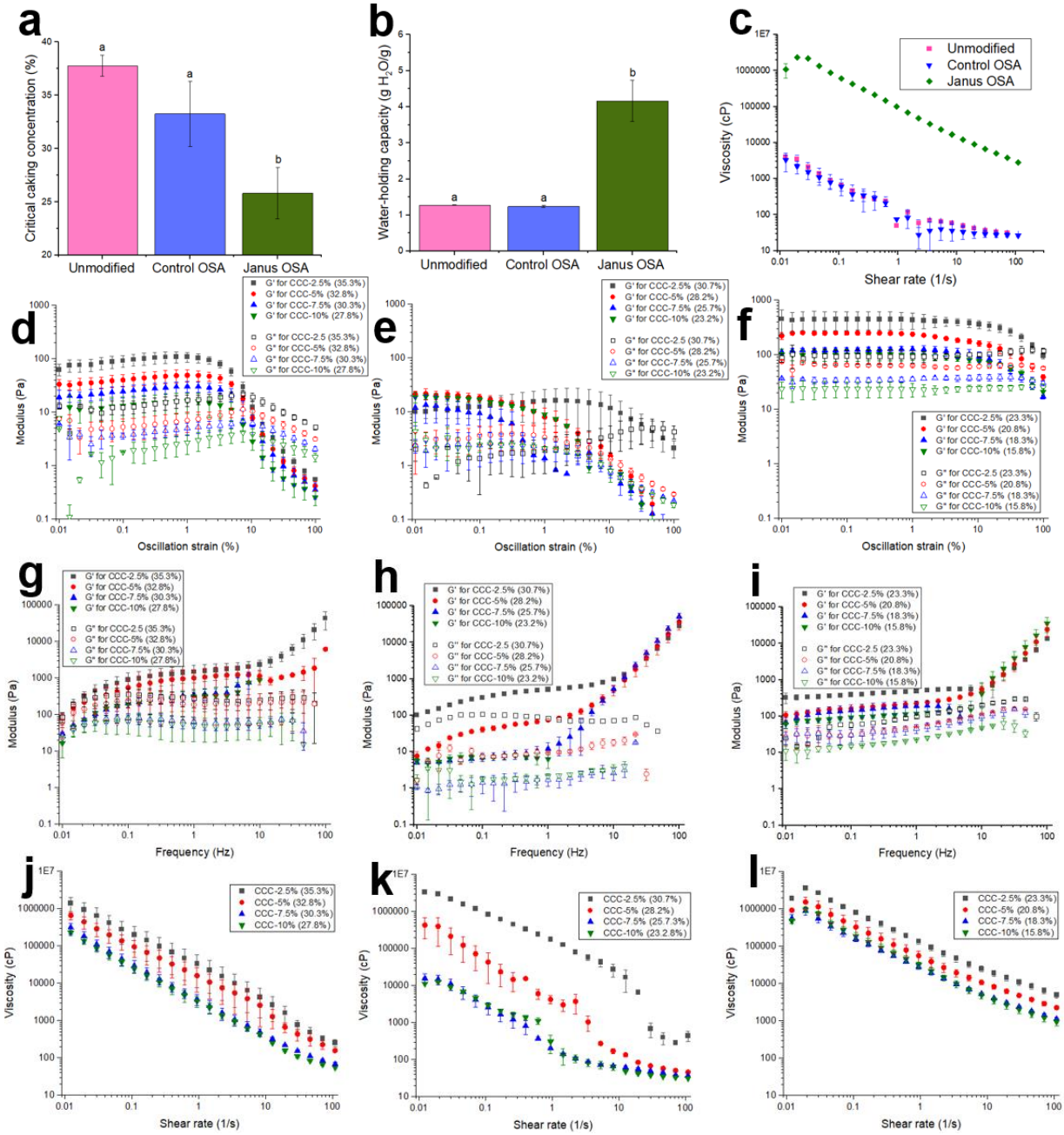

Figure 3.8. Physicochemical properties of Janus particles: Thickening ability. (a) Critical caking concentration, (b) water-holding capacity, and (c) viscosity at 20% (w/w) concentration for unmodified, control OSA, and Janus OSA amaranth starch. Oscillation strain sweep at 1 Hz frequency at four concentrations incrementally lower than the critical caking concentration (-2.5%, -5%, -7.5%, and -10%) for (d) unmodified, (e) control OSA, and (f) Janus OSA amaranth starch. Oscillation frequency sweep at 0.1% strain at the same four concentrations for (g) unmodified, (h) control OSA, and (i) Janus OSA amaranth starch. Viscosity at the same four concentrations for (j) unmodified, (k) control OSA, and (l) Janus OSA amaranth starch.

Compared to both the unmodified starch and the control OSA, however, the Janus OSA starch showed a much lower critical caking concentration (26%) that was statistically significant ($p<0.05$). Because Janus OSA granules self-assemble into small or large worm-like strings that stretch out in different directions and can rotate in solution, as we saw in the previous section (see Figs. 3.7c), they can therefore occupy a much larger effective dispersed phase volume than the actual dispersed phase volume that their constituent granules occupy, allowing them to form a network that can quickly thicken a solution even at low concentration. These networks can also trap water between them, reducing water flow and thus again increasing viscosity. These results indicate that Janus particles have a much better thickening ability than both the unmodified starch and the control.

3.2.9 Water-holding capacity of Janus OSA amaranth starch

Water-holding capacity (WHC) measures the ability of a material to bind or trap water (Elhardallou & Walker, 1993). The more sites in a material that are available to either bind water molecules through hydrogen bonding, or to trap them, the larger will be the WHC (Azfaralariff, Fazial, Sontanosamy, Nazar, & Lazim, 2020). The WHC of the unmodified, control OSA, and Janus OSA starch were found to be 1.27 ± 0.01, 1.24 ± 0.03, and 4.1 ± 0.6 g H_2O /g starch, respectively (see Fig. 3.8b). While the WHC of the unmodified starch and the control OSA starch were not statistically different form each other, the WHC of the Janus OSA was found to be much larger than both, and the difference was statistically significant ($p<0.05$).

The WHC of Janus OSA starch is almost four times higher than that of the unmodified starch and the control OSA, indicating that Janus OSA starch binds and traps water more effectively. This greater WHC may again be attributed to the self-assembly of these Janus particles into wormlike strings, allowing the formation of a network that can trap more water molecules inside it, which can lead to a thicker viscosity because this makes it harder for water molecules to move around. Thus, based on the WHC data, Janus OSA starch appears to have a better thickening ability than unmodified starch and control OSA—a result which is supported by the previous section on critical caking concentration, which showed that Janus OSA thickens in water more quickly even at lower concentrations. The CCC appears to be indirectly proportional to WHC, and in fact the methods used to measure them (filtration for CCC and centrifugation for WHC) have been interchangeably used to measure either, using only different equations to arrive at the same general property of how well water is held by a material (Ngoc, Len, & Lindberg, 2012).

3.2.10 Rheology of Janus OSA amaranth starch

a. Viscosity at one concentration

To compare the thickening abilities between the unmodified, Janus OSA, and control OSA amaranth starch, we measured their viscosities at the same concentration (20%), a concentration high enough to allow us to see any viscosity effects due to inter-granule interactions but still below the critical caking concentrations of all three samples (as determined in *section 3.2.8*). At all shear rates measured, from 0.01 to 100 1/s, all

samples showed shear-thinning behavior, but the viscosity of the Janus OSA was much higher by 2 or 3 orders of magnitude than those of both the unmodified and control OSA starch (see Fig. 3.8c). If we take their viscosities at one shear rate (13 1/s) and perform a t-test, we can verify that the viscosity difference between the Janus OSA and the unmodified starch, and between Janus OSA and the control OSA, are statistically significant ($p<0.05$); on the other hand, there is no statistically significant difference between the viscosity of the unmodified starch and that of control OSA. In general, these viscosity results corroborate the data we've already seen from the critical caking concentration and the water-holding capacity, which verifies that Janus OSA indeed has a greater thickening ability than both unmodified and control OSA starch, producing a more viscous dispersion at the same concentration by 2 or 3 orders of magnitude, across all shear rates tested, a property which may be due to its ability to self-assemble into wormlike strings in water.

b. Oscillatory amplitude sweep at different concentrations

To determine the linear viscoelastic region (LVR), amplitude sweeps were performed for unmodified, control OSA, and Janus OSA starch at four concentrations below (-2.5, -5, -7.5, and -10%) their critical caking concentration (see Figs. 3.8d, e, and f, respectively). For unmodified starch, which has a CCC=37.8%, we performed amplitude sweeps of 35.3% (CCC-2.5%), 32.8% (CCC-5%), 30.3% (CCC-7.5%), and 27.8% (CCC-10%) starch dispersions (Fig 3.8d). Likewise, for control OSA with a CCC=33.2%, we did amplitude sweeps for 30.7%, 28.2%, 25.7%, and 23.2% (Fig 3.8e);

and for Janus OSA with a CCC=25.8%, we did sweeps for 23.3%, 20.8%, 18.3%, and 15.8% (Fig 3.8f).

In general, we see that for all samples, at low strains, G' is larger than G", where G' is the storage modulus (closed symbols) and G" is the loss modulus (open symbols). This indicates that these samples are gel-like or viscoelastic solids at low strains. The region where G' is constant represents the linear viscoelastic range (LVR). However, at higher strains at a certain yield point, G' starts to decline, indicating that the network or gel structure starts to fracture, which defines the limit of the LVR. Further on at even higher strains, the G' and G" cross over at the flow point, at which point the solid gel has been fractured enough that it starts to flow as a liquid. At comparable concentrations (27.8%, 23.2%, and 23.3% for unmodified, control OSA, and Janus OSA), the Janus OSA has G' values about 45 times higher than the unmodified and control OSA, indicating that Janus OSA makes stiffer or more elastic gels. In addition, while for all samples the length of the LVR decreases as concentration decreases, indicating how lower concentrations make gels that fracture more easily, Janus OSA retains its long LVR even at lower concentrations. Likewise, at comparable concentrations, Janus OSA has an LVR (0.01 to 10.5% strain) that is about 7 and 105 times longer than those of the unmodified (0.01 to 1.5% strain) and control OSA (0.01 to 0.1% strain), respectively. This indicates that Janus OSA makes a much more stable or well-dispersed gel network or structure. Likewise, the flow point of the Janus OSA (68%) is about 9 and 20 times higher than those of the unmodified (7.4%) and control OSA (3.3%), respectively, which indicates that the network or structure formed by Janus OSA is much stronger and more resistant to breaking.

c. Oscillatory frequency sweep at different concentrations

Within the LVR, oscillatory frequency sweeps at 0.1% strain and 0.01-100 Hz frequency were performed for the unmodified, control OSA, and Janus OSA at the same four concentrations below their CCCs as in the previous section, in order to study the samples' degree of interparticle association and dispersion (Figs. 3.8g, h, i, respectively). High frequencies simulate fast motion and low frequencies simulate slow motion or slow changes in stress, which can give information about the samples' structural stability.

The moduli of Janus OSA appear to be less affected by the frequency than both the unmodified and the control OSA, which indicates that the Janus starch granules are more strongly associated with each other in a stable network and less likely to sediment. In particular, at low frequencies, the G' and G" of unmodified starch start to converge, which indicates that the undissociated, unmodified starch granules may start to sediment, thus making the gel flow more like a liquid. On the contrary, for both the control OSA and Janus OSA, G'>G" even at low frequencies, which indicates that the particles still float and form a gel network due to inter-particle hydrophobic interactions. In addition, at comparable concentrations, the G' for Janus OSA is about 2 and 50 times higher than those of the unmodified and control OSA, respectively, indicating that Janus OSA again forms a stiffer gel network.

d. Viscosity at different concentrations

The viscosity profiles at 0.01-100 1/s shear rate of the unmodified, control OSA, and Janus OSA at four concentrations below their CCC are shown in Figs. 3.8j, k, and l, respectively. It is clear that low concentrations of Janus OSA form more viscous dispersions than higher concentrations of both unmodified and control OSA starch, demonstrating again the greater thickening ability of Janus OSA starch. In fact, we find that we can achieve a similar viscosity (at 13 1/s) using a 15.8% dispersion of Janus OSA and a 35.3% dispersion of unmodified starch. This suggests that we could potentially reduce the amount of starch used in a formulation by about 55% if we use Janus OSA instead of unmodified starch, pointing to its possible use in lower-calorie food products in the food industry.

3.2.11 Surface activity of Janus OSA amaranth starch

Unmodified, Janus OSA, and control OSA amaranth starch formed O/W emulsions with droplet sizes of 170, 900, and 600μm (with PDI of 1.2, 1.2, 1.4), respectively (see Fig. 3.9a). These emulsions had emulsion indices of 0.64±0.01, 0.47±0.1, 0.47±0.05, respectively (see Fig 3.9b). The O/W interfacial tension over 1000s is shown in Fig. 3.9c.

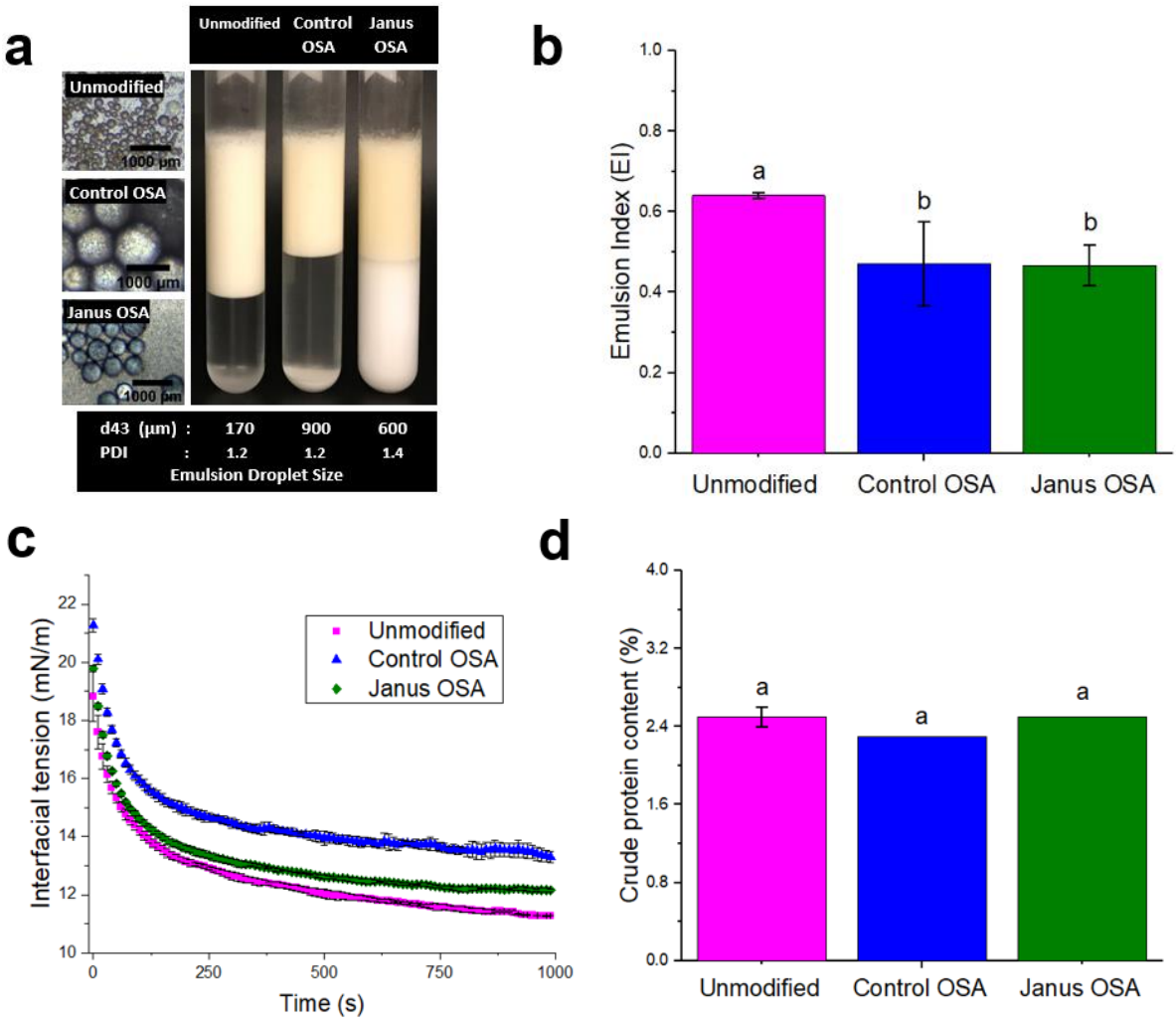

Figure 3.9. Physicochemical properties of Janus particles: Surface activity. (a) Emulsifying ability (droplet size), (b) emulsion index (EI), and interfacial tension of unmodified, control OSA, and Janus OSA amaranth starch.

An effective emulsifier is one that easily adsorbs onto the oil/water interface, effectively lower the O/W interfacial tension, and promotes the formation of smaller oil droplets, which are also more stable over time because they are less prone to creaming according to Stokes' law (McClements, 2016). Because smaller droplets have a larger effective volume fraction—namely, $(1+\delta_x/r)^3$ times that of the actual volume fraction

where δ_x is the adsorbed starch layer thickness and r is droplet radius—effective emulsifiers also give higher emulsion indices (Chanamai & McClements, 2000; Timgren, Rayner, Dejmek, Marku, & Sjoo, 2013). Typically, OSA treatment of starch improves its emulsifying properties, in terms of smaller droplet sizes, larger emulsion indices, and lower interfacial tension (Yu, et al., 2019; Liu, et al., 2019). Our results indicate the opposite trend—both Janus OSA and control OSA starch appear to be less effective emulsifiers than the unmodified starch. There are some possible explanations for this: First, typical OSA treatments are done on commercial, low-protein starches, so OSA treatment increases their hydrophobicity and emulsifying ability. In our case, our unmodified starch is already high in protein and therefore already a good emulsifier (see Fig. 3.9d), and further treatment with OSA (e.g., Janus OSA or control OSA) may have increased its hydrophobicity further, so much so that the increased inter-granule attraction may have reduced the number of granules actually available to participate in oil droplet stabilization. This is particularly evident for Janus OSA, where it is clear that they self-assemble in the water phase below the cream layer (see cloudy lower phase in Fig. 3.9a), making them unable to participate in emulsion stabilization. Thus, while theoretically and experimentally amphiphilic Janus particles are expected to be better emulsifiers than homogeneous particles (Aveyard, 2012; Kumar, Park, Tu, & Lee, 2013), the Janus particles produced here exhibit such strong self-assembly that they prefer to form a network in water. This is why, without oil, these Janus OSA particles form a strong network in water, trapping the water, and making them much more effective texturizers than the controls.

4. Conclusions and perspectives

We developed a scalable method for the bulk synthesis of Janus particles using a natural and safe ingredient like starch as the base material, for the purpose of exploring their possible applications in the food industry. The working principle behind the wax Pickering emulsion method hinges on the fact that high-protein starch granules, because they are moderately hydrophobic, tend to orient themselves at the oil/water interface, causing them to embed themselves halfway into the surface of liquid wax droplets in water, becoming trapped or immobilized when the wax solidifies. With one half of the granule now covered or "masked" by the solid wax droplet (hence the term "3D mask approach"), the other free half can then be modified by any reagent of our choice to make a Janus particle, after which the wax can be effectively removed.

We found that this method produces Janus particles with about 49% Janus balance or coverage. If we use OSA as the reagent, we can make Janus particles—with about 68% of the degree of substitution of the homogeneous control—that self-assemble into worm-like strings in water. This worm-like self-assembly behavior appears to be a unique feature of Janus particles in general, because both unmodified and homogeneously modified particles do not behave in the same way, a result supported by both simulations and experimental data in the literature. We believe that this unique self-assembly behavior, which results in a higher effective dispersed phase volume, may be the reason why Janus particles work as a much better thickener and gelling agent than the control in all the tests we conducted, giving us

a fourfold increase in water-holding capacity, a 30% lower critical caking concentration, a viscosity greater by orders of magnitude, and gels that are stiffer and stronger also by orders of magnitude. We believe that this strong inter-granule interaction may even be responsible for their unexpectedly lower surface activity, preferring to interact with each other rather than participate in emulsification.

In this study we aimed to demonstrate that we can assimilate the extraordinary field of Janus particles into the food space and start a conversation about incorporating smart materials into food. Outside the food industry, Janus particles have been designed as targeted drug delivery vehicles for cancerous tumors, switchable pixels for ultrathin electronic screens, and as self-motile nanomotors that simultaneously detect and remove toxins. Bringing this level of flexibility and extraordinary functionality into the food industry may lead to important, new applications. We've already seen Janus particles being developed to protect blueberries from microbes and to quickly detect Salmonella in milk and mayonnaise. And in this study we have added to those developments by demonstrating that Janus starch particles, because of their unique self-assembly behavior, work as much more effective texturizers than unmodified starch or homogeneously modified starch, and thus can be potentially used to reduce total calories in food products. We have the opportunity here to manufacture binary ingredients with one side having different properties than the other side, allowing them to exhibit synergistic benefits either in the food matrix or in the body after ingestion that far exceed the properties of their constituent parts. As the three-decades-old field of Janus particles has shown, there are indeed still many hurdles

to scale, but we believe their potential vastly outweighs these small difficulties, and we are excited about the possibilities that Janus particles may bring to the food space.

References

Aveyard, R. (2012). Can Janus particles give thermodynamically stable Pickering emulsions? *Soft Matter, 8*, 5233-5240.

Azfaralariff, A., Fazial, F. F., Sontanosamy, R. S., Nazar, M. F., & Lazim, A. M. (2020). Food-grade particle stabilized pickering emulsion using modified sago (Metroxylon sagu) starch nanocrystal. *Journal of Food Engineering , 280*, 109974.

Bhosale, R., & Singhal, R. (2007). Effect of octenylsuccinylation on physicochemicaland functional properties of waxy maize and amaranth starches. *Carbohydrate Polymers, 68*, 447-456.

Chanamai, R., & McClements, D. J. (2000). Dependence of creaming and rheology of monodisperse oil-in-water emulsions on droplet size and concentration. *Colloids and Surfaces A, 172*, 79-86.

Chen, Q., Whitmer, J. K., Jiang, S., Bae, S. C., Luijten, E., & Granick, S. (2011). Supracolloidal Reaction Kinetics of Janus Spheres. *Science , 331*.

Elhardallou, S. B., & Walker, A. F. (1993). The water-holding capacity of three starchy legumes in the raw, cooked and fibre-rich fraction forms. *Plant Foods for Human Nutrition , 44*, 171-179.

Gröschel, A. H., Walther, A., Löbling, T. I., Schmelz, J., Hanisch, A., Schmalz, H., & Müller, A. H. (2012). Facile, Solution-Based Synthesis of Soft, Nanoscale Janus Particles with Tunable Janus Balance. *Journal of the American Chemical Society, 134*(33), 13850-13860.

Hong, L., Jiang, S., & Granick, S. (2006). Simple method to produce Janus colloidal particles in large quantity. *Langmuir , 22*, 9495-99.

Hui, R., Qi-he, C., Ming-liang, F., Qiong, X., & Guo-qing, H. (2009). Preparation and properties of octenyl succinic anhydride modified potato starch. *Food Chemistry, 114*, 81-86.

Jia, R., Jiang, H., Jin, M., Wang, X., & Huang, J. (2015). Silver/chitosan-based Janus particles: Synthesis, characterization, and assessment of antimicrobial activity in vivo and vito. *Food Research International, 78*, 433-441.

Kierulf, A., Azizi, M., Eskandarloo, H., Whaley, J., Liu, W., Perez-Herrera, M., . . . Abbaspourrad, A. (2019). Starch-based Janus particles: Proof-of-concept heterogeneous design via a spin-coating spay approach. *Food Hydrocolloids, 91*, 301-310.

Kierulf, A., Whaley, J., Liu, W., Enayati, M., Tan, C., Perez-Herrera, M., . . . Abbaspourrad, A. (2020). Protein content of amaranth and quinoa starch plays a key role on their ability to form Pickering emulsions. *Food Chemistry, 315*, 126246.

Kim, J.-W., Larsen, R. J., & Weitz, D. A. (2006). Synthesis of Nonspherical Colloidal Particles with Anisotropic Properties. *Journal of the American Chemical Society, 128*(44), 14374-14377.

Kim, S.-H., Abbaspourrad, A., & Weitz, D. A. (2011). Amphiphilic Crescent-Moon-Shaped Microparticles Formed by Selective Adsorption of Colloids. *Journal of the American Chemical Society, 133*(14), 5516-5524.

Kumar, A., Park, B. J., Tu, F., & Lee, D. (2013). Amphiphilic Janus particles at fluid interfaces. *Soft Matter, 9*, 6604.

Latimer, G. (2016). *Official methods of analysis of AOAC International.* AOAC International.

Li, C., Li, Y., Sun, P., & Yang, C. (2013). Pickering emulsions stabilized by native starch granules. *Colloids and surfaces A: Physicochemical and engineering aspects, 431*, 142-149.

Li, Z.-W., Lu, Z.-Y., Sun, Z.-Y., & An, L.-J. (2012). Model, self-assembly structures, and phase diagram of soft Janus particles. *Soft Matter, 8*, 6693-6697.

Liang, F., Zhang, C., & Yang, Z. (2014). Rational Design and Synthesis of Janus Composites . *Advanced Materials, 26*, 6944-6949.

Liu, W., Li, Y., Goff, H. D., Nsor-Atindana, J., Ma, J., & Zhong, F. (2019). Interfacial Activity and Self-Assembly Behavior of Dissolved and Granular Octenyl Succinate Anhydride Starches. *Langmuir , 35*, 4702-4709.

Loget, G., & Kuhn, A. (2012). Bulk synthesis of Janus objects and asymmetric patchy particles. *Journal of Materials Chemistry, 22*, 15457-74.

McClements, D. J. (2016). *Food Emulsions 3rd ed.* Boca Raton, FL: CRC Press.

Miao, M., Li, R., Jiang, B., Cui, S., Zhang, T., & Jin, Z. (2014). Structure and physicochemical properties of octenyl succinic esters of sugary maize soluble starch and waxy maize starch. *Food Chemistry, 151*, 154-160.

Ngoc, T. T., Len, N. T., & Lindberg, J. E. (2012). Chemical Characterization and Water Holding Capacity of Fibre-rich Feedstuffs Used for Pigs in Vietnam. *Asian-Aust. J. Anim. Sci., 25*(6), 861-868.

Pacheco, M., Jurado-Sanchez, B., & Escarpa, A. (2018). Sensitive monitoring of enterobacterial contamination of food using self-propelled Janus microsensors. *Analytical chemistry, 90*, 2912-2917.

Pei, X., Zhai, K., Liang, X., Deng, Y., Xu, K., Tan, Y., . . . Wang, P. (2018). Fabrication of shape-tunable macroparticles by seeded polymerization of styrene using non-cross-linked starch-based seed. *Journal of Colloid and Interface Science, 512*, 600-608.

Robertson, D., van Reenen, A., & Duveskog, H. (2020). A comprehensive investigation into the structure-property relationship of wax and how it influences the properties of hot melt adhesives. *International Journal of Adhesion and Adhesives, 99*, 102559.

Saari, H., Heravifar, K., Rayner, M., Wahlgren, M., & Sjoo, M. (2016). Preparation and characterization of starch particles for use in Pickering emulsions. *Cereal Chemistry, 93*(2), 116-124.

Sharifah, I., ATBS, T. N., & Nor Khairusshima, M. (2017). Thermal modelling and analysis of Batik canting design. *Procedia Engineering, 184*, 326-333.

Shih, F. F., & Daigle, K. W. (2003). Gelatinization and pasting properties of rice starch modifiedwith 2-octen-1-ylsuccinic anhydride. *Nahrung/Food , 47*(1), 64-67.

Singh, N., Sandhu, K. S., & Kaur, M. (2004). Characterization of starches separated from Indian chickpea (Cicer arietinum L.) cultivars. *Journal of Food Engineering, 63*, 441-449.

Takein, H., & Shimizu, N. (1997). Gradient Sensitive Microscopic Probes Prepared by Gold Evaporation and Chemisorption on Latex Spheres. *Langmuir, 13*(7), 1865-1868.

Tanaka, T., Okayama, M., Kitayama, Y., Kagawa, Y., & Okubo, M. (2010). Preparation of “Mushroom-like” Janus Particles by Site-Selective Surface-Initiated Atom Transfer Radical Polymerization in Aqueous Dispersed Systems. *Langmuir , 26*(11), 7843-7847.

Timgren, A., Rayner, M., Dejmek, P., Marku, D., & Sjoo, M. (2013). Emulsion stabilizing capacity of intact starch granules modified by heat treatment or octenyl succinic anhydride. *Food Science and Nutrition, 1*(2), 157-171.

Walther, A., & Müller, A. H. (2013). Janus Particles: Synthesis, Self-Assembly, Physical Properties, and Applications. *Chemical Reviews, 113*(7), 5194-5261.

Xia, X., Li, G., Liao, F., Zhang, F., Jiong, Z., & Kan, J. (2014). Granular structure and physicochemical properties of starches from Amaranth grain. *International Journal of Food Properties*, 1029-1037.

Ye, F., Miao, M., Huang, C., Lu, K., Jiang, B., & Zhang, T. (2014). Elucidation of substituted ester group position in octenylsuccinic anhydride modified sugary maize soluble starch. *Agricultural and Food Chemistry, 62*, 11696-11705.

Yu, Z.-Y., Jiang, S.-W., Zheng, Z., Cao, X.-M., Hou, Z.-G., Xu, J.-J., . . . Pan, L.-J. (2019). Preparation and properties of OSA-modified taro starches and their application for stabilizing Pickering emulsions. *International Journal of Biological Macromolecules, 137*, 277-285.

Zhang, J., Grzybowski, B. A., & Granick, S. (2017). Janus Particle Synthesis, Assembly, and Application. *Langmuir, 33*, 6964-6977.

Zhang, L., Chen, Y., Li, Z., Li, L., Saint-Cricq, P., Li, C., . . . Zink, J. (2016). Tailored synthesis of Octopus-type Janus nanoparticles for synergistic actively-targeted and chemo-photothermal therapy. *Angewandte Chemie Int Ed, 55*, 2118-2121.

Zhao, S., Tian, G., Zhao, C., Lu, C., Bao, Y., & Liu, X. (2018). Emulsifying stability properties of octenyl succinic anhydride (OSA) modified waxy starches with different molecular structures. *Food Hydrocolloids , 85*, 248-256.

CHAPTER 4

Suggestions for future research

As mentioned in the Introduction and Chapter 3, one of the main challenges of Janus particle synthesis is scalability. While the wax Pickering emulsion method has been able to produce Janus particles at the gram scale, yield is still limited by the Soxhlet washing step (Fig. 3.1 a-vi). Future optimization of this washing step is therefore necessary for bulk synthesis. Likewise, concerns over the use of chloroform and Paraffin wax in the 3D mask method can be addressed by searching for alternative materials.

A critical parameter that affects the self-assembly and rheology of starch Janus particles is their Janus balance, and this parameter can be further explored. From the literature, we know that synthetic Janus particles exhibit different self-assembly behaviors at different Janus balances. As shown in Chapter 2, by increasing the residual protein content of starch, we can increase starch's emulsifying ability, or its ability to embed into the wax droplet phase before Janus modification. It would thus be theoretically possible to change the protein content of starch and thus change the Janus balance of the starch Janus particle produced, which would allow us to further control and fine-tune the rheology and texturizing ability of the starch Janus particle produced.

In addition, the thickening and gelling properties of the starch Janus particles measured in Chapter 3 may not exactly reflect their properties in systems involving multiple components other than just starch and water, so further studies involving other components would be helpful in understanding their food applications. Further studies on shear reversibility would also be helpful in understanding their processability.

In addition to heterogeneous starch modification at the granular level that was performed in this dissertation, heterogeneous starch modification at the molecular or nanoscale level via enzymes may also be explored that can lead to improved texturizing and emulsifying abilities.